

2010

Comparison of Full-Wave and Ray-Tracing Analysis of Mode Conversion in Plasmas

Yanli Xiao
College of William & Mary - Arts & Sciences

Follow this and additional works at: <https://scholarworks.wm.edu/etd>



Part of the [Plasma and Beam Physics Commons](#)

Recommended Citation

Xiao, Yanli, "Comparison of Full-Wave and Ray-Tracing Analysis of Mode Conversion in Plasmas" (2010). *Dissertations, Theses, and Masters Projects*. William & Mary. Paper 1539623573.
<https://dx.doi.org/doi:10.21220/s2-nkkd-jc45>

This Dissertation is brought to you for free and open access by the Theses, Dissertations, & Master Projects at W&M ScholarWorks. It has been accepted for inclusion in Dissertations, Theses, and Masters Projects by an authorized administrator of W&M ScholarWorks. For more information, please contact scholarworks@wm.edu.

Comparison of Full-Wave and Ray-Tracing Analysis of Mode Conversion in
Plasmas

Yanli Xiao

Shanghai, China

B.S. Fudan University, 2004
M.S. The College of William and Mary, 2005

A Dissertation presented to the Graduate Faculty
of the College of William and Mary in Candidacy for the Degree of
Doctor of Philosophy

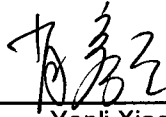
Department of Physics

The College of William and Mary
August 2010

APPROVAL PAGE

This Dissertation is submitted in partial fulfillment of
the requirements for the degree of

Doctor of Philosophy



Yanli Xiao

Approved by the Committee, May 2010



Committee Chair

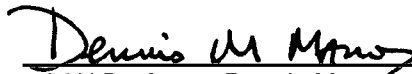
Chancellor Professor Eugene Tracy, Physics
The College of William and Mary



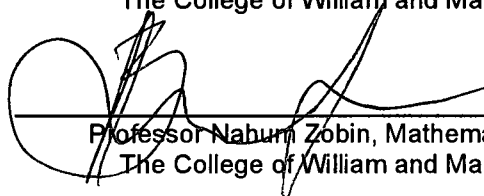
Professor William Cooke, Physics
The College of William and Mary



Professor John Delos, Physics
The College of William and Mary



CSX Professor Dennis Manos, Applied Science
The College of William and Mary



Professor Nabum Zobin, Mathematics
The College of William and Mary

ABSTRACT PAGE

This dissertation reports on the first direct comparison between the results of ray-based and full-wave calculations for mode conversion in plasma. This study was motivated by the modular method originally developed by Ye and Kaufman to treat a magnetosonic wave crossing a cold minority-ion gyroresonance layer. We start with the cold plasma fluid model and introduce a system of evolution equations for electrons and two ion species: deuterium and hydrogen. We first study this system of equations for uniform plasma by Fourier methods, which gives the dispersion relations. We discuss how the traditional approach – which eliminates all other dynamical variables in terms of the electric field – leads to singular denominators at the resonances. We then introduce the Kaufman & Ye approach, which retains the ion velocities as dynamical variables. In this formulation, the ion resonances appear as ‘avoided crossings’ between the familiar ‘fast wave’ and a zero-group-velocity ion ‘mode’ associated with the particle velocities. We then extend our problem to nonuniform plasma where the resonance is localized in space. Away from the resonance, WKB methods apply, but they break down in the vicinity of the resonance. In this region, we introduce the notion of ‘uncoupled modes’ and discuss how to use them to systematically carry out a simplification of the problem. This leads directly to the modular method of Kaufman & Ye in the mode conversion region, and provides the connection coefficients for the WKB solutions across the resonance layer. We specialize to an incoming wave packet and use the full-wave equations and the reduced 2×2 form to numerically study the wave packet conversion. This allows us to observe the emission of the reflected wave packet after a time delay (the linear ‘ion-cyclotron echo’). We calculate the incoming, transmitted and reflected wave packet energies. We compare them to the transmission and reflection coefficients predicted by the S matrix approach of Kaufman and Ye for a wide range of ion density ratios and find good agreement.

To my parents, Gang Xiao and Yimo Huang and my husband, Jacob Xiao for
their love and support.

TABLE OF CONTENTS

ACKNOWLEDGEMENTS	VI
LIST OF FIGURES	VII
CHAPTER 1 INTRODUCTION	1
CHAPTER 2 COLD PLASMA MODEL	7
2.1 FUNDAMENTAL EQUATIONS FOR THE DEUTERIUM-HYDROGEN-ELECTRON SYSTEM	7
2.1.1 Maxwell's Equations	7
2.1.2 Mass Conservation	8
2.1.3 Momentum conservation equation	11
2.2 TOTAL PHYSICAL ENERGY FOR THE DEUTERIUM-HYDROGEN-ELECTRON PLASMA	15
2.3 Nondimensionalization	16
2.4 LINEARIZATION	19
CHAPTER 3 WAVES IN UNIFORM PLASMA	22
3.1 FOURIER TRANSFORMATION	23
3.1.1 Wave packets	24
3.2 TRADITIONAL METHOD	26
3.3 THE RESONANCES	36
3.4 THE KAUFMAN & YE MODEL	48
CHAPTER 4 WAVES IN NONUNIFORM PLASMA FAR FROM RESONANCE	54
4.1 LOCAL RESONANCES	55
4.2 THE WKB METHOD	58
4.3 WKB METHOD ON AN EXAMPLE VECTOR PROBLEM	64
4.4 WKB METHOD ON THE COLD PLASMA PROBLEM	74
CHAPTER 5 WAVES IN NONUNIFORM PLASMA AT RESONANCES	77
5.1 REDUCTION TO THE 2x2 FORM	77
5.2 DOUBLE CONVERSION FOR THE COLD PLASMA MODELS	82
CHAPTER 6 NUMERICAL CALCULATIONS AND COMPARISON WITH THEORETICAL PREDICTIONS	85
6.1 CRANK-NICOLSON METHOD	85
6.2 INITIAL WAVE PACKETS	89
6.3 NUMERICAL RESULTS	91
6.3.1 Wave packet propagation	91
CHAPTER 7 SUMMARY AND CONCLUSION	103
APPENDIX A	108
APPENDIX B	116
APPENDIX C	123
BIBLIOGRAPHY	127
VITA	132

ACKNOWLEDGEMENTS

I would like to express my sincere gratitude to Professor Eugene Tracy for his patient guidance, encouragement and friendship to me during my time as a graduate student at the College of William and Mary. Dr. Tracy has been both a friend and a mentor. Without his encouragement and constant support, I could not have finished this research work.

I would also like to thank my defense committee members: Drs. Eugene Tracy, William Cooke, John Delos, Dennis Manos and Nahum Zobin. They provided me with insightful suggestions in my research work. Thanks also to Dr. Manos for providing me helpful comments and corrections.

Many thanks to Dr. Allan Kaufman for pointing me in the right direction and providing a foundation for my work. I would also like to thank my friends: Sadie Tedder, for helping me adjust to American life and for all the fun you brought me outside of my studies, for Qiujie Lv and Cheng Sun, for pushing me to keep working, listening to my ramblings, and giving me their insights.

Last but not least, I would like to thank my family: my parents Gang Xiao and Yimo Huang, for educating me, for unconditional love, support and encouragement; my husband: Jacob Xiao, for patiently listening to my complaints and frustrations all the time and cheering me up and easing my troubles afterwards; and my parents-in-laws: Bob and Beth Godwin-Jones for bringing happiness and warmth to me, and giving me their useful life advice.

This work was supported by the National Science Foundation and the Department of Energy.

LIST OF FIGURES

FIGURE 3.1 THE COORDINATE SYSTEM IN THE WAVE PROPAGATION OF THE UNIFORM MAGNETIC UNPERTURBED PLASMA	29
FIGURE 3.2 THE DIRECTIONS OF INDUCED ELECTRIC AND MAGNETIC FIELDS.....	32
FIGURE 3.3 THE DISPERSION RELATION FOR ORDINARY MODE.	34
FIGURE 3.4 THE POSITIVE BRANCH OF THE GROUP VELOCITY AND PHASE VELOCITY FOR THE ORDINARY MODE.....	35
FIGURE 3.5 THE DIRECTION OF THE INDUCED ELECTRIC FIELD AND MAGNETIC FIELD FOR THE SECOND EIGENVALUE.....	36
FIGURE 3.6 R AS A FUNCTION OF FREQUENCY IN THE POSITIVE FREQUENCY RANGE	38
FIGURE 3.6 (A) FUNCTION R IN THE ION CYCLOTRON FREQUENCY REGION	38
FIGURE 3.6 (B) FUNCTION R IN THE ELECTRON CYCLOTRON FREQUENCY REGION	39
FIGURE 3.7 L AS A FUNCTION OF FREQUENCY OVER THE FULL RANGE	40
FIGURE 3.7 (A) FUNCTION L IN THE ION CYCLOTRON FREQUENCY REGION	40
FIGURE 3.7 (B) FUNCTION L IN THE ELECTRON CYCLOTRON FREQUENCY REGION	41
FIGURE 3.8 (A) FUNCTION S IN THE ION CYCLOTRON FREQUENCY REGION.....	42
FIGURE 3.8 (B) FUNCTION S IN THE ELECTRON CYCLOTRON FREQUENCY REGION	42
FIGURE 3.9 (A) FUNCTION N^2 IN THE FIRST $S=0$ ROOT REGION	43
FIGURE 3.9 (B) FUNCTION N^2 IN THE SECOND $S=0$ ROOT REGION	44
FIGURE 3.9 (C) FUNCTION N^2 IN THE THIRD $S=0$ ROOT REGION	45
FIGURE 3.10 THE INDEX OF REFRACTION AS A FUNCTION OF FREQUENCY NOT TO SCALE FOR 50%DEUTERIUM AND 50%HYDROGEN.	46
FIGURE 3.11 THE INDEX OF REFRACTION AS A FUNCTION OF FREQUENCY NOT TO SCALE FOR 99%DEUTERIUM AND 1%HYDROGEN	47
FIGURE 3.12 THE INDEX OF REFRACTION AS A FUNCTION OF FREQUENCY NOT TO SCALE FOR ONLY ONE SPECIES OF ION: DEUTERIUM	47
FIGURE 3.13 THE DISPERSION RELATION IN THE POSITIVE FREQUENCY REGION FOR 50%DEUTERIUM AND 50%HYDROGEN	51
FIGURE 3.14 THE DISPERSION RELATION IN THE POSITIVE FREQUENCY REGION FOR 99%DEUTERIUM AND 1%HYDROGEN	52
FIGURE 4.1 THE DISPERSION CURVES FOR FIXED SPATIAL POSITION X.....	66
FIGURE 4.2 THE 3D DISPERSION SURFACE FOR THE FAST WAVE	68
FIGURE 4.3 THE 3D DISPERSION SURFACE FOR THE GYROFREQUENCY STANDING WAVE MODE.....	69
FIGURE 4.4 THE 3D DISPERSION SURFACE FOR THE TWO MODES	70
FIGURE 4.5 THE DISPERSION CURVES FOR FIXED FREQUENCY.....	71
FIGURE 4.6 MODE CONVERSION IN ω -K SPACE FOR FIXED POSITION x_0 . THESE ARE DISPERSION CURVES. NOTE THE AVOIDED CROSSINGS	73
FIGURE 4.7 MODE CONVERSION IN X-K SPACE FOR FIXED FREQUENCY ω_0 . THE BLACK CURVES ARE RAYS.....	73
FIGURE 4.8 DISPERSION CURVES FOR 50% DEUTERIUM-50% HYDROGEN WITH ELECTRON IN ω -K SPACE FOR A FIXED POSITION $x_0 > x_*$. THESE ARE DISPERSION CURVES CALCULATED USING THE FULL COLD PLASMA EQUATIONS.	74
FIGURE 5.1 DISPERSION CURVES FOR THE COLD PLASMA EQUATIONS IN PHASE SPACE FOR A FIXED FREQUENCY ω_* . THESE ARE RAYS, BUT NEAR THE CONVERSIONS WKB BREAKS DOWN.....	78
FIGURE 5.2 LOCAL RAY GEOMETRY AND THE POLARIZATION AT EACH POINT ON THE RAYS. $\hat{e}_\alpha(k_*, x_*)$ IS CONSTRUCTED BY LINEARLY TRANSPORTING THE INCOMING AND OUTGOING RED POLARIZATIONS TO THE ORIGIN, THEN AVERAGING $\hat{e}_\alpha(in)$ AND	

$\hat{e}_b(out); \hat{e}_\lambda(k_*, x_*)$ IS CONSTRUCTED SIMILARLY BY AVERAGING THE BLUE POLARIZATIONS $\hat{e}_a(out)$ AND $\hat{e}_b(in)$	79
FIGURE 6.1 DISPERSION RELATION OF THE FULL 6×6 COLD PLASMA PROBLEM FOR A FIXED POSITION	87
FIGURE 6.2 THE SHADED REGION INDICATES THE INCOMING WAVE PACKET FOR THE FULL 6×6 COLD PLASMA PROBLEM. THE RED LINES ARE THE MODE CONVERSION REGIONS. THE INCOMING WAVE PACKET MOVES TO THE LEFT. THE INCOMING ENERGY IS COMPUTED USING THE SHADED REGION.	92
FIGURE 6.3 THE SHADED REGION INDICATES THE TRANSMITTED WAVE PACKET FOR THE FULL 6×6 COLD PLASMA PROBLEM. THE RED LINES ARE THE MODE CONVERSION REGIONS. THE WAVE PACKET MOVES TO THE LEFT. THIS IS THE TRANSMITTED WAVE PACKET AND ITS ENERGY IS COMPUTED USING THE SHADED REGION.	93
FIGURE 6.4 THE SHADED REGION INDICATES THE REFLECTED WAVE PACKETS FOR THE FULL 6×6 COLD PLASMA PROBLEM. THE RED LINES ARE THE MODE CONVERSION REGIONS. THE REFLECTED WAVE PACKET MOVES TO THE RIGHT. ITS ENERGY IS COMPUTED USING THE SHADED REGION.	94
FIGURE 6.5 THE SHADED REGION INDICATES THE INCOMING WAVE PACKET FOR THE 2×2 REDUCED FORM. THE INCOMING ENERGY IS COMPUTED USING THE SHADED REGION.....	95
FIGURE 6.6 THE SHADED REGION INDICATES THE TRANSMITTED WAVE PACKET FOR THE 2×2 REDUCTION FORM. NOTE THE DISTURBANCE REMAINING IN THE VICINITY OF THE RESONANCE IN THE LOWER FRAME (WHICH IS LARGELY A COMBINATION OF THE PARTICLE VELOCITIES), AND THE EMERGENCE OF THE REFLECTED WAVE PACKET (WHICH IS LARGELY THE ELECTRIC FIELD).	96
FIGURE 6.7 THE SHADED REGION INDICATES THE REFLECTED WAVE PACKET FOR THE 2×2 REDUCED FORM. THE REFLECTED ENERGY IS COMPUTED USING THE SHADED REGION.	97
FIGURE 6.8 THE TRANSMISSION COEFFICIENT FROM THE ‘FULL-WAVE’ 6×6, ‘REDUCED’ 2×2 FULL WAVE AND ‘RAY-BASED’ S MATRIX PREDICTIONS FOR DIFFERENT ION DENSITIES.	100
FIGURE 6.9 THE REFLECTION COEFFICIENT FROM THE ‘FULL-WAVE’ 6×6, ‘REDUCED’ 2×2 FULL WAVE AND ‘RAY-BASED’ S MATRIX PREDICTIONS FOR DIFFERENT ION DENSITIES.	101

Chapter 1

Introduction

Current estimates suggest that most of the matter in the universe interacts only by gravitational forces; hence it is 'dark'. Of the remaining 'ordinary' matter, the large majority of it is ionized to some degree and, hence, a plasma. Plasmas consist of free electrons and ions that can be acted upon by electric and magnetic fields to a far greater degree than neutral matter. One big characteristic of plasma that is different from a collection of discrete particles is that plasma has collective behavior, such as waves and flows. Furthermore, plasmas carry current and charge densities which act as sources for the electromagnetic field. This leads to a rich variety of phenomena that are of interest in astrophysics, space physics, and laboratory plasmas. Plasmas are also of technological importance and are used routinely, for example, in material science and surface processing. The most direct application of the ideas described in this thesis concern radio frequency (RF) heating [1, 2, 3, 4] of fusion machines where the phenomenon of interest (mode conversion in the ion-cyclotron range of frequencies) is used to convert RF energy injected by an antenna at the plasma edge into particle kinetic energy, thereby heating the ions.

When there is a magnetic field, a moving charged particle gyrates with a characteristic frequency: the gyrofrequency. If the collective oscillatory motion of a plasma wave resonates with this particle motion there can be a

significant exchange of energy, either from the wave to the particles (heating) or *vice versa* (wave emission). In the problem we study here *both* processes occur because what is commonly called *mode conversion* [5, 6] in RF plasmas is in fact a *two-step* process: 1] in the first step an incoming collective wave converts partially to a disturbance in the motion of resonant ions, 2] in the second step the motion of these ions converts again to emit a reflected collective wave. In traditional treatments of mode conversion in the plasma literature, this is usually treated as a single-step process, *even though there is a time delay between the first and second steps*. As we will show, following the method of Ye and Kaufman [7, 8, 9], if the process is studied using ray phase space methods [10, 11, 12, 13, 14, 15], it becomes clear that two distinct events are involved: they are separated in phase space and the time delay arises because information has to be transported from one point in phase space to another. A great advantage of the Ye and Kaufman approach is that, because the two events are separated in phase space it is possible to develop local simplified approximations that lead to phase space connection coefficients for incoming and outgoing rays. In this way, we arrive at a simple theoretical prediction for how energy is shared among the incoming and outgoing collective waves, and how much is deposited with the particles.

The modular approach to mode conversion developed by Ye and Kaufman has been used to great advantage by our group [16,17,18], and we have extended it to include particle kinetic effects, multidimensionality, multiple resonances, cavity effects, etc. However, this thesis provides the first

direct comparison between a ‘primitive’ full-wave calculation of the phenomenon and the ray-based predictions. This is important because ray-based methods – which involve finding solutions of *ordinary differential equations* – run much faster than full-wave simulations, which involve *partial differential equations*, or even *integro-partial differential equations*. For example, to find the spatial heating profile for RF heating scenarios in tokamaks, a full-wave simulation can take a week on a supercomputer but a ray-tracing calculation can take only a few minutes on a desktop computer to map out where the conversion will occur, provide an estimate of how energy is transported through the machine, and predict where it will be deposited [19]. Because they take so long, full-wave simulations cannot currently be used real-time to analyze experimental data. The CPU overhead for each simulation also implies it will be difficult to use full-wave methods to do thorough studies of parameter space for the design of future fusion machines. This suggests that ray-based and full-wave methods can work together, with ray-based methods providing insight in real-time during experiments, as well as helping to identify critical points in parameter space where full-wave methods should take a more detailed look.

We now provide an outline of the rest of the thesis. We introduce the cold plasma model in Chapter 2. In this model each particle species (electrons, hydrogen and deuterium ions) are treated as interpenetrating cold ideal fluids. They are ‘cold’ because we do not allow for a thermal spread of velocities about the local fluid velocity. The evolution equations are derived by

imposing two fundamental conservation laws: we insist on mass and momentum conservation for each species separately. The different particle species interact only via the electromagnetic fields, and they act as sources for these fields. We then linearize the cold fluid equations and nondimensionalize. This allows us to identify the relevant small parameters in the problem.

In chapter 3, we study the uniform plasma case. We will use the Fourier transformation to derive the dispersion relations for collective motions and introduce both the traditional method and the Kaufman & Ye approach. In the Kaufman & Ye approach, certain singular denominators associated with resonances turn into “avoided crossings”, also called mode conversion. Mode conversion results in energy and action exchange between two nearly-degenerate modes.

In Chapter 4, we specialize to one spatial dimension and allow the background to be nonuniform, which makes all the resonances local in x . We can no longer use Fourier transforms as in the nonuniform plasma, so we introduce the WKB (ray tracing) method when away from the mode conversion. To motivate some of the mathematics, a simple pedagogic example is given of a vector wave equation solved using WKB methods.

In Chapter 5, we continue to consider nonuniform plasma, but focus now on the mode conversion region where the WKB approximation breaks down. We discuss the modular methods developed by Kaufman *et al.* to connect the incoming and outgoing WKB solutions. An interesting twist here

is that the two ‘avoided crossings’ that occur in this problem are associated with two modes that are dramatically different in physical character: the magnetosonic ‘fast’ wave is a nondispersive electromagnetic disturbance, while the ion-hybrid resonance has zero group velocity. This means the conversion occurs ‘at a caustic’, and that both conversions lie over one another in x -space. This projection singularity is what leads the traditional methods of analysis – which use the x -space representation for numerical analysis – to have difficulty because the problem is numerically stiff with a wide range of spatial scales. In phase space, as we shall show, there is no problem dealing with the conversion. We will show how to simplify our resulting 6×6 evolution equations to a 2×2 reduced form. Using Weyl symbol methods (which are particularly simple to apply in the current setting) we can construct a local wave equation in the vicinity of each mode conversion. This local 2×2 wave equation is then solved to find the standard S matrix (WKB connection) coefficients. This gives the transmission and conversion coefficients, and predicts how energy will be distributed after the mode conversion occurs. We will revisit the cold plasma model and present the double conversions.

In Chapter 6, we will numerically calculate both 6×6 and 2×2 ‘full-wave’ equations, which will give the wave packet evolution along with the incoming, transmitted and reflected packet energies. We will then compare the transmitted and reflected energy coefficients with the S matrix theoretical prediction for a range of ion density ratios. We will see that the agreement is

quite good over a wide range of density ratios for hydrogen-deuterium plasmas. These particular ion species were chosen because they are of interest in real fusion experiments studying conversion. We emphasize that these are the first direct comparisons between ray-based and full-wave methods for a three-species cold plasma model that includes the ion-hybrid resonance. Earlier comparisons between the two approaches used much simpler models constructed for illustrative purposes [20] [21]. Also, we note that Cally *et al.* have recently examined the reflection of a fast wave at the Alfvén resonance in a solar MHD model and found good agreement with ray-based estimates of reflection and absorption – based upon the modular methods discussed here -- for some parameter ranges, but not all [22]. For some of the parameter values studied by Cally *et al.* the local approximations used in our approach break down, so the disagreement is not really surprising. But, the results point to interesting directions for further development of the method.

In Chapter 7 we end with a summary and discuss possible future lines of research.

Chapter 2

Cold Plasma Model

The plasma model we studied is an ionized gas consisting of positively and negatively charged particles with overall of charge neutrality for the unperturbed background. To maintain the ionization, of course, the plasma is usually at a very high temperature. The presence of free charges makes the plasma respond strongly to the existence of electromagnetic fields. These unique characteristics make plasma a fourth state of matter.

We model the plasma as a cold fluid. This means there is no thermal velocity spread around the local mean velocities (the fluid velocity for each species). The cold plasma model provides a significant simplification, but still gives a reasonably accurate description of some waves that occur in real plasma.

2.1 Fundamental equations for the Deuterium-Hydrogen-Electron System

2.1.1 Maxwell's Equations

Plasmas are ionized gases. We assume that our plasmas are quasineutral, on average at each point they have an equal amounts of positive and negative charge. The model we studied consists of electrons and two

different species of ions: deuterium and hydrogen. We start with Maxwell's equations [23]:

$$\nabla \times \vec{B} = \mu_0 \vec{J} + \epsilon_0 \mu_0 \frac{\partial \vec{E}}{\partial t} \quad (2.1)$$

$$\nabla \times \vec{E} = -\frac{\partial \vec{B}}{\partial t} \quad (2.2)$$

$$\nabla \cdot \vec{E} = \frac{\rho}{\epsilon_0} \quad (2.3)$$

$$\nabla \cdot \vec{B} = 0 \quad (2.4)$$

Where $\rho = \sum_s n_s e_s$, $\vec{J} = \sum_s n_s e_s \vec{v}_s$, the subscript s denotes different particle species. Each particle species is also assumed to satisfy two fundamental fluid conservation laws: conservation of mass and momentum.

2.1.2 Mass Conservation

We treat the Deuterium-Hydrogen-Electron plasma as three ideal interpenetrating fluids that interact only through the electromagnetic fields [24]. The evolution equations for such fluids are the mass conservation equation -- also called the continuity equation -- and momentum conservation -- also known as the force balance equation.

Consider any *fixed* volume V_0 in the space. The mass of fluid s contained in this volume is

$$M_{sV_0}(t) = \int_{V_0} m_s n_s(\vec{x}, t) dV. \quad (2.5)$$

Where $n_s(\bar{x}, t)$ is the fluid number density for fluid species s at the position $\bar{x} = (x, y, z)$ at time t ; m_s is the mass per particle for fluid species s and the integration is taken over V_0 . Following Newton, the time derivative of the mass in V_0 is

$$\begin{aligned}
\frac{dM_{sV_0}(t)}{dt} &= \lim_{\Delta t \rightarrow 0} \frac{M_{sV_0}(t + \Delta t) - M_{sV_0}(t)}{\Delta t} \\
&= \lim_{\Delta t \rightarrow 0} \frac{\int_{V_0} m_s n_s(\bar{x}, t + \Delta t) dV - \int_{V_0} m_s n_s(\bar{x}, t) dV}{\Delta t} \\
&= \lim_{\Delta t \rightarrow 0} \int_{V_0} \frac{m_s n_s(\bar{x}, t + \Delta t) - m_s n_s(\bar{x}, t)}{\Delta t} dV \\
&= \int_{V_0} \lim_{\Delta t \rightarrow 0} m_s \frac{n_s(\bar{x}, t + \Delta t) - n_s(\bar{x}, t)}{\Delta t} dV = \int_{V_0} m_s \frac{\partial n_s(\bar{x}, t)}{\partial t} dV
\end{aligned} \tag{2.6}$$

Note that at a critical step we have exchanged the order of the integration and the limit. This is justified if the integrand satisfies certain smoothness conditions, which we will assume hold, without proof. The number of particles of each species is assumed to be constant; hence the total mass in the volume can only change by having particles flow in – or out – of the volume.

At the time t , the mass of fluid flowing through an infinitesimal surface area on the boundary of V_0 , denote dA , in the short time Δt is $m_s n_s(\bar{x}, t) \vec{v}_s(\bar{x}, t) \cdot \hat{n} dA \Delta t$, where \vec{v}_s is the local fluid velocity of species s at the position $\bar{x} = (x, y, z)$ and time t , and \hat{n} is the outward-pointing normal direction of the area dA . Hence, by convention, when $m_s n_s(\bar{x}, t) \vec{v}_s(\bar{x}, t) \cdot \hat{n} dA \Delta t$ is positive, the fluid is flowing out of the volume

and when it is negative, the fluid is flowing into the volume through dA .

Dividing by Δt and integrating over the surface of the volume V_0 , the rate of change of the total mass of fluid species s is

$$\frac{dM_s(t)}{dt} = - \oint_{V_0, \text{surface}} m_s n_s(\vec{x}, t) \vec{v}_s(\vec{x}, t) \cdot \hat{n} dA. \quad (2.7)$$

The negative sign appears because of our sign convention for the unit normal: an outward flux is *positive* and contributes to a *decrease* in the total mass.

From equations (2.6) and (2.7), we get

$$\int_{V_0} \frac{\partial n_s(\vec{x}, t)}{\partial t} dV = - \oint_{V_0, \text{surface}} n_s(\vec{x}, t) \vec{v}_s(\vec{x}, t) \cdot \hat{n} dA. \quad (2.8)$$

By Green's formula, the surface integral can be transformed into a volume integral, so (2.8) becomes

$$\int_{V_0} \frac{\partial n_s(\vec{x}, t)}{\partial t} dV = - \int_{V_0} \nabla \cdot (n_s(\vec{x}, t) \vec{v}_s(\vec{x}, t)) dV \quad (2.9)$$

Thus,

$$\int_{V_0} \left[\frac{\partial n_s(\vec{x}, t)}{\partial t} + \nabla \cdot (n_s(\vec{x}, t) \vec{v}_s(\vec{x}, t)) \right] dV = 0. \quad (2.10)$$

Since the volume V_0 is arbitrary and (2.10) must be valid for any region in space, hence the integrand has to be zero. Therefore we get a local statement of conservation of mass:

$$\frac{\partial n_s(\vec{x}, t)}{\partial t} + \nabla \cdot (n_s(\vec{x}, t) \vec{v}_s(\vec{x}, t)) = 0. \quad (2.11)$$

This is the continuity equation and it holds for each species of our cold plasma model. This is a special case of a *conservation law*, which equates the time

derivative of a *density* of some quantity with the divergence of the *flux* of that quantity, where the flux is the density times the local fluid velocity. The force balance equation – discussed in the next section -- is another example of such a conservation law: it holds for each component of the momentum density for each species. An additional complication in the momentum conservation law is the need to treat external forces.

2.1.3 Momentum conservation equation

The total momentum for the fluid species s of any volume V_0 is

$$\vec{P}_s(t) = \int_{V_0} m_s n_s(\vec{x}, t) \vec{v}_s(\vec{x}, t) dV . \quad (2.12)$$

So the rate of momentum change is

$$\frac{d\vec{P}_s(t)}{dt} = \int_{V_0} \left[m_s \vec{v}_s(\vec{x}, t) \frac{\partial n_s(\vec{x}, t)}{\partial t} + m_s n_s(\vec{x}, t) \frac{\partial \vec{v}_s(\vec{x}, t)}{\partial t} \right] dV . \quad (2.13)$$

Substituting (2.11) into (2.13) gives:

$$\frac{d\vec{P}_s(t)}{dt} = \int_{V_0} \left[-m_s \nabla \cdot [n_s(\vec{x}, t) \vec{v}_s(\vec{x}, t)] \vec{v}_s + m_s n_s(\vec{x}, t) \frac{\partial \vec{v}_s(\vec{x}, t)}{\partial t} \right] dV . \quad (2.14)$$

The time rate of change of the total momentum on the fluid s is now equated to the net external forces $\vec{F}_s^{external}$ acting on the matter in the volume. These forces are of two different types: *volume* forces \vec{F}_s^{volume} – that act throughout the volume (important examples are gravitational forces, or electric and magnetic forces) – and what are called *tractive* forces $\vec{F}_s^{tractive}$ that act at the surface.

$$\frac{d\bar{P}_s(t)}{dt} = \int_{V_0} dV \bar{F}_s^{external} = \int_{V_0} dV \bar{F}_s^{volume} + \int_{\partial V_0} dA \bar{F}_s^{tractive} \quad (2.15)$$

For cold ideal fluids, the tractive forces are assumed to be due only to the advection of momentum in or out of the volume due to the fluid motion.

Hence, it is a momentum flux. The j^{th} component of the momentum flux for species s is simply $m_s n_s v_s^j$ times the local flow velocity. Therefore, the j^{th} component of equation (2.15) is:

$$\begin{aligned} \frac{dP_s^j(t)}{dt} &= \int_{V_0} dV (\bar{F}_s^{external})^j = \left(\int_{V_0} dV \bar{F}_s^{volume} + \int_{\partial V_0} dA \bar{F}_s^{tractive} \right)^j \\ &= \int_{V_0} dV (\bar{F}_s^{volume})^j + \int_{\partial V_0} dA \hat{n} \cdot (m_s n_s v_s^j \bar{v}_s) \end{aligned} \quad (2.16)$$

With Green's formula, we can replace the surface integral with a volume integral:

$$\int_{\partial V_0} dA \hat{n} \cdot (m_s n_s v_s^j \bar{v}_s) = - \int_{V_0} dV \sum_k m_s \partial_k (n_s v_s^j v_s^k). \quad (2.17)$$

Where $j, k = x, y, z$ lies in the three-dimensional configuration space, and the minus sign indicates that a positive (outward) momentum flux corresponds to a decreasing momentum of the fluid in the volume.

Substitute equation (2.16) with (2.17),

$$\begin{aligned} \frac{dP_s^j(t)}{dt} &= \int_{V_0} dV (\bar{F}_s^{volume})^j - \int_{V_0} dV \sum_k m_s \partial_k (n_s v_s^j v_s^k) \\ &= \int_{V_0} dV (\bar{F}_s^{volume})^j - \int_{V_0} dV m_s \sum_k v_s^j \partial_k (n_s v_s^k) - \int_{V_0} dV m_s n_s \sum_k v_s^k \partial_k v_s^j \end{aligned} \quad (2.18)$$

Equation (2.14) has the j^{th} -component:

$$\frac{dP_s^j(t)}{dt} = \int_{V_0} \left[-m_s \sum_k v_s^j \partial_k (n_s v_s^k) + m_s n_s \frac{\partial v_s^j}{\partial t} \right] dV \quad (2.19)$$

Combining (2.19) with (2.18), we get:

$$\begin{aligned} \int_{V_0} dV (\vec{F}_s^{volume})^j &= \int_{V_0} dV m_s n_s \sum_k v_s^k \partial_k v_s^j + \int_{V_0} m_s n_s \frac{\partial v_s^j}{\partial t} dV \\ &= \int_{V_0} dV m_s n_s (\vec{v}_s \cdot \nabla) v_s^j + \int_{V_0} m_s n_s \frac{\partial v_s^j}{\partial t} dV \end{aligned}$$

Expressing this in the vector form,

$$\int_{V_0} dV m_s n_s(\vec{x}, t) \left[\vec{v}_s(\vec{x}, t) \cdot \nabla \vec{v}_s(\vec{x}, t) + \frac{\partial \vec{v}_s(\vec{x}, t)}{\partial t} \right] = \int_{V_0} dV \vec{F}_s^{volume}(\vec{x}, t). \quad (2.20)$$

This is the momentum conservation equation for the fluid species s of volume V_0 . Using the fact that the equation is valid for any volume V_0 , the integrands have to be equal, thus we get the equation of motion:

$$m_s n_s(\vec{x}, t) \left[\vec{v}_s(\vec{x}, t) \cdot \nabla \vec{v}_s(\vec{x}, t) + \frac{\partial \vec{v}_s(\vec{x}, t)}{\partial t} \right] = \vec{F}_s^{volume}(\vec{x}, t) \quad (2.21).$$

The result (2.21) is general and applies for any external (volume) forces.

We now specialize our model by assuming the volume force is the Lorentz force law for charge particle motion in EM fields. Therefore, we have (in SI units):

$$\vec{F}_s^{volume}(\vec{x}, t) = \sum_s q_s n_s(\vec{x}, t) \left[\vec{E}(\vec{x}, t) + \vec{v}_s(\vec{x}, t) \times \vec{B}(\vec{x}, t) \right]. \quad (2.22)$$

Where q_s is the charge of the fluid species s ; \vec{E} is the electric field and \vec{B} is the magnetic field.

Combining equation (2.21) and (2.22), we get the equation of motion:

$$(\vec{v}_s(\vec{x},t) \cdot \nabla) \vec{v}_s(\vec{x},t) + \frac{\partial \vec{v}_s(\vec{x},t)}{\partial t} = \frac{q_s}{m_s} [\vec{E}(\vec{x},t) + \vec{v}_s(\vec{x},t) \times \vec{B}(\vec{x},t)]. \quad (2.23)$$

For the cold plasma model with two ion species (deuterium and hydrogen) and electrons, the six fundamental evolution equations are (2.1), (2.2), (2.3), (2.4), (2.11) and (2.23). These form a closed set of equations and, combined with a choice of initial conditions, provide a complete description of the plasma.

Let's count variables. These are: the three electric field components; the three magnetic field components; the deuterium, hydrogen and electron densities $(n_D(\vec{x},t), n_H(\vec{x},t), n_e(\vec{x},t))$; and the velocities:

$$\vec{v}_D(\vec{x},t) = [v_{D_x}(\vec{x},t), v_{D_y}(\vec{x},t), v_{D_z}(\vec{x},t)] \quad (\text{Deuterium})$$

$$\vec{v}_H(\vec{x},t) = [v_{H_x}(\vec{x},t), v_{H_y}(\vec{x},t), v_{H_z}(\vec{x},t)] \quad (\text{Hydrogen})$$

$$\vec{v}_e(\vec{x},t) = [v_{e_x}(\vec{x},t), v_{e_y}(\vec{x},t), v_{e_z}(\vec{x},t)] \quad (\text{Electrons})$$

This gives a total of 18 unknowns.

Because we are using a cold ideal fluid model for each species, we have neglected the direct particle-particle interactions, which would lead to collisions at the micro level, and viscosity and drag effects at the macro – or fluid -- level. At the present level of description, the particles interact with each other only through the intermediary of the macroscopic electromagnetic fields. The particles act as sources for these fields, but because the particles are treated as a smooth fluid, the fields are also assumed to be smooth in space. While noting how much of the microscopic physics has been neglected, it is also important to emphasize that the cold fluid model captures some of the essential wave physics observed in laboratory plasmas. In particular, the

wave mode that will concern us in later chapters (e.g. the fast Alfvén wave) is well-established as having many of the properties predicted by the simple cold-plasma equations.

The most important effect that has been neglected at this level of description is thermal broadening of the resonant wave-particle interaction. For cold fluids with single-frequency harmonic wave motion, this resonant interaction is ‘sharp’: the resonance condition is either satisfied or it isn’t. For uniform plasma, the resonance is global while for nonuniform plasma (which is of more interest to us) the resonance occurs at a well-defined spatial position where the gyrofrequency of species s equals the wave frequency. If there is a thermal spread, then each subpopulation of particles – moving at different velocities – can resonate at slightly different spatial positions due to Doppler effects, leading to a broadening of the spatial region where resonance occurs. Phase mixing among the different populations of particles also leads to wave absorption via Landau damping. These ideas were discussed in [25,26]. Thermal effects are not treated in this thesis, but will be pursued in later work.

2.2 Total Physical Energy for the Deuterium-Hydrogen-Electron Plasma

The total energy of the cold plasma is conserved by the evolution equations derived in the previous section, and it will be used to compare our various methods of analysis in later chapters. The total energy consists of two parts: the electromagnetic field energy and the particle kinetic energy.

The electromagnetic field energy is

$$\mathcal{E}_{field} = \int_V \frac{\epsilon_0}{2} \left(|\vec{E}(\vec{x}, t)|^2 + c^2 |\vec{B}(\vec{x}, t)|^2 \right) dV. \quad (2.24)$$

The particle kinetic energy is

$$\mathcal{E}_{kinetic} = \int_V \frac{1}{2} \left(m_D n_D(\vec{x}, t) |\vec{v}_D(\vec{x}, t)|^2 + m_H n_H(\vec{x}, t) |\vec{v}_H(\vec{x}, t)|^2 + m_e n_e(\vec{x}, t) |\vec{v}_e(\vec{x}, t)|^2 \right) dV \quad (2.25)$$

The total energy is

$$\mathcal{E}_{total} = \mathcal{E}_{field} + \mathcal{E}_{kinetic} \quad (2.26)$$

Taking the time derivative of (1.25), and using the evolution equations, a straightforward calculation shows the total energy is conserved.

2.3 Nondimensionalization

We will eventually solve our evolution equations numerically, which requires that they be nondimensionalized. We nondimensionalize the evolution equations of section 2.1 by first choosing reference scales for mass, charge, time scales, and spatial scales. The ‘*’ quantities are nondimensional.

$$\vec{x} = x_0 \vec{x}_*, \quad t = t_0 t_*, \quad m = m_p m_*, \quad q = e e_*. \quad (2.27)$$

Here m_p is the proton mass, e is the proton charge; x_0 and t_0 are the rescaled length and time scales. We will choose these scales in a moment.

For electric field \vec{E} and magnetic field \vec{B} will be nondimensionalized - along with each fluid species density n_s , and velocity \vec{v}_s -- as follows:

$$\begin{aligned} n_s(\vec{x}, t) &= n_0 n_{s*}(\vec{x}_*, t_*), & \vec{v}_s(\vec{x}, t) &= v_0 \vec{v}_{s*}(\vec{x}_*, t_*) \\ \vec{E}(\vec{x}, t) &= E_0 \vec{E}_*(\vec{x}_*, t_*), & \vec{B}(\vec{x}, t) &= B_0 \vec{B}_*(\vec{x}_*, t_*) \end{aligned} \quad (2.28)$$

where all notations with 0 subscripts represent reference values.

There are, of course, relations between some of these choices. For example: we have $x_0 = c_A t_0$, $E_0 = c B_0$, where c is the speed of light. We define

$$\Omega_{p0} \equiv \frac{e B_0}{m_p}, \quad \omega_p^2 \equiv \frac{n_0 e^2}{\epsilon_0 m_p}, \quad c_A \equiv \left(\frac{B_0^2}{\mu_0 m_p n_0} \right)^{1/2}, \quad (2.29)$$

Where Ω_{p0} is the proton gyrofrequency, ω_p is the proton plasma frequency and c_A is the Alfvén wave speed for the proton [27].

Rescaling the six equations (2.1), (2.2), (2.3), (2.4), (2.11) and (2.23) using (2.27) and (2.28), we get:

$$\nabla_* \times \vec{B}_* = \frac{\omega_p^2 t_0}{\Omega_{p0}} \frac{c_A^2}{c^2} \sum_s n_{s*} e_{s*} \vec{v}_{s*} + \frac{c_A}{c} \frac{\partial \vec{E}_*}{\partial t_*} \quad (2.30)$$

$$\nabla_* \times \vec{E}_* = -\frac{c_A}{c} \frac{\partial \vec{B}_*}{\partial t_*} \quad (2.31)$$

$$\nabla_* \cdot \vec{B}_* = 0 \quad (2.32)$$

$$\nabla_* \cdot \vec{E}_* = \frac{\omega_p^2 t_0}{\Omega_{p0}} \frac{c_A}{c} \sum_s e_{s*} n_{s*} \quad (2.33)$$

$$\frac{\partial n_{s*}}{\partial t_*} + \nabla_* \cdot (n_{s*} \vec{v}_{s*}) = 0 \quad (2.34)$$

$$(\vec{v}_{s*} \cdot \nabla_*) \vec{v}_{s*} + \frac{\partial \vec{v}_{s*}}{\partial t_*} = \Omega_{p0} t_0 \frac{c}{c_A} \frac{e_{s*}}{m_{s*}} \vec{E}_* + \Omega_{p0} t_0 \frac{e_{s*}}{m_{s*}} \vec{v}_{s*}(\vec{x}, t) \times \vec{B}_*(\vec{x}, t) \quad (2.35)$$

where $\nabla_* = \left(\frac{\partial}{\partial x_*}, \frac{\partial}{\partial y_*}, \frac{\partial}{\partial z_*} \right)$ is the gradient operation in dimensionless spatial

variables.

Now define the constants $f_1 \equiv \frac{c_A}{c}$, $f_2 \equiv \Omega_p t_0$, $f_3 \equiv \omega_p t_0$. We use the

freedom to pick the time scale t_0 such that $f_2 = 1$. They are pure numbers that

will characterize the physical regime we are working in. For simplicity we

now drop all the *'s in the above equations. This gives:

$$\nabla \times \vec{B} = f_1^2 f_3^2 \sum_s n_s e_s \vec{v}_s + f_1 \frac{\partial \vec{E}}{\partial t} \quad (2.36)$$

$$\nabla \times \vec{E} = -f_1 \frac{\partial \vec{B}}{\partial t} \quad (2.37)$$

$$\nabla \cdot \vec{E} = f_1 f_3^2 \sum_s e_s n_s \quad (2.38)$$

$$\nabla \cdot \vec{B} = 0 \quad (2.39)$$

$$\frac{\partial n_s(\vec{x}, t)}{\partial t} + \nabla \cdot (n_s(\vec{x}, t) \vec{v}_s) = 0 \quad (2.40)$$

$$(\vec{v}_s(\vec{x}, t) \cdot \nabla) \vec{v}_s(\vec{x}, t) + \frac{\partial \vec{v}_s(\vec{x}, t)}{\partial t} = \frac{1}{f_1} \frac{e_s}{m_s} \vec{E}(\vec{x}, t) + \frac{e_s}{m_s} \vec{v}_s(\vec{x}, t) \times \vec{B}(\vec{x}, t) \quad (2.41)$$

Equations (2.36) – (2.41) are the nondimensionalized version of the six

fundamental equations for the system. We still have 18 unknowns.

2.4 Linearization

We now linearize the cold plasma equations about a static background in order to study the dynamics of small-amplitude waves. Following the standard approach, all the dependent variables for each plasma species s , $n_s, \vec{v}_s(\vec{x}, t), \vec{E}(\vec{x}, t), \vec{B}(\vec{x}, t)$ are assumed to have a static zeroth-order term with a first-order small perturbation term. The static background will be allowed to have a nonuniform spatial dependence. The zeroth-order magnetic field is assumed to be non-zero. We assume it points everywhere in the same direction, for simplicity, and we take its direction as our z -direction. The field strength is allowed to depend on x : $\vec{B}^0 = B^0(\vec{x})\hat{z}$.

The zeroth-order velocity fields are assumed to be zero: $\vec{v}^0(\vec{x}, t) = 0$.

The zeroth-order electric field has to be zero; otherwise it would conflict with the assumed static unperturbed state of the particles: $\vec{E}^0(\vec{x}, t) = 0$.

From these assumptions, we have

$$\begin{aligned}
 \vec{v}_s(\vec{x}, t) &= \vec{v}_s^1(\vec{x}, t) \\
 \vec{E}(\vec{x}, t) &= \vec{E}^1(\vec{x}, t) \\
 \vec{B}(\vec{x}, t) &= B^0(\vec{x})\hat{z} + \vec{B}^1(\vec{x}, t) \\
 n_s(\vec{x}, t) &= n_s^0(\vec{x}) + n_s^1(\vec{x}, t)
 \end{aligned}
 \tag{2.42}$$

Where the superscript 0 represents the zero-order term and 1 represents the first-order term and s represents different particle species. Also, for the

unperturbed state, the total charge has to be neutral, so we set $\sum_s e_s n_s^0 = 0$ and

the undisturbed density is assumed to be homogeneous in space and constant in time, so n_s^0 is a constant.

After inserting the definitions of the zeroth- and first-order terms of (2.42) into equations (2.36) – (2.41), and keeping only the resulting first-order equations, we find the following *linear* system of evolution equations:

$$\nabla \times \bar{B}^1(\bar{x}, t) = f_1^2 f_3^2 \sum_s n_s^0 e_s \bar{v}_s^1(\bar{x}, t) + f_1 \frac{\partial \bar{E}^1(\bar{x}, t)}{\partial t} \quad (2.43)$$

$$\nabla \times \bar{E}^1(\bar{x}, t) = -f_1 \frac{\partial \bar{B}^1(\bar{x}, t)}{\partial t} \quad (2.44)$$

$$\nabla \cdot \bar{E}^1(\bar{x}, t) = f_1 f_3^2 \sum_s n_s^1(\bar{x}, t) e_s \quad (2.45)$$

$$\nabla \cdot \bar{B}^1(\bar{x}, t) = 0 \quad (2.46)$$

$$\frac{\partial n_s^1(\bar{x}, t)}{\partial t} + \nabla \cdot (n_s^0 \bar{v}_s^1(\bar{x}, t)) = 0 \quad (2.47)$$

$$\frac{\partial \bar{v}_s^1(\bar{x}, t)}{\partial t} = \frac{1}{f_1} \frac{e_s}{m_s} \bar{E}^1(\bar{x}, t) + \frac{e_s}{m_s} \bar{v}_s^1(\bar{x}, t) \times B^0(\bar{x}) \hat{z} \quad (2.48)$$

This system of equations is the focus of our study in the next few chapters.

We will first consider the special case of uniform plasma in Chapter 3. Using standard Fourier methods we will identify the important features of the various modes supported by the plasma in this case. In Chapter 4 we consider the effects of nonuniformity and find that – away from resonances – WKB methods can be used, provided the background variation is on a longer spatial scale than the wavelength of the waves. Then, in Chapter 5 we move to the central topic of this thesis: how to connect the incoming and outgoing WKB solutions across the resonance layer using modular methods developed by

Kaufman and co-workers. In Chapter 6 we then perform a direct comparison of numerical simulations and various methods of approximation.

Chapter 3

Waves in uniform plasma

We introduced the six differential equations that govern the Deuterium-Hydrogen-Electron plasma system in the Chapter 2. In Section 2.4 we linearized the electric field about a zero background, and the magnetic field about a constant zeroth-order term with a first-order small perturbation term $\vec{B}(\vec{x}, t) = B^0(\vec{x})\hat{z} + \vec{B}^1(\vec{x}, t)$. In this chapter, we make a further assumption: the zeroth-order magnetic field is not only constant in time but also homogenous in space. Again, we take the zeroth-order magnetic field direction as the z-direction:

$$\vec{B}^0 = B^0\hat{z} \quad (3.1)$$

where B^0 , the magnitude of the unperturbed magnetic field.

The six linearized partial differential equations are:

$$\nabla \times \vec{B}^1(\vec{x}, t) = f_1^2 f_3^2 \sum_s n_s^0 e_s \vec{v}_s^1(\vec{x}, t) + f_1 \frac{\partial \vec{E}^1(\vec{x}, t)}{\partial t} \quad (3.2)$$

$$\nabla \times \vec{E}^1(\vec{x}, t) = -f_1 \frac{\partial \vec{B}^1(\vec{x}, t)}{\partial t} \quad (3.3)$$

$$\nabla \cdot \vec{E}^1(\vec{x}, t) = f_1 f_3^2 \sum_s n_s^1(\vec{x}, t) e_s \quad (3.4)$$

$$\nabla \cdot \vec{B}^1(\vec{x}, t) = 0 \quad (3.5)$$

$$\frac{\partial n_s^1(\vec{x}, t)}{\partial t} + \nabla \cdot (n_s^0 \vec{v}_s^1(\vec{x}, t)) = 0 \quad (3.6)$$

$$\frac{\partial \bar{v}_s^1(\bar{x}, t)}{\partial t} = \frac{1}{f_1} \frac{e_s}{m_s} \bar{E}^1(\bar{x}, t) + \frac{e_s}{m_s} \bar{v}_s^1(\bar{x}, t) \times \mathbf{B}^0(\bar{x}) \hat{z} \quad (3.7)$$

Where the superscript 0 represents the zero-order term, 1 represents the first-order term, and s represents different particle species.

3.1 Fourier transformation

Because the coefficients of this system of PDEs are constant, we know the solutions can be found as superposition of exponentials. Any function $g(\bar{x}, t)$ can be represented by a Fourier integral of the form:

$$g(\bar{x}, t) = \frac{1}{2\pi} \int_{-\infty}^{\infty} \tilde{g}(\vec{k}, \omega) e^{i(\vec{k} \cdot \bar{x} - \omega t)} d^3 k d\omega \quad (3.8)$$

Where $\tilde{g}(\vec{k}, \omega)$ is the Fourier transform of the function $g(\bar{x}, t)$. By converting the system of PDEs into a system of algebraic equations, the Fourier transform makes the linear differential equations easier to solve. From the Fourier transform, it is easy to derive the following relations:

$$\begin{aligned} \frac{\partial g}{\partial t} &= \frac{1}{(2\pi)^2} \int_{-\infty}^{\infty} (-i\omega \tilde{g}) e^{i(\vec{k} \cdot \bar{x} - \omega t)} d^3 k d\omega \\ \nabla g &= \frac{1}{(2\pi)^2} \int_{-\infty}^{\infty} (i\vec{k} \tilde{g}) e^{i(\vec{k} \cdot \bar{x} - \omega t)} d^3 k d\omega \end{aligned} \quad (3.9)$$

Therefore, we have the following familiar correspondences between operators in (x, t) space and multiplication by numbers in (k, ω) space:

$$\omega \rightarrow i \frac{\partial}{\partial t}, \quad \vec{k} \rightarrow -i \nabla \quad (3.10)$$

Fourier transforming the equations (3.2) – (3.7), we get:

$$i\vec{k} \times \vec{\tilde{B}}^1(\vec{k}, \omega) = f_1^2 f_3^2 \sum_s n_s^0 e_s \tilde{v}_s^1(\vec{k}, \omega) + f_1(-i\omega) \vec{\tilde{E}}^1(\vec{k}, \omega) \quad (3.11)$$

$$i\vec{k} \times \vec{\tilde{E}}^1(\vec{k}, \omega) = i\omega f_1 \vec{\tilde{B}}^1(\vec{k}, \omega) \quad (3.12)$$

$$i\vec{k} \cdot \vec{\tilde{E}}^1(\vec{k}, \omega) = f_1 f_3^2 \sum_s e_s n_s^1(\vec{k}, \omega) \quad (3.13)$$

$$i\vec{k} \cdot \vec{\tilde{B}}^1(\vec{k}, \omega) = 0 \quad (3.14)$$

$$-i\omega \vec{n}_s^1(\vec{k}, \omega) + i\vec{k} \cdot (n_s^0 \vec{\tilde{v}}_s^1(\vec{k}, \omega)) = 0 \quad (3.15)$$

Fourier transforming equation (3.7) and expressing the result in x, y, z components:

$$\begin{aligned} -i\omega \tilde{v}_{sx}^1(\vec{k}, \omega) &= \frac{1}{f_1} \frac{e_s}{m_s} \tilde{E}_x^1(\vec{k}, \omega) + \frac{e_s B^0}{m_s} \tilde{v}_{sy}^1(\vec{k}, \omega) \\ -i\omega \tilde{v}_{sy}^1(\vec{k}, \omega) &= \frac{1}{f_1} \frac{e_s}{m_s} \tilde{E}_y^1(\vec{k}, \omega) - \frac{e_s B^0}{m_s} \tilde{v}_{sx}^1(\vec{k}, \omega) \\ -i\omega \tilde{v}_{sz}^1(\vec{k}, \omega) &= \frac{1}{f_1} \frac{e_s}{m_s} \tilde{E}_z^1(\vec{k}, \omega) \end{aligned} \quad (3.16)$$

Where the “ \sim ” represents the Fourier transform of its original function.

3.1.1 Wave packets

When we Fourier transformed the equations, we assumed the solution is a superposition of plane waves. Let's consider a more general wave function such as a wavepacket, which will be used for our numerical comparisons. First, let's treat a simple scalar wave equation of the form: $D(-i\partial_x, i\partial_t)\psi(x, t) = 0$. If the wave packet has a well-defined carrier wave number k_0 , it is useful to write the solution for $\psi(x, t)$ as:

$$\psi(x, t) = e^{i(k_0 x - \omega_0 t)} \phi(x, t).$$

ω_0 is where $D(k_0, \omega_0) = 0$. Insert this ansatz into the wave equation,

$$\begin{aligned} D(-i\partial_x, i\partial_t)\psi(x, t) &= D(-i\partial_x, i\partial_t)e^{i(k_0x - \omega_0t)}\phi(x, t) \\ &= e^{i(k_0x - \omega_0t)}D(k_0 - i\partial_x, \omega_0 + i\partial_t)\phi(x, t) = 0 \end{aligned}$$

Expand $D(k_0 - i\partial_x, \omega_0 + i\partial_t)$ in Taylor series around ω_0, k_0 and keep only the first order:

$$\begin{aligned} D(k_0 - i\partial_x, \omega_0 + i\partial_t)\phi(x, t) &\approx \left[D(k_0, \omega_0) - i \left. \frac{\partial D}{\partial k} \right|_{k_0, \omega_0} \partial_x + i \left. \frac{\partial D}{\partial \omega} \right|_{k_0, \omega_0} \partial_t \right] \phi(x, t) = 0 \\ D(k_0, \omega_0) = 0 &\Rightarrow \left[\left. \frac{\partial D}{\partial \omega} \right|_{k_0, \omega_0} \partial_t - \left. \frac{\partial D}{\partial k} \right|_{k_0, \omega_0} \partial_x \right] \phi(x, t) = 0 \\ &\Rightarrow \left[\partial_t - \frac{\left. \frac{\partial D}{\partial k} \right|_{k_0, \omega_0}}{\left. \frac{\partial D}{\partial \omega} \right|_{k_0, \omega_0}} \partial_x \right] \phi(x, t) = 0 \end{aligned}$$

This gives the group velocity, the velocity of the propagation of the envelope

of the wave packet definition: $v_g = - \left. \frac{\partial D / \partial k}{\partial D / \partial \omega} \right|_{k_0, \omega_0} = \frac{\partial \omega}{\partial k}$. This is also the speed

at which the energy propagates. The phase velocity, which is the speed at

which the phase fronts move, is $v_p = \frac{\omega_0}{k_0}$. We derived here the group velocity

and phase velocity for the uniform case and they do not depend on x -space.

For the nonuniform case we will discuss in Chapter 4, the phase and group

velocities are no longer constant. The wave packet's energy propagation

depends on the local group velocity and the carrier oscillation wave fronts

propagate according to the local phase velocity.

Consider now a more general situation where more than one mode is present. When the phase velocities for different modes are equal, there occur mode conversions. These are points where the local (in x) wavenumbers and frequencies of the two modes are equal.

After the Fourier transformation, traditionally all of the unknowns are eliminated in favor of the electric field. As we shall see in the next section this leads to resonant denominators at certain frequencies. By contrast, the method proposed by Kaufman and Ye retains the velocity field for the resonant species. This makes the problem look much more like a standard avoided crossing or mode conversion. We will find this approach more appropriate to study resonance crossing in nonuniform plasmas,

3.2 Traditional method

The results in this section are well known and are included here for completeness. Readers already familiar with the topic of RF waves can skip ahead. In Chapter 2, we introduced the fact that there are 18 variables $(\vec{E}(\vec{x},t), \vec{B}(\vec{x},t), n_s(\vec{x},t), \vec{v}_s(\vec{x},t))$ of the Deuterium-Hydrogen-Electron plasma system whose dynamics are governed by and Maxwell equations and mass and momentum conservation equations. A traditional way to solve this system is to write all other variables in favor of electric field $\vec{E}(\vec{x},t)$. After we get the solution for the electric field, we can use the Maxwell's equations and mass and momentum conservation equations to solve for the other variables.

We can define the gyrofrequency, which is also called cyclotron

frequency $\Omega_s = \frac{e_s B_0}{m_s}$ for each particle species s and rewrite equation (3.16)

into a matrix form:

$$\begin{pmatrix} -i\omega & -\Omega_s & 0 \\ \Omega_s & -i\omega & 0 \\ 0 & 0 & -i\omega \end{pmatrix} \begin{pmatrix} \tilde{v}_{sx} \\ \tilde{v}_{sy} \\ \tilde{v}_{sz} \end{pmatrix} = \frac{1}{f_1} \frac{e_s}{m_s} \begin{pmatrix} \tilde{E}_x \\ \tilde{E}_y \\ \tilde{E}_z \end{pmatrix} \quad (3.17)$$

Here all the superscripts l representing the first-order terms have been dropped for simplicity. Inverting the matrix and solving for the velocity function in terms of the electric field gives:

$$\begin{pmatrix} \tilde{v}_{sx} \\ \tilde{v}_{sy} \\ \tilde{v}_{sz} \end{pmatrix} = \frac{1}{f_1} \frac{e_s}{m_s} \begin{pmatrix} \frac{-i\omega}{\Omega_s^2 - \omega^2} & \frac{\Omega_s}{\Omega_s^2 - \omega^2} & 0 \\ \frac{\Omega_s}{\Omega_s^2 - \omega^2} & \frac{-i\omega}{\Omega_s^2 - \omega^2} & 0 \\ 0 & 0 & \frac{i}{\omega} \end{pmatrix} \begin{pmatrix} \tilde{E}_x \\ \tilde{E}_y \\ \tilde{E}_z \end{pmatrix} \quad (3.18)$$

Combining the equations (3.18) and (3.11), we obtain:

$$i\vec{k} \times \vec{\tilde{B}} = f_1^2 f_3^2 \sum_s n_s^0 e_s \tilde{v}_s + (-i\omega) \vec{\tilde{E}} f_1 = -i\omega \left(\vec{I} - \frac{\vec{\sigma}}{i\omega f_1} \right) \vec{\tilde{E}} f_1 \quad (3.19)$$

Where \vec{I} is the identity matrix and the matrix $\vec{\sigma}$ is defined as:

$$\begin{aligned}
\vec{\sigma} &\equiv \sum_s \frac{n_s^0 e_s^2}{m_s} f_1 f_3^2 \begin{pmatrix} \frac{-i\omega}{\Omega_s^2 - \omega^2} & \frac{\Omega_s}{\Omega_s^2 - \omega^2} & 0 \\ \frac{\Omega_s}{\Omega_s^2 - \omega^2} & \frac{-i\omega}{\Omega_s^2 - \omega^2} & 0 \\ 0 & 0 & \frac{i}{\omega} \end{pmatrix} \\
&= \sum_s \omega_{ps}^2 f_1 \begin{pmatrix} \frac{-i\omega}{\Omega_s^2 - \omega^2} & \frac{\Omega_s}{\Omega_s^2 - \omega^2} & 0 \\ \frac{\Omega_s}{\Omega_s^2 - \omega^2} & \frac{-i\omega}{\Omega_s^2 - \omega^2} & 0 \\ 0 & 0 & \frac{i}{\omega} \end{pmatrix}
\end{aligned} \tag{3.20}$$

with the definition of the plasma frequency for each plasma species

$$\omega_{ps}^2 \equiv \frac{n_s^0 e_s^2}{m_s} f_3^2 \text{ and the plasma frequency for the system is defined}$$

$$\omega_p^2 \equiv \sum_s \omega_{ps}^2.$$

Multiply both sides of equation (3.12) from the left by \vec{k} using the cross product and substitute for $\vec{k} \times \vec{B}$ using equation (3.19) yielding:

$$\vec{k} \times (i\vec{k} \times \vec{E}) = i\omega(\vec{k} \times \vec{B})f_1 = -i\omega^2(\vec{I} - \frac{\vec{\sigma}}{i\omega f_1})\vec{E}f_1^2 \tag{3.21}$$

Rearranging and using the definition of the index of refraction

$$\vec{N} \equiv \frac{\vec{k}}{f_1 \omega} :$$

$$\vec{N} \times (\vec{N} \times \vec{E}) + (\vec{I} - \frac{\vec{\sigma}}{i\omega f_1})\vec{E} = 0 \tag{3.22}$$

Recall that we defined the z-direction to lie along the zeroth-order magnetic field. We still have freedom to choose our x-y direction. Choose the x-y

direction such that the \bar{N} -direction lies in the x - z plane at an angle θ to the z -direction $\bar{N} = (N \sin \theta, 0, N \cos \theta)$.

Figure 3.1 illustrates the coordinates of the wave propagation direction of uniform magnetized cold plasma.

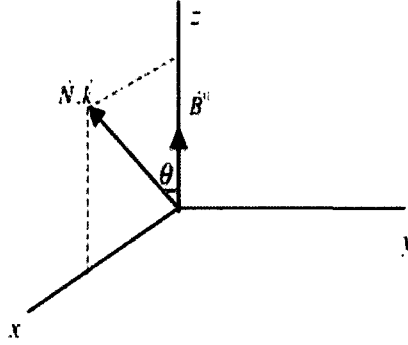


FIGURE 3.1 THE COORDINATE SYSTEM IN THE WAVE PROPAGATION OF THE UNIFORM MAGNETIC UNPERTURBED PLASMA

Expanding equation (3.22) in matrix form yields:

$$\begin{pmatrix} S - N^2 \cos^2 \theta & -iD & N^2 \sin \theta \cos \theta \\ iD & S - N^2 & 0 \\ N^2 \sin \theta \cos \theta & 0 & P - N^2 \sin^2 \theta \end{pmatrix} \begin{pmatrix} \tilde{E}_x \\ \tilde{E}_y \\ \tilde{E}_z \end{pmatrix} = 0 \quad (3.23)$$

Where, following Stix's notation [28], we define

$$S \equiv 1 - \sum_s \frac{\omega_{ps}^2}{(\omega^2 - \Omega_s^2)}, \quad D \equiv \sum_s \frac{\omega_{ps}^2 \Omega_s}{\omega(\omega^2 - \Omega_s^2)}, \quad P \equiv 1 - \sum_s \frac{\omega_{ps}^2}{\omega^2} = 1 - \frac{\omega_p^2}{\omega^2}.$$

It is also useful to introduce Stix's R and L functions, which separate out the left- and right-circular resonance behaviors. These functions are defined as:

$$R \equiv 1 - \sum_s \frac{\omega_{ps}^2}{\omega(\omega + \Omega_s)}, \quad L \equiv 1 - \sum_s \frac{\omega_{ps}^2}{\omega(\omega - \Omega_s)}$$

Note that $S = \frac{R+L}{2}$, $D = \frac{R-L}{2}$.

Equation (3.23) is a matrix equation of the form $\underline{\underline{D}}(\vec{k}, \omega) \cdot \vec{\tilde{E}}(\vec{k}, \omega) = 0$.

This can have a nontrivial solution for $\vec{\tilde{E}}(\vec{k}, \omega)$ if and only if

$\det(\underline{\underline{D}}(\vec{k}, \omega)) = 0$. Let's take a moment to understand the geometrical meaning

of this condition. The matrix $\underline{\underline{D}}(\vec{k}, \omega)$ is a function of \vec{k} (which has three

components) and ω . Therefore, consider the function $\det(\underline{\underline{D}}(\vec{k}, \omega))$ on the

four-dimensional space (\vec{k}, ω) . The condition $\det(\underline{\underline{D}}(\vec{k}, \omega)) = 0$ forces a single

scalar relation among the four variables, hence it defines a three-dimensional

surface which we call the *dispersion manifold*. This surface might have

multiple sheets, but each sheet is locally smooth at most points. We have

found this manner of visualizing the dispersion surface to be useful because it

generalizes straightforwardly to the nonuniform case (by expanding the size of

the space to include \vec{x}).

Traditionally, however, Equation (3.23) is viewed as a condition on N

and θ . The $\det(\underline{\underline{D}}(\vec{k}, \omega)) = 0$ condition becomes a sixth-order polynomial

(more precisely, a cubic in N^2) for the magnitude of N , with θ -dependent

and ω -dependent coefficients. Note the resonant denominators in R and L .

To better understand the problem, we will examine a special case

where the wave propagates perpendicular to the magnetic field: $\theta = \frac{\pi}{2}$.

Equation (3.23) reduces to:

$$\begin{pmatrix} S & -iD & 0 \\ iD & S - N^2 & 0 \\ 0 & 0 & P - N^2 \end{pmatrix} \begin{pmatrix} \tilde{E}_x \\ \tilde{E}_y \\ \tilde{E}_z \end{pmatrix} = 0 \quad (3.24)$$

For the nontrivial electric field solution, the determinant of the matrix

$$\text{has to be zero: } \det \begin{pmatrix} S & -iD & 0 \\ iD & S - N^2 & 0 \\ 0 & 0 & P - N^2 \end{pmatrix} = 0, \text{ which gives two eigenvalues}$$

for N^2 .

(1) The first eigenvalue with its corresponding eigenvector is

$$\begin{aligned} N^2 &= P \\ \tilde{\vec{E}} &= (0, 0, E_0) \end{aligned} \quad (3.25)$$

This is called ordinary mode because the undisturbed magnetic field has no effect on the particle motion. From equation (3.18), we get

$$\tilde{\vec{v}}_s = \left(0, 0, \frac{1}{f_1} \frac{iE_0}{\omega} \frac{e_s}{m_s} \right), \text{ so } \tilde{\vec{v}}_s \times \vec{B}^0 = 0, \text{ the Lorentz force (3.16) reduces to a}$$

simpler version $-i\omega \tilde{\vec{v}}_s(\vec{k}, \omega) = \frac{1}{f_1} \frac{e_s}{m_s} \tilde{\vec{E}}(\vec{k}, \omega)$. Figure 3.2 illustrates the

directions of the induced electric and magnetic fields, $\tilde{\vec{E}}_z$ and $\tilde{\vec{B}}_y$ are the

induced electric field and magnetic field.

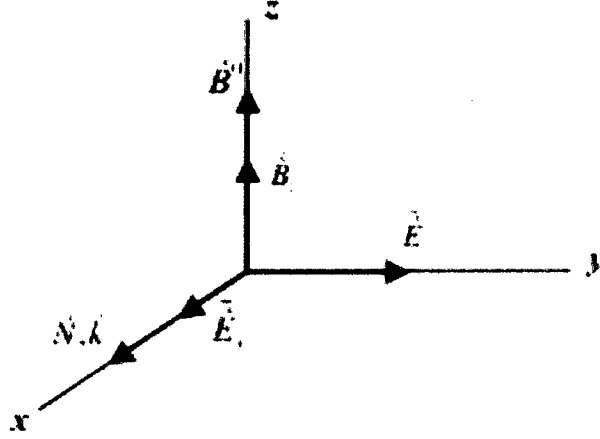


FIGURE 3.2 THE DIRECTIONS OF INDUCED ELECTRIC AND MAGNETIC FIELDS

From the definition of P and N , we will have

$$P = 1 - \frac{\omega_p^2}{\omega^2} = N^2 = \frac{|\vec{k}|^2}{f_1^2 \omega^2}. \text{ Rearrange the equation, we will get the dispersion}$$

relation: $\omega^2 = \frac{|\vec{k}|^2}{f_1^2} + \omega_p^2$. This result that does not carry units because of the

nondimensionlization we performed in Chapter 2.3. To better understand the

physics, we reintroduce units. Multiplying by frequency units on both sides:

$$\begin{aligned} \omega_*^2 \frac{1}{t_0^2} &= \frac{|\vec{k}_*|^2}{f_1^2} \frac{1}{t_0^2} + \omega_{p*}^2 \frac{1}{t_0^2} \\ \Rightarrow \omega^2 &= c^2 \frac{|\vec{k}_*|^2}{c_A^2 t_0^2} + \omega_p^2 = c^2 \frac{|\vec{k}_*|^2}{x_0^2} + \omega_p^2 = c^2 |\vec{k}|^2 + \omega_p^2 \end{aligned} \quad (3.26)$$

where all the * terms represent the dimensionless terms and the notations

subscribed with 0 represent reference values. Also we used the relation

introduced in Chapter 2.3 that $f_1 \equiv \frac{c_A}{c}$, $x_0 = c_A t_0$. Equation (3.26) is the

familiar dispersion relation for electromagnetic waves in a plasma.

It is interesting to note in passing that, after multiplying by \hbar (Planck's constant divided by 2π) on both sides of equation (3.26), we get:

$$\hbar^2 \omega^2 = c^2 p^2 + \hbar^2 \omega_p^2 \quad (3.27),$$

with the definition of momentum $p^2 \equiv \hbar^2 |\vec{k}|^2$. This looks very similar to the

Klein-Gordon equation [29] for a free particle with the mass-energy

$\varepsilon^2 \equiv \hbar^2 \omega^2 = c^2 p^2 + m^2 c^4$. Comparing this mass-energy relationship for

relativistic massive particles with equation (3.27), the plasma frequency for the system plays a role of mass, although it is purely classical effect.

Figure 3.3 shows positive ω branch of the dispersion relation of this mode. It illustrates that as ω and k increases, it asymptotes to the straight lines $\omega = \pm k / f_1$. And there do not exist waves with real ω below the plasma frequency ω_p .

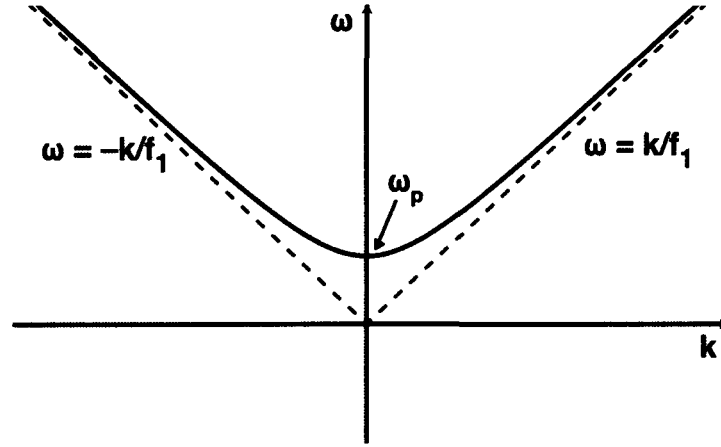


FIGURE 3.3 THE DISPERSION RELATION FOR ORDINARY MODE.

Solving the dispersion relation, it will give the wave number value

$\vec{k} = \pm f_1 \sqrt{\omega^2 - \omega_p^2} \hat{x}$ for propagation in the x-direction. The group velocity is

defined as $\vec{v}_g = \frac{\partial \omega}{\partial \vec{k}} = \pm \frac{1}{f_1} \sqrt{1 - \frac{f_1^2 \omega_p^2}{k^2 + f_1^2 \omega_p^2}} \hat{x}$.

In the wave packet, different plane waves move at different phase velocities.

The phase velocity is defined as $\vec{v}_p = \frac{\omega}{|\vec{k}|} \hat{k} = \pm \sqrt{\frac{1}{f_1^2} + \frac{\omega_p^2}{k^2}} \hat{x}$ for propagation

in the x-direction.

Figure 3.4 shows the positive branch of group velocity and phase velocity. At the plasma frequency, the group velocity at which speed energy propagates will go to zero and the phase velocity is infinite. As ω increases, these two velocities asymptotically approach one another.

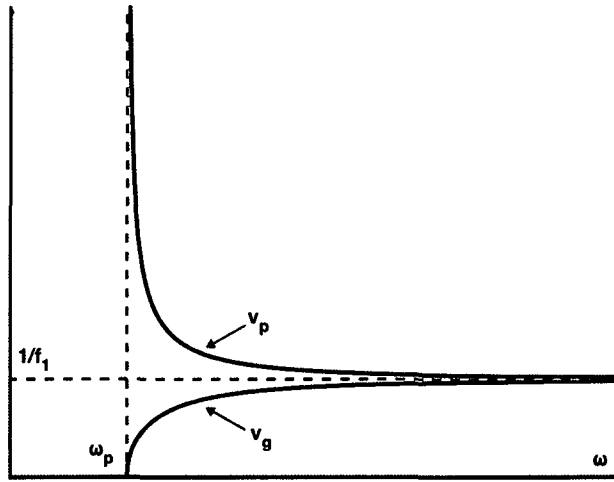


FIGURE 3.4 THE POSITIVE BRANCH OF THE GROUP VELOCITY AND PHASE VELOCITY FOR THE ORDINARY MODE

(2) The second eigenvalue and its corresponding eigenvector is:

$$N^2 = \frac{RL}{S} \quad (3.28)$$

$$\tilde{\vec{E}} = \left(\frac{iD}{\sqrt{R^2 + L^2}} E_0, \frac{S}{\sqrt{R^2 + L^2}} E_0, 0 \right)$$

This is called the extraordinary mode and it has a more complicated behavior than the previous ordinary mode. The electric field has components both parallel and perpendicular to \vec{k} . We will discuss the phase and group velocities, and the polarization, momentarily.

After we get the solutions for the electric field, we can use Maxwell's equations, the mass conservation equation and the momentum equation to solve all of the other fifteen dependent variables $\tilde{\vec{B}}^1, \tilde{\vec{v}}^1, \tilde{\vec{n}}_s^1$.

Figure 3. illustrates the orientation of the induced electric and magnetic fields for this root.

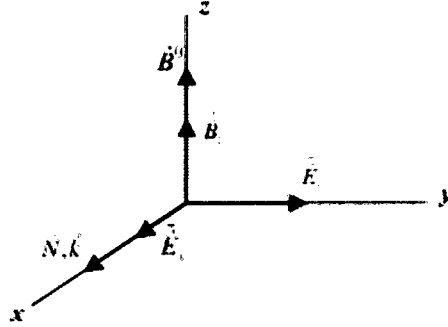


FIGURE 3.5 THE DIRECTION OF THE INDUCED ELECTRIC FIELD AND MAGNETIC FIELD FOR THE SECOND EIGENVALUE.

From the definition of S , there exist a few poles and zeros. The poles occur when the wave frequency equals the gyrofrequency of one of the particle species, and the zeros of S occur either where R or L equals zero. It is not generic for both R and L to go to zero together. We will examine the plots of R , L , S and N^2 in next section.

3.3 The resonances

In section 3.2 we showed when the wavevector is perpendicular to the unperturbed magnetic field, one of the eigenmodes is $N^2 = \frac{RL}{S}$. The index of refraction N^2 is zero when R or L is zero and infinite when S is zero. Recall the definition for R , L and S :

$$R \equiv 1 - \sum_s \frac{\omega_{ps}^2}{\omega(\omega + \Omega_s)}, \quad L \equiv 1 - \sum_s \frac{\omega_{ps}^2}{\omega(\omega - \Omega_s)}$$

$$\text{Note that } S \equiv \frac{R+L}{2} = 1 - \sum_s \frac{\omega_{ps}^2}{(\omega^2 - \Omega_s^2)}.$$

Next, we will discuss these functions in detail and use a Deuterium-Hydrogen-Electron plasma where the deuterium and hydrogen are both present at 50% of the number density as an example.

As the wave frequency ω goes to zero, R and L appear to diverge because ω appears in the denominator. However, a careful analysis shows the term $\frac{1}{\omega}$ is well behaved in the limit because of our assumption of charge neutrality. In that case, a little algebra shows that:

$$R = 1 - \frac{\left[\omega(\omega_{pH}^2 + \omega_{pD}^2 + \omega_{pe}^2) + \omega_{pH}^2(\Omega_D + \Omega_e) + \omega_{pD}^2(\Omega_H + \Omega_e) + \omega_{pe}^2(\Omega_D + \Omega_H) \right]}{(\omega + \Omega_H)(\omega + \Omega_D)(\omega + \Omega_e)}$$

$$L = 1 - \frac{\left[\omega(\omega_{pH}^2 + \omega_{pD}^2 + \omega_{pe}^2) - \omega_{pH}^2(\Omega_D + \Omega_e) - \omega_{pD}^2(\Omega_H + \Omega_e) - \omega_{pe}^2(\Omega_D + \Omega_H) \right]}{(\omega - \Omega_H)(\omega - \Omega_D)(\omega - \Omega_e)}$$

When ω is zero, R and L equal the same value, called the Alfvén index of refraction of index, N_A .

$$R|_{\omega=0} = L|_{\omega=0} = 1 - \frac{\left[\omega_{pH}^2(\Omega_D + \Omega_e) + \omega_{pD}^2(\Omega_H + \Omega_e) + \omega_{pe}^2(\Omega_D + \Omega_H) \right]}{\Omega_H \Omega_D \Omega_e} \equiv N_A.$$

Figure 3.6 showed the function R in the positive wave frequency region, where we concentrate on. Because the electron cyclotron frequency and the ion cyclotron frequencies are so far away apart

$$|\Omega_e| = \frac{m_H}{m_e} \Omega_H = 1836 \Omega_H, \text{ we will look at them separately. Figure 3.6 (a)}$$

focuses on the ion cyclotron frequency region while Figure 3.6 (b) focuses on the electron cyclotron frequency region.

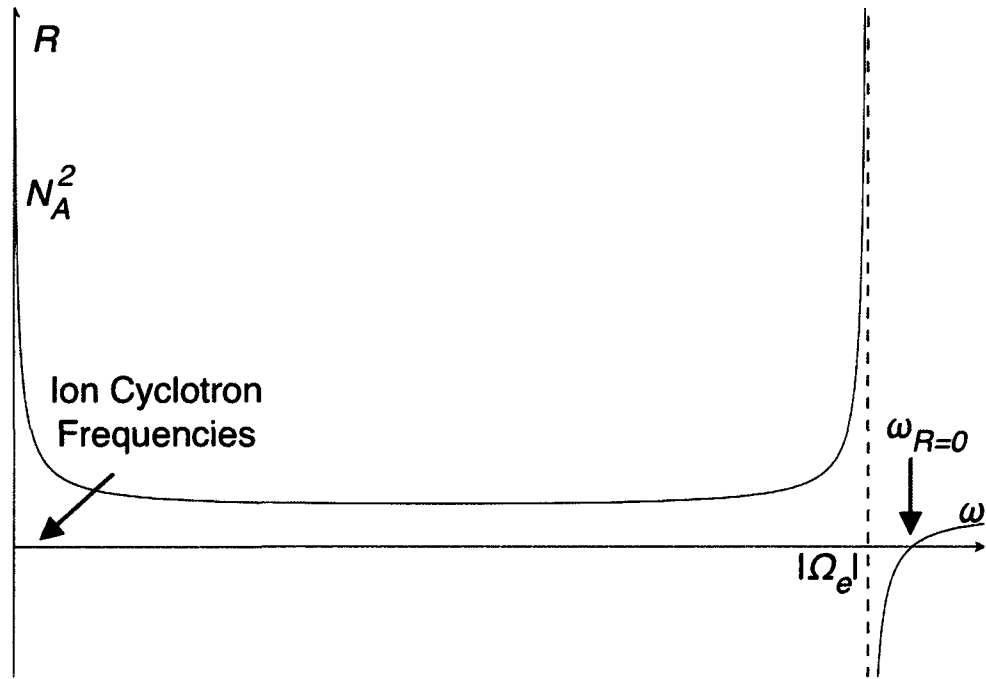


FIGURE 3.6 R AS A FUNCTION OF FREQUENCY IN THE POSITIVE FREQUENCY RANGE

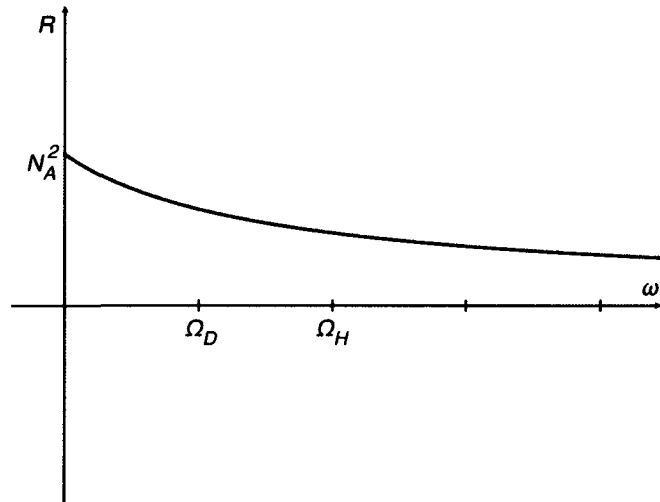


FIGURE 3.6 (A) FUNCTION R IN THE ION CYCLOTRON FREQUENCY REGION

Then we will focus on the absolute value of the electron frequency region.

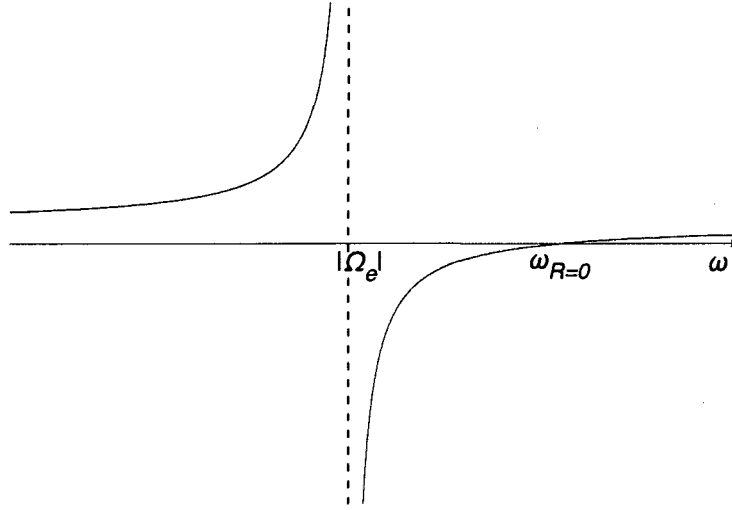


FIGURE 3.6 (B) FUNCTION R IN THE ELECTRON CYCLOTRON FREQUENCY REGION

When $\omega = \omega_{R=0}$, $R = 0$ and $N^2 = 0$ correspondingly. The condition when N^2 goes to zero is called a *cutoff*. Recall that N^2 is a smooth function of ω , therefore there will be frequencies in the vicinity of the cutoff where $N^2 < 0$, implying that waves of that frequency are evanescent, hence they are ‘cut off’ from propagating. We will see in the nonuniform case that cutoffs are associated with caustics where rays must turn back from nonpropagating regions.

In the present case there is only one root for $\omega_{R=0}$. The cutoff occurs at ω_R , bigger than the absolute value of electron cyclotron frequency, which is much higher than the ion cyclotron frequency. Therefore, at the cutoff of $\omega_{R=0}$, the ion motions can be neglected.

$$\omega \sim \omega_{R=0}, \quad R \approx 1 - \frac{\omega_{es}^2}{\omega(\omega + \Omega_e)}$$

Which gives the value of $\omega_{R=0} \approx \frac{|\Omega_e|}{2} + \sqrt{\left(\frac{\Omega_e}{2}\right)^2 + \omega_{pe}^2}$. When $\omega = |\Omega_e|$, R diverges. And when $\omega \rightarrow \infty$, $R \rightarrow 1$.

Figure 3.7 indicated the function L in the positive wave frequency region. Again, the ion and electron cyclotron frequencies are very well separated; Figure 3.7 (a) focuses on the ion cyclotron frequency region while Figure 3.7 (b) focuses on the electron cyclotron frequency region.

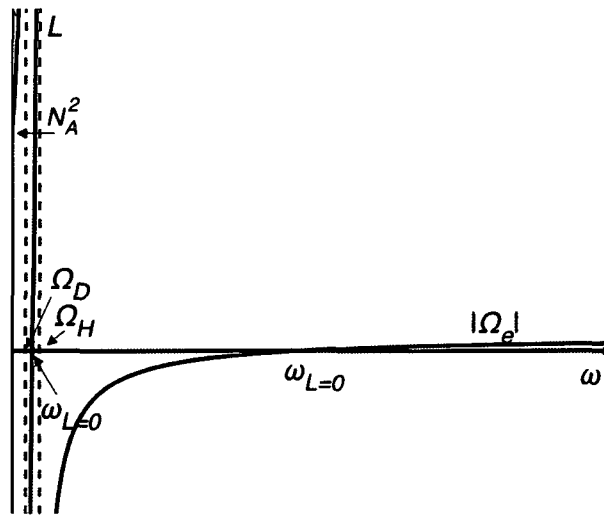


FIGURE 3.7 L AS A FUNCTION OF FREQUENCY OVER THE FULL RANGE

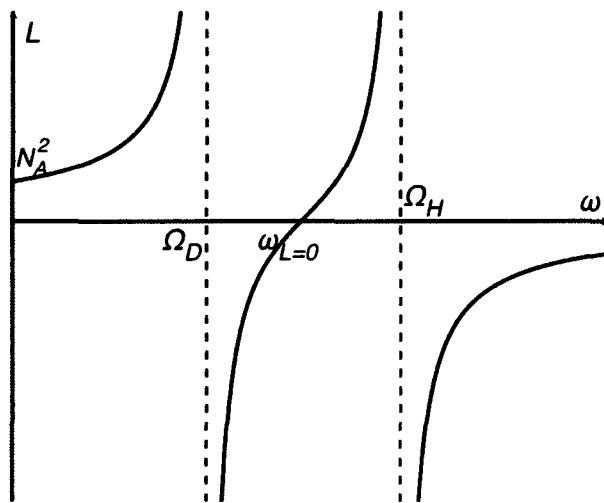


FIGURE 3.7 (A) FUNCTION L IN THE ION CYCLOTRON FREQUENCY REGION

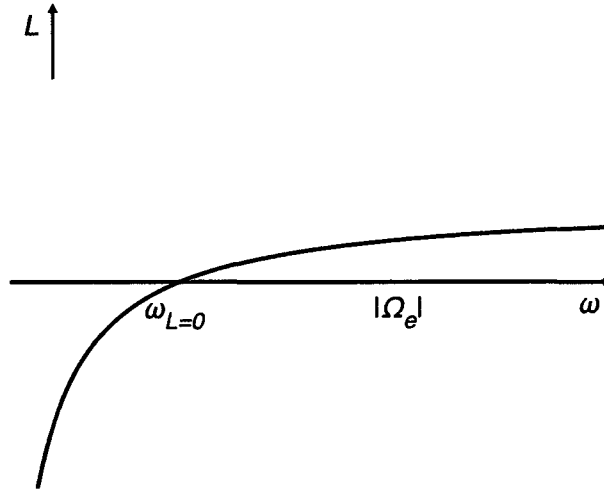


FIGURE 3.7 (B) FUNCTION L IN THE ELECTRON CYCLOTRON FREQUENCY REGION

There are two roots where $\omega = \omega_{L=0}$, which gives $L=0$, where we again have cutoffs where $N^2 = 0$. When $\omega \rightarrow \infty$, $L \rightarrow 1$, same as R does. The cutoff occurs at $\omega_{L=0}$, which can occur in the ion cyclotron range of frequencies.

At the ion cyclotron frequencies L blows up. R blows up at the electron cyclotron frequency. This is because positive ions gyrate so as to resonate with left-circular polarized waves, while electrons resonate with right-circular polarized waves. (Hence, the purpose of the L and R notation is now clear.). We will discuss these conditions more in detail later.

Function S is defined as $S = \frac{R+L}{2}$. Figure 3.8(a) shows S in the ion cyclotron frequency region while Figure 3.8 (b) shows S in the electron cyclotron frequency region.

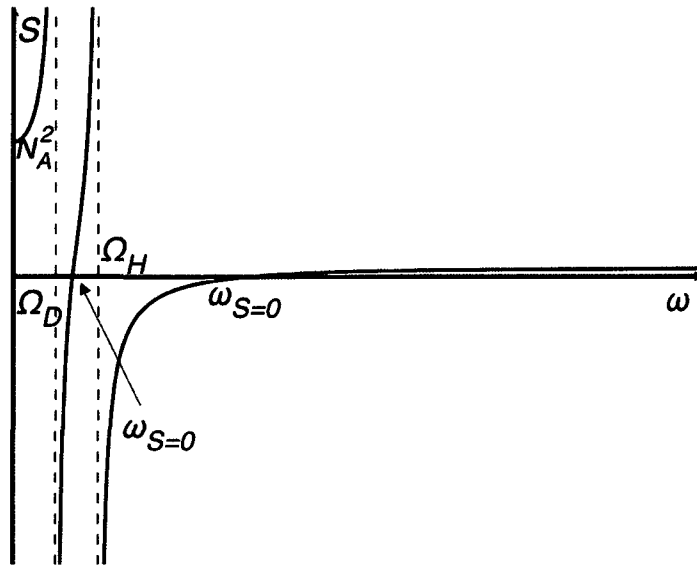


FIGURE 3.8 (A) FUNCTION S IN THE ION CYCLOTRON FREQUENCY REGION

Next we will focus on the absolute value of the electron cyclotron frequency region.

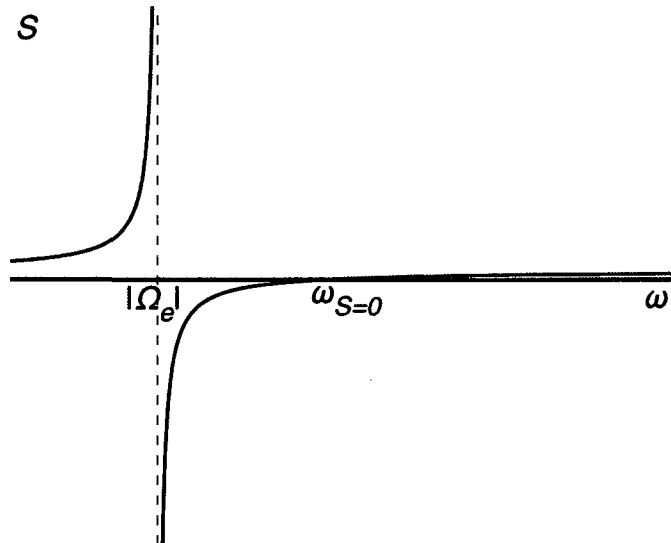


FIGURE 3.8 (B) FUNCTION S IN THE ELECTRON CYCLOTRON FREQUENCY REGION

When $\omega = \omega_{S=0}, S = 0, |\vec{N}|^2 = \frac{RL}{S} \rightarrow \infty$. The condition when the index

of refraction goes to infinity is called a *resonance*. Because this particular resonance involves both the Hydrogen and Deuterium ions in combination, it

is called the ion-ion *hybrid resonance*, or just the ‘ion-hybrid’ resonance. Each additional species in the plasma will result in one hybrid resonance. Also, S blows up at the ion cyclotron frequencies because L does, and it diverges at the electron cyclotron frequency because R does. Although functions R , L and S diverge in the ion and electron frequencies, the index of refraction (which involves the ratio RL/S) does not.

Figure 3.9(a) (b) and (c) show how the function N^2 behaves. There are three roots corresponding to $S=0$. For a clearer view, we will look at them one by one.

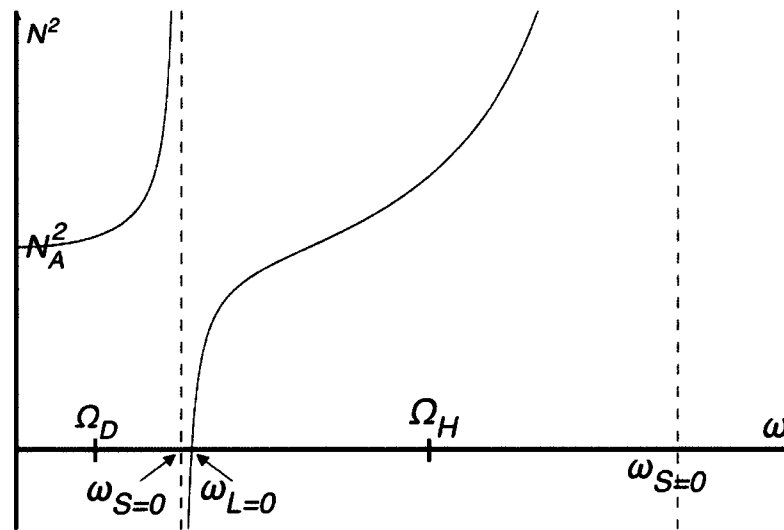


FIGURE 3.9 (A) FUNCTION N^2 IN THE FIRST $S=0$ ROOT REGION

When $\omega = 0$, the index of refraction equals to the Alfvén index of refraction. N^2 diverges at the first root where $\omega = \omega_{s=0}, S = 0$. This is the ion hybrid resonance. An ion hybrid resonance always lies between each adjacent pair of ion cyclotron frequencies and, in general, they must be numerically calculated.

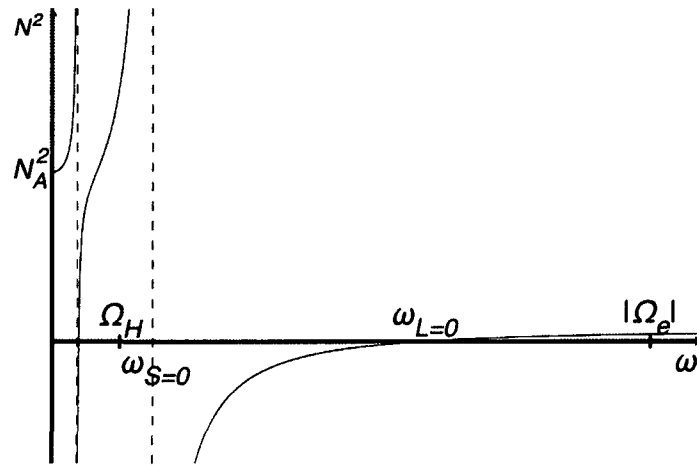


FIGURE 3.9 (B) FUNCTION N^2 IN THE SECOND $S=0$ ROOT REGION

Figure 3.9 (b) illustrates the second root of $S = 0$, where the hybrid resonance lies between the Hydrogen cyclotron frequency and the electron cyclotron frequency. This is called ‘lower hybrid’ resonance. The lower hybrid resonance is located between the highest ion cyclotron frequency and the electron gyrofrequency. For more cases with more than one ion species, the lower hybrid resonance usually cannot be calculated analytically but must be computed numerically.

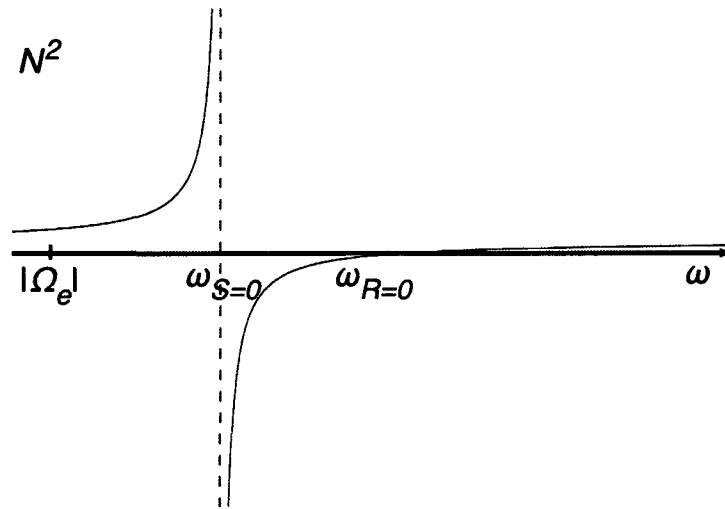


FIGURE 3.9 (C) FUNCTION N^2 IN THE THIRD $S=0$ ROOT REGION

Figure 3.9(c) shows the third root of $S = 0$ and this hybrid resonance is located at a frequency greater than the electron cyclotron frequency. This one is called the ‘upper hybrid’ resonance. The upper hybrid resonance is mainly due to the motion of electrons.

The above figures 3.4-3.9 are all shown to scale. As discussed, the plots span a very wide frequency range from the ion cyclotron frequency to the electron cyclotron frequency and above, so we have to show multiple figures in the different frequency regions for a clearer view. Next I want to show the figure not to the scale to give a better idea how the index of refraction changes as the frequency changes. Figure 3.10 shows the relations of S and N^2 for the Deuterium-Hydrogen-Electron plasma for deuterium and hydrogen are both 50% of the density. The main difference is that the upper hybrid resonance should be very far to the right.

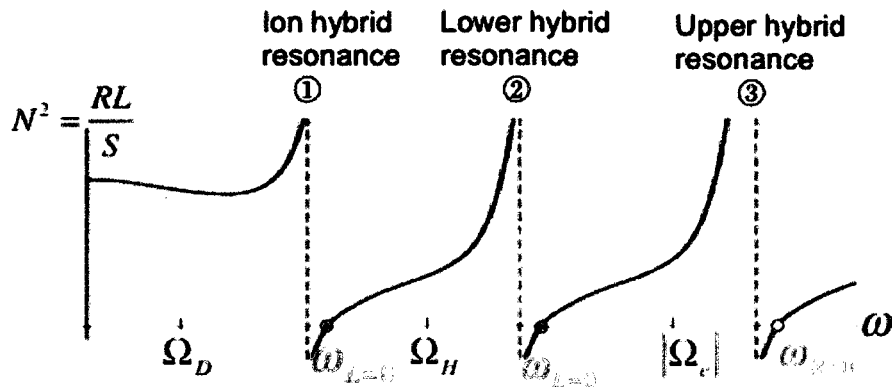


FIGURE 3.10 THE INDEX OF REFRACTION AS A FUNCTION OF FREQUENCY NOT TO SCALE FOR 50%DEUTERIUM AND 50%HYDROGEN.

At cutoffs, the index of refraction N^2 is zero. This occurs when R or L are zero. The index of refraction is infinite when S is zero, which occurs at resonances. For our Deuterium-Hydrogen-Electron plasma, there are two ion species and electrons, so there exist three resonances. The ① ② ③ dashed lines corresponding to three different roots when $S = 0$ are the ion hybrid resonances, lower hybrid resonances and upper hybrid resonances respectively. Cutoffs occur at ω_R , the root where $R=0$ and ω_L two roots where $L=0$. As we mentioned earlier, each species in the plasma will result in one hybrid resonance. If we change the density of the two ion species instead of 50% each, but 99% Deuterium with 1% Hydrogen and the plasma is still neutral.

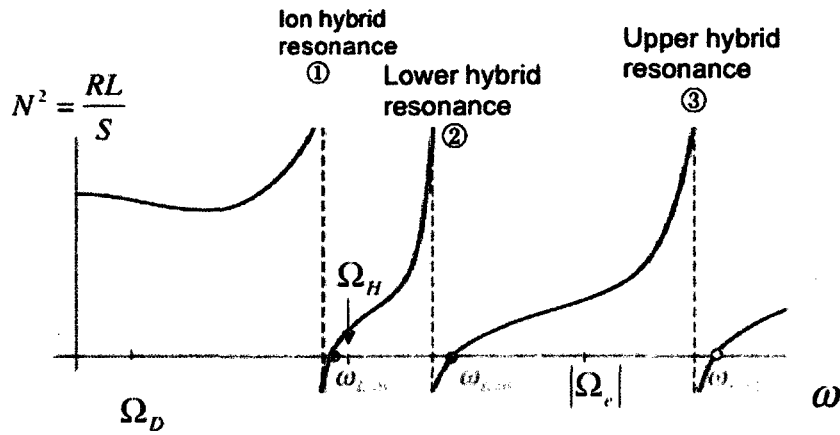


FIGURE 3.11 THE INDEX OF REFRACTION AS A FUNCTION OF FREQUENCY NOT TO SCALE FOR 99%DEUTERIUM AND 1%HYDROGEN

Compare Figure 3.10 and 3.11, the upper hybrid resonance is unchanged because it is dominated by the electron motions as discussed. The ion hybrid resonance and lower hybrid resonance move closer to each other. If we eliminate the Hydrogen from the system, only one ion and one electron species remain.

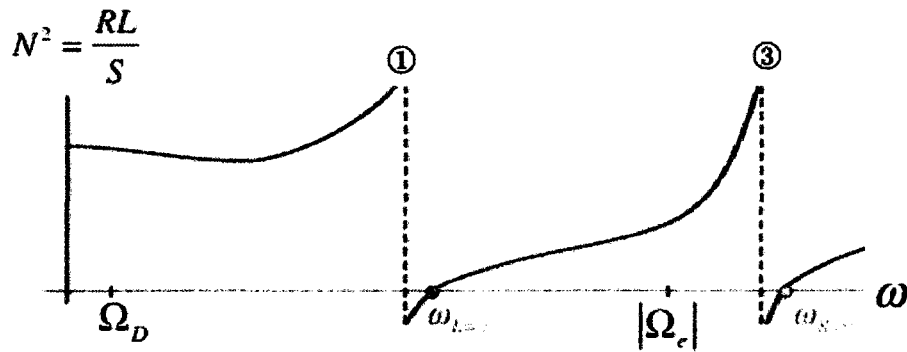


FIGURE 3.12 THE INDEX OF REFRACTION AS A FUNCTION OF FREQUENCY NOT TO SCALE FOR ONLY ONE SPECIES OF ION: DEUTERIUM

Figure 3.12 shows as there is only one ion species, there are no longer three hybrid resonances only two. One of the remaining resonances is the lower hybrid resonance; the other is the upper hybrid. This matches what we discussed earlier, each ion species results in one hybrid resonance. The hybrid resonance because of the electron motion is again unchanged in this limit.

3.4 The Kaufman & Ye model

Because the traditional methods eliminate all variables in terms of the electric field, they can obscure an important phenomenon: when a collective wave crosses a minority gyroresonance layer there is a disturbance that evolves in the velocity channel which carries energy and momentum [30] [31]. Following this disturbance in the velocity field becomes particularly useful when we want to understand resonance crossing in nonuniform plasma. For the uniform case, we simply note that by keeping the velocity field and electric field on an equal footing means we return to Equation (3.17) and keep nine variables (the velocities and the electric field).

In summary, following Kaufman and Ye, we eliminate all the variables in favor of the electric field, *and the particle velocities*. Because we are concerned with frequencies in the ion-cyclotron range, which is far from the electron cyclotron resonance frequency, we also eliminate the electron disturbance in terms of the ion velocity fields and the electric field. We used Equations (3.11) and (3.12) to eliminate the magnetic field and electron particle velocities in terms of the electric field and ion velocities. Equation (3.16) gives a relation between the electric field and the ion particle

disturbance. So the eighteen unknown variables $\vec{E}(\vec{x}, t), \vec{B}(\vec{x}, t), n_s(\vec{x}, t), \vec{v}_s(\vec{x}, t)$ ($s = \text{deuterium, hydrogen and electron}$) will reduce to nine variables:

$\vec{E}(\vec{x}, t), \vec{v}_D(\vec{x}, t), \vec{v}_H(\vec{x}, t)$. Appendix A shows in detail how to get the equations for the nine remaining unknowns from the cold plasma equations. We consider a special case that selects the unperturbed magnetic field as the z direction and then pick the particle disturbance direction as the x direction, which means $\vec{k} = k\hat{x}, k_y = 0, k_z = 0$. In this situation, the dynamics along and across the magnetic field decouple and the wave equation in (k, ω) space will reduce to two uncoupled block matrices (the off-diagonal blocks are zero):

$$\begin{pmatrix} \underline{\underline{R}}_{6 \times 6}^{x,y} & \\ & \underline{\underline{R}}_{3 \times 3}^z \end{pmatrix} \begin{pmatrix} \underline{\underline{V}}_{6 \times 1}^{x,y} \\ \underline{\underline{V}}_{3 \times 1}^z \end{pmatrix} = 0$$

$$\underline{\underline{V}}_{6 \times 1}^{x,y} \equiv \begin{pmatrix} \tilde{E}_R \\ \tilde{v}_{DR} \\ \tilde{v}_{HR} \\ \tilde{E}_L \\ \tilde{v}_{DL} \\ \tilde{v}_{HL} \end{pmatrix}, \underline{\underline{V}}_{3 \times 1}^z \equiv \begin{pmatrix} \tilde{E}_z \\ \tilde{v}_{Dz} \\ \tilde{v}_{Hz} \end{pmatrix}$$

$$\underline{\underline{R}}_{6 \times 6}^{x,y} \equiv \begin{pmatrix} \tilde{D}_{11} & -i\omega f_1^3 f_3^2 n_D^0 e_D & -i\omega f_1^3 f_3^2 n_H^0 e_H & -\frac{1}{2}k^2 & 0 & 0 \\ \frac{1}{f_1} \frac{e_D}{m_D} & i(\omega + \Omega_D) & 0 & 0 & 0 & 0 \\ \frac{1}{f_1} \frac{e_H}{m_H} & 0 & i(\omega + \Omega_H) & 0 & 0 & 0 \\ -\frac{1}{2}k^2 & 0 & 0 & \tilde{D}_{22} & -i\omega f_1^3 f_3^2 n_D^0 e_D & -i\omega f_1^3 f_3^2 n_H^0 e_H \\ 0 & 0 & 0 & \frac{1}{f_1} \frac{e_D}{m_D} & i(\omega - \Omega_D) & 0 \\ 0 & 0 & 0 & \frac{1}{f_1} \frac{e_H}{m_H} & 0 & i(\omega - \Omega_H) \end{pmatrix} \quad (3.29)$$

$$\underline{\underline{R}}_{3 \times 3}^z \equiv \begin{pmatrix} \tilde{D}_{33} & -i\omega f_1^3 f_3^2 n_D^0 e_D & -i\omega f_1^3 f_3^2 n_H^0 e_H \\ \frac{1}{f_1} \frac{e_D}{m_D} & i\omega & 0 \\ \frac{1}{f_1} \frac{e_H}{m_H} & 0 & i\omega \end{pmatrix}$$

$$\tilde{D}_{11} \equiv -f_1^2 \omega^2 + \frac{k^2}{2} + f_1^2 f_3^2 \frac{n_e^0 e^2}{m_e} \frac{\omega}{\omega + \Omega_e}$$

$$\tilde{D}_{22} \equiv -f_1^2 \omega^2 + \frac{k^2}{2} + f_1^2 f_3^2 \frac{n_e^0 e^2}{m_e} \frac{\omega}{\omega - \Omega_e}$$

$$\tilde{D}_{33} \equiv -f_1^2 \omega^2 + k^2 + f_1^2 f_3^2 \frac{n_e^0 e^2}{m_e}$$

(3.30)

In summary, the dynamics across the magnetic field (the x - y direction) decouples from the dynamics along the magnetic field (the z -direction). For the z component, because the uncoupled magnetic field and the particles are moving in the same direction, the term $\tilde{v}^1 \times \tilde{B}^0$ in the Lorentz force vanishes and the solution to this problem is discussed in [32]. We will be more interested in how the electric field interacts with the particle motion in the x - y

direction. So we will concentrate on that six-dimensional block, with the notation defined in Equation (3.28):

$$\underline{\underline{R}}_{6 \times 6}^{x,y}(k, \omega) \cdot \underline{V}_{6 \times 1}^{x,y}(k, \omega) = 0.$$

For nontrivial solutions $\underline{V}_{6 \times 1}^{x,y}(k, \omega)$, the determinant of $\underline{\underline{R}}_{6 \times 6}^{x,y}(k, \omega) = 0$, which gives the dispersion relation of ω and k .

We will look at two examples. Figure 3.13 shows Deuterium and Hydrogen both at 50% density.

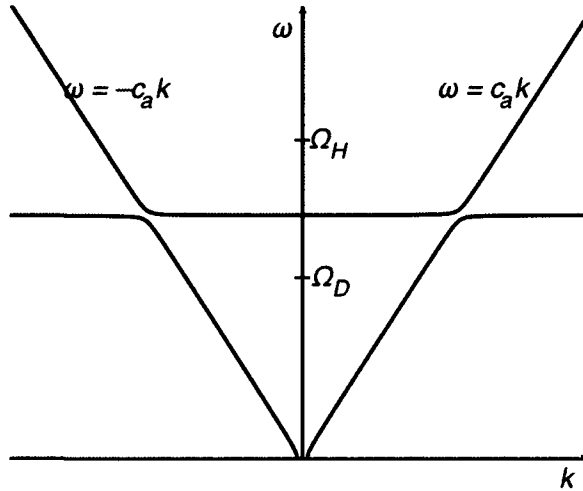


FIGURE 3.13 THE DISPERSION RELATION IN THE POSITIVE FREQUENCY REGION FOR 50%DEUTERIUM AND 50%HYDROGEN

Figure 3.13 shows that there are two fast wave modes $\omega = \pm c_a k$, where C_a is the Alfvén wave speed of the system. The standing wave mode, which crosses the middle of two ion cyclotron frequencies, occurs because we used the Kaufman-Ye approach, keeping the velocities of the two ion species as dynamical variables. This ‘mode’ used to appear as a singular denominator in the traditional approach, but it now appears as a new branch of the dispersion

relation, with avoided crossings. The ion hybrid resonance appears as a horizontal dispersion curve, implying that ‘mode’ has zero group velocity. We will see what this means physically in the next Chapter.

Next we will look at a different density for the two ion species, when one of the ions is a minority: 99% Deuterium and 1% Hydrogen as Figure 3.14.

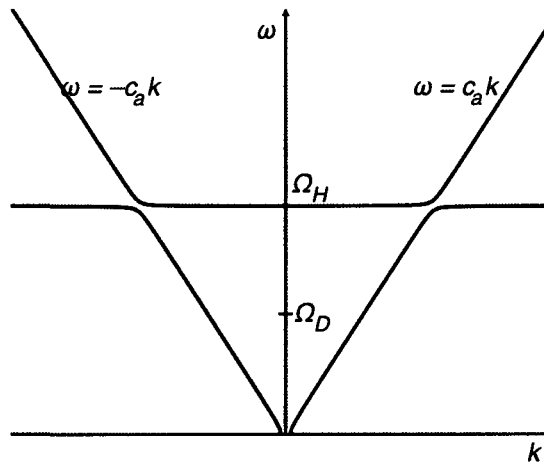


FIGURE 3.14 THE DISPERSION RELATION IN THE POSITIVE FREQUENCY REGION FOR 99%DEUTERIUM AND 1%HYDROGEN

When Hydrogen becomes the minority, the fast waves are still the same, but the ion hybrid resonance moves up to the vicinity of the Hydrogen cyclotron frequency.

As we will see, in the nonuniform problem the region where two modes are nearly degenerate, the ‘avoided crossings’, now become local in x . When waves cross these resonance layers, they can exchange energy and action with each other. In the nonuniform setting this is called *mode conversion*. The Kaufman-Ye approach shows that resonance crossing in

plasmas is really a pair of avoided crossings, which is obscured in the traditional approach.

Chapter 4

Waves in nonuniform plasma far from resonance

We discussed waves in uniform plasma in Chapter 3. There we carried out the Fourier transformation for linearized cold-plasma model of Deuterium-Hydrogen-Electron plasma. We introduced both the traditional method and the Kaufman & Ye method to perform the calculation and described the dispersion relations in both formulations, noting that certain resonances that appear as singular denominators in the determinant using the traditional approach appear as zeros of the determinant (*i.e.* they are related to dispersion curves) in the Kaufman-Ye formulation. Therefore, in the KY formulation, a resonance crossing will look like an avoided crossing. This shows that what is called ‘mode conversion’ in plasma physics is in fact deeply connected to Landau-Zener [33, 34] or ‘level-crossing’ [35,36] phenomena that are familiar in condensed matter or AMO physics.

In the current chapter, we will study these cold-plasma waves in nonuniform plasma. The undisturbed magnetic field strength will be allowed to vary in space. For simplicity, we assume the non-uniformity is only in the x -direction. The zeroth order magnetic field is again assumed to lie in the z -direction: $B^0 = B(x)\hat{z}$. These assumptions can be relaxed without changing the

WKB analysis described below, but for ease of comparison with the uniform plasma results of the previous chapter we restrict ourselves to adding only one new twist to the problem.

4.1 Local resonances

In the nonuniform case we must be careful about operator orderings. Because the background is constant in time we can still Fourier transform from the time to the frequency domain. However, we will be using wave packets to study the resonance crossing numerically, hence we will return to the time domain at that time. The linearized cold plasma model (Maxwell + mass and momentum conservation) consists of Equations (3.2)-(3.6) once again, while equation (3.7) becomes:

$$\frac{\partial \tilde{v}_s^1(\vec{x}, t)}{\partial t} = \frac{1}{f_1} \frac{e_s}{m_s} \tilde{E}^1(\vec{x}, t) + \frac{e_s}{m_s} \tilde{v}_s^1(\vec{x}, t) \times B^0(x) \hat{z} \quad (4.1)$$

Thus the six fundamental equations are:

$$\nabla \times \tilde{\tilde{B}}^1(\vec{x}, \omega) = f_1^2 f_3^2 \sum_s n_s^0 e_s \tilde{\tilde{v}}_s^1(\vec{x}, \omega) + f_1 (-i\omega) \tilde{\tilde{E}}^1(\vec{x}, \omega) \quad (4.2)$$

$$\nabla \times \tilde{\tilde{E}}^1(\vec{x}, \omega) = i\omega f_1 \tilde{\tilde{B}}^1(\vec{x}, \omega) \quad (4.3)$$

$$\nabla \cdot \tilde{\tilde{E}}^1(\vec{x}, \omega) = f_1 f_3^2 \sum_s e_s \tilde{\tilde{n}}_s^1(\vec{x}, \omega) \quad (4.4)$$

$$\nabla \cdot \tilde{\tilde{B}}^1(\vec{x}, \omega) = 0 \quad (4.5)$$

$$-i\omega \tilde{\tilde{n}}_s^1(\vec{x}, \omega) + \nabla \cdot (n_s^0 \tilde{\tilde{v}}_s^1(\vec{x}, \omega)) = 0 \quad (4.6)$$

And the momentum conservation law is written in x, y, z components:

$$\begin{aligned}
-i\omega\tilde{v}_{sx}^1(\bar{x},\omega) &= \frac{1}{f_1} \frac{e_s}{m_s} \tilde{E}_x^1(\bar{x},\omega) + \Omega_s(x)\tilde{v}_{sy}^1(\bar{x},\omega) \\
-i\omega\tilde{v}_{sy}^1(\bar{x},\omega) &= \frac{1}{f_1} \frac{e_s}{m_s} \tilde{E}_y^1(\bar{x},\omega) - \Omega_s(x)\tilde{v}_{sx}^1(\bar{x},\omega) \\
-i\omega\tilde{v}_{sz}^1(\bar{x},\omega) &= \frac{1}{f_1} \frac{e_s}{m_s} \tilde{E}_z^1(\bar{x},\omega)
\end{aligned} \tag{4.7}$$

The gyrofrequency for each plasma species, denoted as $\Omega_s(x) \equiv \frac{e_s B^0(x)}{m_s}$, is

now x -dependent. The “ \sim ” indicates the Fourier transform in time of its original function. Because we again assume the plasmas are cold, we can employ the Kaufman & Ye model as in Chapter 3.

Appendix B shows the details of how to express this system of PDEs in a compact matrix operator form for the Deuterium-Hydrogen-Electron system:

$$\underline{\underline{\tilde{D}}}^{9 \times 9}(-i\partial_x, -i\partial_y, -i\partial_z, x; \omega)\underline{\underline{\psi}}(\bar{x}, \omega) = 0 \tag{4.8}$$

where $\underline{\underline{\tilde{D}}}^{9 \times 9}$ is a 9×9 matrix operator and $\underline{\underline{\psi}}$ is a 9-component wave function.

For simplicity, and to minimize the computational overhead, the background medium is assumed to vary only in the x direction. Also, our work currently restricts the problem to variation in only one spatial dimension, hence

$\underline{\underline{\psi}} = \underline{\underline{\psi}}(x, t)$. In Eq.(4.8), therefore, when acting on $\underline{\underline{\psi}}$, we set $i\partial_y = 0, i\partial_z = 0$.

As in the uniform case described in Chapter 3, in this setting the 9×9 matrix operator decomposes into two uncoupled matrix operators, one 3×3 block governs the dynamics along the unperturbed magnetic field (along z), while

the remaining 6×6 block governs the dynamics across the background

magnetic field:

$$\begin{pmatrix} \tilde{D}_{11} & -i\omega f_1^3 f_3^2 n_D^0 e_D & -i\omega f_1^3 f_3^2 n_H^0 e_H & \frac{1}{2}\partial_x^2 & 0 & 0 \\ \frac{1}{f_1} \frac{e_D}{m_D} & i(\omega + \Omega_D(x)) & 0 & 0 & 0 & 0 \\ \frac{1}{f_1} \frac{e_H}{m_H} & 0 & i(\omega + \Omega_H(x)) & 0 & 0 & 0 \\ \frac{1}{2}\partial_x^2 & 0 & 0 & \tilde{D}_{22} & -i\omega f_1^3 f_3^2 n_D^0 e_D & -i\omega f_1^3 f_3^2 n_H^0 e_H \\ 0 & 0 & 0 & \frac{1}{f_1} \frac{e_D}{m_D} & i(\omega - \Omega_D(x)) & 0 \\ 0 & 0 & 0 & \frac{1}{f_1} \frac{e_H}{m_H} & 0 & i(\omega - \Omega_H(x)) \end{pmatrix} \begin{pmatrix} \tilde{E}_R \\ \tilde{v}_{DR} \\ \tilde{v}_{HR} \\ \tilde{E}_L \\ \tilde{v}_{DL} \\ \tilde{v}_{HL} \end{pmatrix} = 0 \quad (4.9)$$

Where we have introduced the operators

$$\begin{aligned} \hat{\tilde{D}}_{11} &\equiv -f_1^2 \omega^2 - \frac{\partial_x^2}{2} + f_1^2 f_3^2 \frac{n_e^0 e^2}{m_e} \frac{\omega}{\omega + \Omega_e(x)}, \\ \hat{\tilde{D}}_{22} &\equiv -f_1^2 \omega^2 - \frac{\partial_x^2}{2} + f_1^2 f_3^2 \frac{n_e^0 e^2}{m_e} \frac{\omega}{\omega - \Omega_e(x)}. \end{aligned}$$

We note that, because we are interested in frequencies that lie in the ion-cyclotron range, the denominators associated with the electron cyclotron resonance are non-singular.

In Chapter 3, where we discussed waves in uniform plasma, we mentioned that the Fourier transform converts the wave operator to an ordinary matrix that depends upon k and ω . The determinant of this matrix is the dispersion function, and the zeros of this function define the dispersion curves. In the current chapter we are dealing with nonuniform – though stationary -- plasma. Therefore we can only Fourier transform in time. However, the models we have derived have an important special property: there are no terms that mix x and $-i\partial_x$ in the current 6×6 matrix. Therefore,

ordering issues don't appear and we don't need to invoke the full generality of the Weyl symbol calculus [37], which would be needed for more general cases. The *symbol* of the 6×6 cold plasma operator is therefore what we would naively write down by simply replacing $-i\partial_x$ by k :

$$\underline{\underline{R}}_{6 \times 6}^{\nu, \nu} \equiv \begin{pmatrix} \tilde{D}_{11} & -i\omega \frac{f_1^3 f_3^2}{f_2} n_D^0 e_D & -i\omega \frac{f_1^3 f_3^2}{f_2} n_H^0 e_H & -\frac{1}{2}k^2 & 0 & 0 \\ \frac{f_2}{f_1} \frac{e_D}{m_D} & i(\omega + \Omega_D(x)) & 0 & 0 & 0 & 0 \\ \frac{f_2}{f_1} \frac{e_H}{m_H} & 0 & i(\omega + \Omega_H(x)) & 0 & 0 & 0 \\ -\frac{1}{2}k^2 & 0 & 0 & \tilde{D}_{22} & -i\omega \frac{f_1^3 f_3^2}{f_2} n_D^0 e_D & -i\omega \frac{f_1^3 f_3^2}{f_2} n_H^0 e_H \\ 0 & 0 & 0 & \frac{f_2}{f_1} \frac{e_D}{m_D} & i(\omega - \Omega_D(x)) & 0 \\ 0 & 0 & 0 & \frac{f_2}{f_1} \frac{e_H}{m_H} & 0 & i(\omega - \Omega_H(x)) \end{pmatrix} \quad (4.10)$$

$$\tilde{D}_{11} \equiv -f_1^2 \omega^2 + \frac{k^2}{2} + f_1^2 f_3^2 \frac{n_e^0 e^2}{m_e} \frac{\omega}{\omega + \Omega_e(x)}$$

$$\tilde{D}_{22} \equiv -f_1^2 \omega^2 + \frac{k^2}{2} + f_1^2 f_3^2 \frac{n_e^0 e^2}{m_e} \frac{\omega}{\omega - \Omega_e(x)}$$

Before considering the cold plasma problem, we consider WKB theory for vector wave equations more generally, introducing notation and deriving some important general results. We then return to the cold plasma problem in subsequent sections.

4.2 the WKB method

In this section, we will review the WKB method for solving vector wave problems. When there are no caustics or mode conversions, the WKB method --also known as the ray tracing method -- is effective for solving wave equations.

Here I want to talk about the general case of a wave equation in multiple spatial dimensions. We also assume we have a vector wave problem. The medium is time-independent but varying in space. We assume the wave operator is finite-order in the derivatives. (This could be generalized using the Weyl calculus, but the assumption is sufficient for the problem of interest in this thesis.) Hence, we consider a general wave equation of the form:

$$\underline{\underline{D}}(\vec{x}, -i\nabla, i\partial_t) \cdot \underline{\underline{\psi}}(\vec{x}, t) = 0 \quad (4.11)$$

where $\vec{x} = x_1, x_2 \dots x_n$.

Fourier transforming in time gives:

$$\underline{\underline{D}}(\vec{x}, -i\nabla; \omega) \cdot \underline{\underline{\tilde{\psi}}}(\vec{x}, \omega) = 0 \quad (4.12)$$

Since the frequency ω is just a fixed parameter, we can suppress it for notational simplicity but emphasize that all the results that follow hold for a fixed frequency. We will have to revisit this when we talk about wave packets later. Our wave equation is now of the form:

$$\underline{\underline{D}}(\vec{x}, -i\nabla) \cdot \underline{\underline{\tilde{\psi}}}(\vec{x}) = 0 \quad (4.13)$$

We are interested in solutions of this equation which have a phase that is rapidly varying compared to the background. To set up the asymptotic calculation, we now introduce a formal small parameter ε in front of the gradient. Doing the calculation in this manner allows us to keep the background variation on a fixed spatial scale while taking the wavelength of the oscillations to zero as ε becomes small. We start with a trial solution, which is called an *eikonal* ansatz:

$$\underline{\tilde{\psi}}(\vec{x}) = A(\vec{x}) e^{i \frac{\theta(\vec{x})}{\varepsilon}} \hat{e}(\vec{x}) \quad (4.14)$$

We assume the background medium is weakly inhomogeneous, the phase factor $\frac{\theta(\vec{x})}{\varepsilon}$ varies more quickly than both the amplitude $A(\vec{x})$ and the polarization vector $\hat{e}(\vec{x})$.

We assume the wave operator is self-adjoint. The system then has an action principle:

$$\mathcal{A} \equiv \int d^n x \underline{\tilde{\psi}}^\dagger(\vec{x}) \underline{D}(\vec{x}, -i\nabla) \cdot \underline{\tilde{\psi}}(\vec{x}). \quad (4.15)$$

Insert the eikonal wave ansatz (4.14) into it. To leading order in ε this gives:

$$\mathcal{A} \equiv \int d^n x A^2(\vec{x}) \hat{e}^\dagger(\vec{x}) \underline{D}(\vec{x}, \nabla\theta(\vec{x})) \cdot \hat{e}(\vec{x}). \quad (4.16)$$

The variation with respect to $\hat{e}^\dagger(\vec{x})$ gives

$$A^2(\vec{x}) \underline{D}(\vec{x}, \nabla\theta(\vec{x})) \cdot \hat{e}(\vec{x}) = 0. \quad (4.17)$$

For nontrivial solutions ($A(\vec{x}) \neq 0$), we must have:

$$\underline{D}(\vec{x}, \nabla\theta(\vec{x})) \cdot \hat{e}(\vec{x}) = 0. \quad (4.18)$$

At each spatial position, the polarization $\hat{e}(\vec{x})$ must be an eigenvector of the matrix $\underline{D}(\vec{x}, \nabla\theta(\vec{x}))$ with zero eigenvalue. Define the local wavevector:

$$\vec{k}(\vec{x}) \equiv \nabla\theta(\vec{x}).$$

Following the development of the uniform medium theory, we now define the dispersion function \mathcal{D} which is the determinant of the matrix $\underline{D}(\vec{x}, \vec{k}(\vec{x}))$:

$$\mathcal{D}(\vec{x}, \vec{k}(\vec{x})) \equiv \det\left(\underline{D}(\vec{x}, \vec{k}(\vec{x}))\right).$$

For nontrivial solutions we must have:

$$\mathcal{D}(\vec{x}, \vec{k}(\vec{x})) = 0 \quad (4.19).$$

This is the Hamilton-Jacobi equation. It is a nonlinear partial differential equation for the unknown phase. Equation (4.19) can be solved locally – but not globally in general -- using ray tracing methods in phase space.

Ray phase space is formed by adjoining the n -dimensional space \vec{x} and n -dimensional wavevector space \vec{k} into a $2n$ -dimensional space $\vec{z} = (\vec{x}, \vec{k}) = (z_1, z_2 \dots z_{2n})$ where the wavevector space \vec{k} is now treated an independent variable. When we enforced the relation that $\vec{k} \equiv \vec{k}(\vec{x}) \equiv \nabla\theta(\vec{x})$, we defined an n -dimensional surface $(\vec{x}, \vec{k}(\vec{x}))$ in the $2n$ -dimensional phase space, and this surface is called a *Lagrangian manifold*. The phase function $\theta(\vec{x})$ can be constructed by launching a family of rays with the given initial conditions. This family of rays on the *Lagrangian* manifold can be used to construct the phase function by integrating kdx along each, as described on the next page.

Since we assumed the wave operator is self-adjoint, the matrix $\underline{\underline{D}}(\vec{z}) \equiv \underline{\underline{D}}(\vec{x}, \vec{k}(\vec{x}))$ is Hermitian. Therefore, there are n real eigenvalues $D_j(\vec{z})$. If they are nondegenerate, there will be n corresponding eigenvectors $\hat{e}_j(\vec{z}), j = 1, 2 \dots n$ that are orthogonal. Therefore they form a basis. Because we assume we are in the area away from resonances -- which means away from the degeneracy -- there is at most one zero eigenvalue, for example, $D_1(\vec{z}) = 0$ with eigenvector $\hat{e}_1(\vec{z})$. The determinant of the dispersion

matrix can be written as the product of the eigenvalues:

$\mathcal{D}(\vec{z}) = D_1(\vec{z}) \cdot D_2(\vec{z}) \cdots D_n(\vec{z})$. The locus of points for which $D_1(\vec{z}) = 0$ gives the dispersion surface of wave 1. On this dispersion surface, rays will propagate with the ray Hamiltonian $\mathcal{D}(\vec{z})$. Also, $D_1(\vec{z})$ can be chosen as the ray Hamiltonian. This gives the same rays, but with a different parameterization.¹

For any two scalar functions $f(\vec{z})$ and $g(\vec{z})$, the Poisson bracket is defined as $\{f, g\} \equiv \nabla_{\vec{x}} f \cdot \nabla_{\vec{k}} g - \nabla_{\vec{k}} f \cdot \nabla_{\vec{x}} g$. The ray Hamiltonian $\mathcal{D}(\vec{z})$ generates the ray by

$$\dot{\vec{z}} \equiv \frac{d\vec{z}}{d\sigma} = \{\mathcal{D}(\vec{z}), \vec{z}\} \quad (4.20)$$

Thus we have $\dot{\vec{x}} = -\nabla_{\vec{k}} \mathcal{D}(\vec{z})$, $\dot{\vec{k}} = \nabla_{\vec{x}} \mathcal{D}(\vec{z})$ and the associated phase can be

$$\text{constructed as } \theta_1(\vec{x}) = \theta_0 + \int_{\vec{x}_0}^{\vec{x}} \vec{k}(\vec{x}') \cdot d\vec{x}' = \theta_0 + \int_{\sigma_0}^{\sigma_1} \vec{k}(\vec{x}, \sigma') \cdot \frac{d\vec{x}}{d\sigma'} d\sigma' \text{ by}$$

following the ray σ_1 , where θ_0 is the initial condition for the phase; σ_0 is the initial point of this ray. Note that we must choose initial conditions where

$$\mathcal{D}(\vec{z}_0) = 0. \quad [38]$$

¹ Consider $n=2$ as an example for simplicity: $\mathcal{D}(\vec{z}) = D_1(\vec{z}) \cdot D_2(\vec{z})$, and suppose $D_1(\vec{z}) = 0$, but use the determinant as ray Hamiltonian. Then:

$$\dot{\vec{z}} \equiv \frac{d\vec{z}}{d\sigma} = \{\mathcal{D}(\vec{z}), \vec{z}\} = \{D_1 D_2, \vec{z}\} = D_1 \{D_2, \vec{z}\} + D_2 \{D_1, \vec{z}\} = D_2 \{D_1, \vec{z}\}. \text{ The}$$

factor of D_2 can be absorbed into a new ray parameter via: $\frac{d\sigma}{d\sigma'} = D_2$. Then

$$\frac{d\vec{z}}{d\sigma'} = D_2 \{D_1, \vec{z}\}.$$

Because the phase $\theta(\vec{x})$ appears in equation (4.16) only through its gradient we can shift the phase $\theta(\vec{x})$ by an overall constant leaving the action invariant $\theta(\vec{x}) \rightarrow \theta(\vec{x}) + \theta_0$. By Noether's theorem [39], there is an associated conserved quantity, which is the wave action flux density

$$\vec{J}(\vec{x}) \equiv -A^2(\vec{x}) \left[\nabla_{\vec{k}} (\hat{e}^\dagger(\vec{x}) \underline{D}(\vec{x}, \vec{k}) \cdot \hat{e}(\vec{x})) \right]_{\vec{k}=\nabla\theta(\vec{x})}. \text{ Varying the action with}$$

respect to the phase gives the conservation law (recall we are assuming no time-dependence here) $\nabla \cdot \vec{J} = 0$. The conserved action flux density associated with the zero eigenvalue $D_1(\vec{z})$ is:

$$\vec{J}_1(\vec{x}) \equiv -A^2(\vec{x}) \left[\nabla_{\vec{k}} D_1(\vec{x}, \vec{k}) \right]_{\vec{k}=\nabla\theta_1(\vec{x})} \text{ and } \nabla \cdot \vec{J}_1 = 0 \text{ will give an explicit}$$

expression for the amplitude propagation. This equation typically does not have global solutions: it breaks down near caustics or in conversion regions. The proper treatment of caustics is discussed in the work of Delos [40], Littlejohn [41] and others. In the problem considered in this thesis, however, we are concerned with the breakdown of WKB in conversion regions, so we consider a simplified problem where the 'caustic' that appears is straightforward to deal with (as we'll see, the conversion from the 'fast wave' to the 'ion hybrid' mode looks like conversion at a caustic).

The polarization propagation is discussed in [42, 43, 17]. We will not need the polarization transport results here, however, because we will be carrying out direct numerical simulations on the one hand, and using a local construction on the other hand for finding the 'uncoupled' polarizations (sometimes called the 'adiabatic basis' in the AMO literature).

4.3 WKB method on an example vector problem

We discussed WKB methods for generic vector wave problems in section 4.2. In this section, we will introduce a simple wave problem in a background that is weakly varying in space and constant in time as an example.

$$\begin{pmatrix} (i\partial_t)^2 - (-i\partial_x)^2 & \eta \\ \eta^* & i\partial_t - \Omega_H(x) \end{pmatrix} \begin{pmatrix} \psi_a(x,t) \\ \psi_b(x,t) \end{pmatrix} = 0 \quad (4.21)$$

Where η is the constant coupling and $\Omega_H(x)$ is a spatially dependent gyrofrequency for Hydrogen. There is a very simplified version of the local wave equation governing the interaction between the fast wave (in channel ‘a’) and the hydrogen gyroresonance (in channel ‘b’). In later chapters we will provide a more formal derivation of a similar 2×2 model directly from the cold plasma model, so this simple model is actually more than a ‘toy’.

Because the matrix $\begin{pmatrix} (i\partial_t)^2 - (-i\partial_x)^2 & \eta \\ \eta^* & i\partial_t - \Omega_H(x) \end{pmatrix}$ acting on the wave vector $\begin{pmatrix} \psi_a(x,t) \\ \psi_b(x,t) \end{pmatrix}$ is time independent, we can Fourier transform the

equation in time by inserting $\begin{pmatrix} \psi_a(x,t) \\ \psi_b(x,t) \end{pmatrix} = \begin{pmatrix} \tilde{\psi}_a(x) \\ \tilde{\psi}_b(x) \end{pmatrix} e^{-i\omega t}$, which gives us:

$$e^{-i\omega t} \begin{pmatrix} \omega^2 - (-i\partial_x)^2 & \eta \\ \eta^* & \omega - \Omega_H(x) \end{pmatrix} \begin{pmatrix} \tilde{\psi}_a(x) \\ \tilde{\psi}_b(x) \end{pmatrix} = 0 \quad (4.22)$$

If we insert a WKB ansatz $\begin{pmatrix} \tilde{\psi}_a(x) \\ \tilde{\psi}_b(x) \end{pmatrix} = e^{i\theta(x)} \begin{pmatrix} A_a(x) \\ A_b(x) \end{pmatrix}$, assuming the

two-component wave function has a rapidly varying phase $\theta(x)$ and slowly

varying amplitude and polarization $\begin{pmatrix} A_a(x) \\ A_b(x) \end{pmatrix}$, we get:

$$e^{-i\omega t} e^{i\theta(x)} \begin{pmatrix} \omega^2 - k^2 & \eta \\ \eta^* & \omega - \Omega_H(x) \end{pmatrix} \begin{pmatrix} A_a(x) \\ A_b(x) \end{pmatrix} = 0 \quad (4.23)$$

where $k \equiv \frac{d\theta}{dx}$. For any nontrivial solution for the equation: $\begin{pmatrix} A_a(x) \\ A_b(x) \end{pmatrix} \neq 0$, we

have

$$\det \begin{pmatrix} \omega^2 - k^2 & \eta \\ \eta^* & \omega - \Omega_H(x) \end{pmatrix} = 0 \quad (4.24)$$

Equation (4.24) defines a 2-dimensional dispersion surface in 3-dimensional space (x, k, ω) .

If the coupling η is zero, the dispersion function (4.24) becomes

$$\mathcal{D}(\omega, k, x) = \det \begin{pmatrix} \omega^2 - k^2 & 0 \\ 0 & \omega - \Omega_H(x) \end{pmatrix} = (\omega^2 - k^2)(\omega - \Omega_H(x)) \quad (4.25)$$

which has two eigenvalues, one associated with the fast wave, and the other the hydrogen gyroresonance. Considered, instead, as a function of ω for fixed x there are three distinct branches of the dispersion function:

$$\omega = \pm k, \omega = \Omega_H(x).$$

For each spatial position x_0 , the zero eigenvalue gives a condition on the wave number $\omega = \pm k$ and the gyrofrequency is $\omega = \Omega_H(x_*)$.

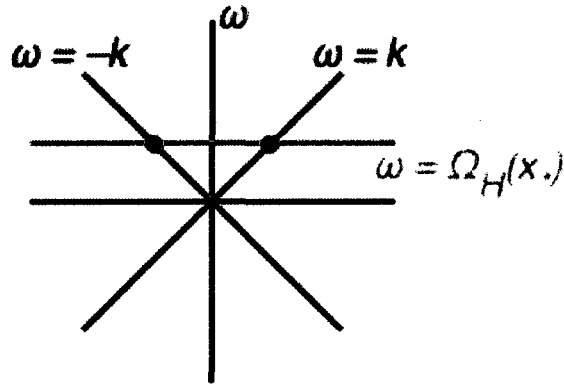


FIGURE 4.1 THE DISPERSION CURVES FOR FIXED SPATIAL POSITION x .

In Chapter 3, we mentioned the group velocity that describes the propagation of the energy/ amplitude or envelope of the wave packet and phase velocity that describe how the carrier oscillation of the wave packet changes.

According to the definition, $v_g \equiv \frac{\partial \omega}{\partial k}$, $v_p \equiv \frac{\omega}{k}$. The eigenmode

$$\omega = \pm k \text{ gives } \begin{cases} \omega = k \Rightarrow v_g = 1, v_p = 1 \\ \omega = -k \Rightarrow v_g = -1, v_p = -1 \end{cases} \text{ and it is the 'fast wave' mode; the}$$

positive mode is the right-moving direction while the negative mode is the left-moving direction.

In figure 4.1, the blue $\mathcal{D}_{11} \equiv \omega^2 - k^2$ mode is the fast moving wave mode with the left (the minus k_0 branch) and right propagation waves (the positive k_0 branch) in space x . The group velocity and the phase velocity have the same value for all ω , hence these waves are dispersionless. We will derive the ray equations momentarily.

The dispersion curve $\omega = \Omega_H(x_*)$ has $v_g = 0$, $v_p = \frac{\omega}{k} = \frac{\Omega_H(x_*)}{k}$. It is a standing wave because the group velocity is zero. The red curve in Figure 4.1

is where $\mathcal{D}_{22} \equiv \omega - \Omega_H(x) = 0$. Because there is no constraint on the wave number for this mode, the phase velocity can be freely changed. In figure 4.1, the two modes cross at the green dots, where the phase velocities of the two modes are equal. This is called the “mode conversion” region, for each choice of frequency it will occur at a different position x_* determined by the condition $\Omega_H(x_*) = \omega_0$, hence the resonance for a given frequency is now localized in x .

Ignoring mode conversion for the moment, we can ask what ray orbits look like for these two modes. In order to do that we must therefore extend our point of view to include the x -domain and view the dispersion functions on the three-dimensional space (x, k, ω) .

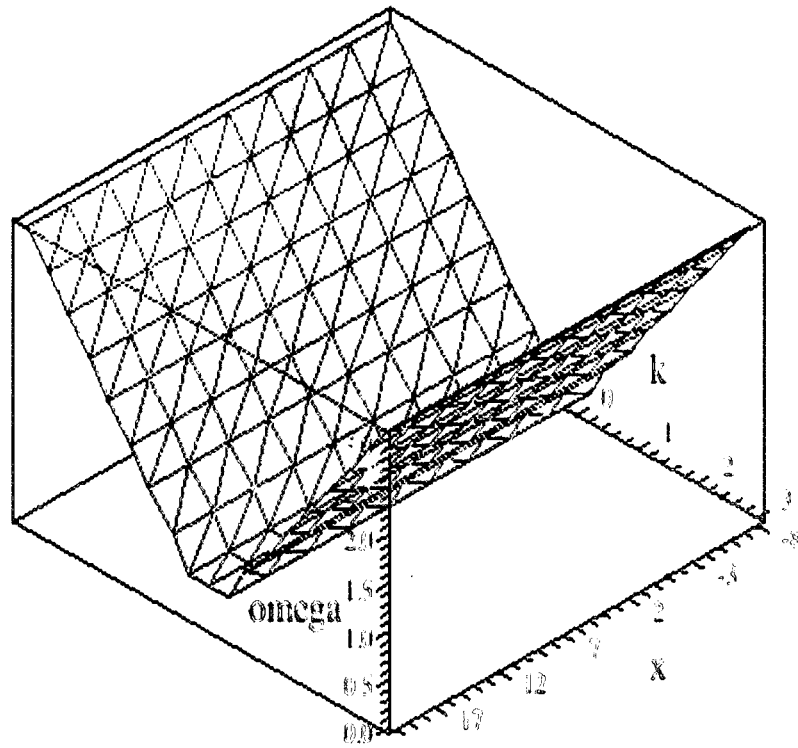


FIGURE 4.2 THE 3D DISPERSION SURFACE FOR THE FAST WAVE

Figure 4.2 shows the fast wave dispersion surface where $\mathcal{D}_{11} \equiv \omega^2 - k^2 = 0$ in the three-dimensional space (x, k, ω) . It is independent of x , so it is invariant in the x -direction.

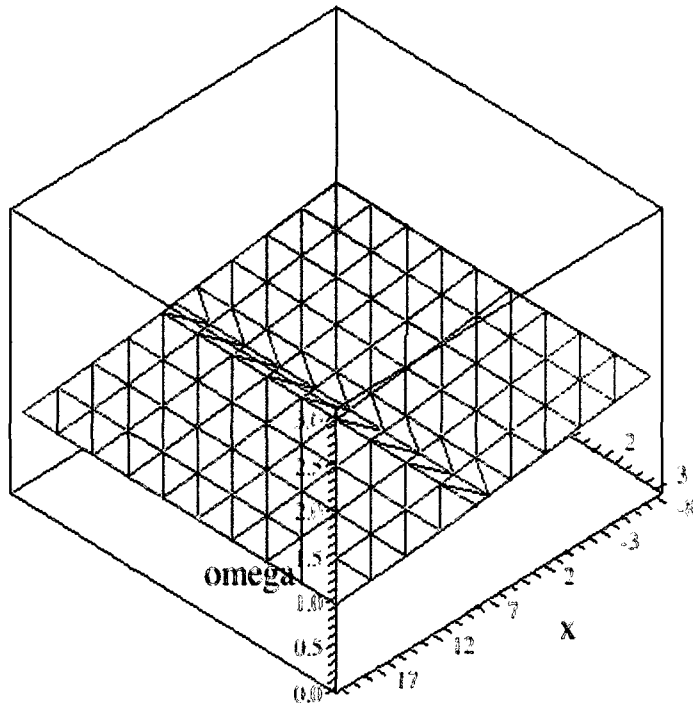


FIGURE 4.3 THE 3D DISPERSION SURFACE FOR THE GYROFREQUENCY STANDING WAVE MODE

Figure 4.3 shows the dispersion surface where $\mathcal{D}_{22} \equiv \omega - \Omega_H(x) = 0$, there is no k dependence, so the surface is invariant in k .

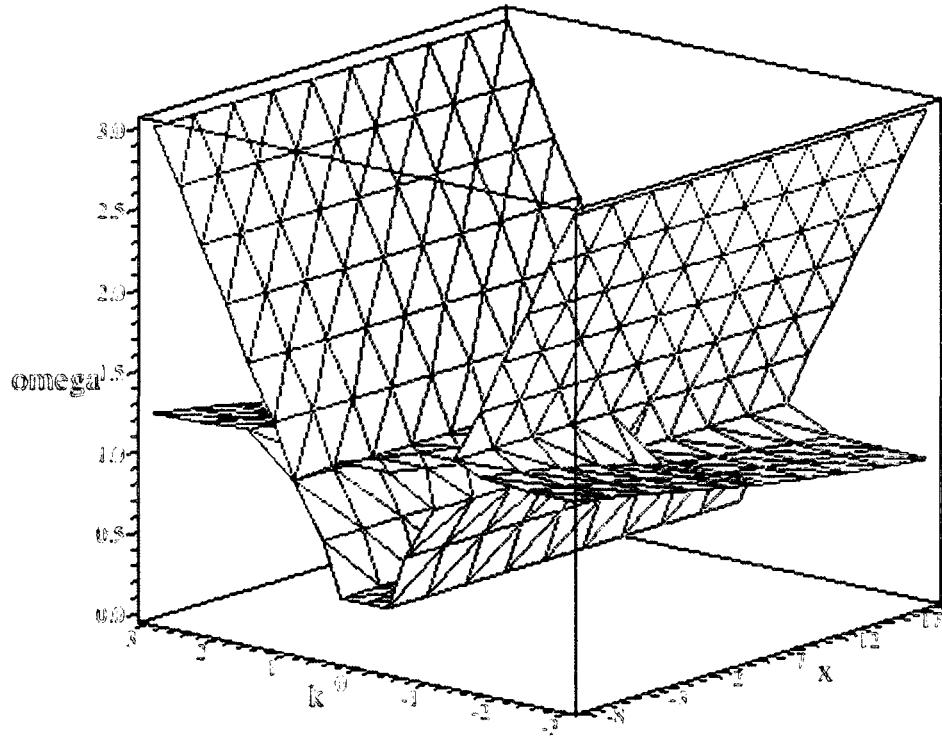


FIGURE 4.4 THE 3D DISPERSION SURFACE FOR THE TWO MODES

Figure 4.4 shows the dispersion surface where $\mathcal{D}_{11} \cdot \mathcal{D}_{22} = 0$. The two modes intersect at places that are x -dependent. For a wave with a fixed frequency carrier, it will cross the resonance at a certain space x point with a definite wavenumber.

Figure 4.5 illustrates the ray orbits in x - k phase space of the two different modes. The blue positive branch is for the right-moving wave while the blue negative branch is for the left-moving wave. The red one is the standing wave – i.e. the hydrogen gyroresonance. Equation (4.20) gives the motion in k space: $\dot{\vec{k}} = \nabla_{\vec{x}} \mathcal{D}(\vec{z})$. The fast wave mode $\mathcal{D}_{11} \equiv \omega^2 - k^2$ is space-independent so it is motionless in k as indicated in Figure 4.2. The standing

wave mode $\mathcal{D}_{22} \equiv \omega - \Omega_H(x)$ is x -dependent. Thus $\frac{\partial k}{\partial t} = \frac{\partial \mathcal{D}(\bar{z})}{\partial x} = -\frac{\partial \Omega_H(x)}{\partial x}$,

the standing wave mode, which is stationary in x space, but propagates in k space.

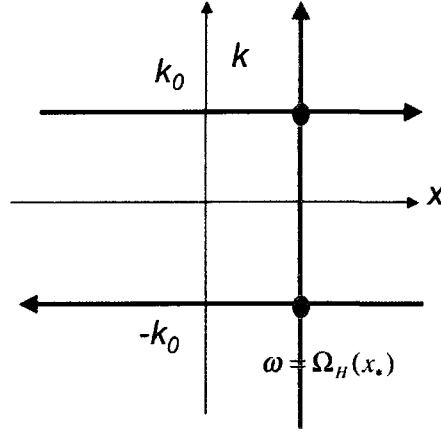


FIGURE 4.5 THE DISPERSION CURVES FOR FIXED FREQUENCY.

Notice that the red ray, associated with the hydrogen gyroresonance, is vertical and, hence, looks like a (highly degenerate!) caustic in x -space. This is what we were referring to earlier when we mentioned that in this problem ‘conversion occurs at a caustic’. In fact, Figure 4.5 shows we have two conversions lying over one another in x -space. They are separated in phase space, however, which will allow us to develop a modular approach to the resonance crossing problem, treating the two conversions in isolation.

If the coupling is not zero, then the two pictures will be modified in the area when two modes cross. The dispersion function is now:

$$\mathcal{D}(\omega, k, x) = \det \begin{pmatrix} \omega^2 - k^2 & \eta \\ \eta^* & \omega - \Omega_H(x) \end{pmatrix} = (\omega^2 - k^2)(\omega - \Omega_H(x)) - |\eta|^2.$$

We mentioned previously when the phase velocities for the two modes are equal, they are degenerate and mode conversion occurs and the WKB methods fail.

Away from the mode conversion area, we use the WKB method to calculate how the waves propagate. Initial conditions are chosen so that

ω_0, k_0, x_0 satisfy $\det \begin{pmatrix} \omega_0^2 - k_0^2 & \eta \\ \eta^* & \omega_0 - \Omega_H(x_0) \end{pmatrix} = 0$. The corresponding null

eigenvector completes the WKB ansatz at x_0 : $\begin{pmatrix} \tilde{\psi}_a(x_0) \\ \tilde{\psi}_b(x_0) \end{pmatrix} = \begin{pmatrix} A_a(x_0) \\ A_b(x_0) \end{pmatrix} e^{ik_0x}$.

Away from x_0 the amplitude is chosen to be a Gaussian with a width that is large compare to a wavelength of the carrier oscillation, but small compared to the length scale over which the background changes. When $\omega_0 = -k_0$, this gives a left-moving wave packet; while for $\omega_0 = k_0$ we would get a right-moving wave packet. The envelope of the wave packet is updated using the group velocity while the carrier is updated using the phase velocity.

Figure 4.6 indicates the avoided crossing phenomenon in the (ω, k) -space for fixed x_0 . The dispersion curves clearly show an avoided crossing at two points. The fact that the dispersion curves reconnect in the manner shown is physically important: for all real values of k there are only real roots of the dispersion relation $\omega(k)$. If the avoided crossing had a gap for some values of real k , it would imply that for those values of k there were complex frequencies, hence the possibility of instabilities.

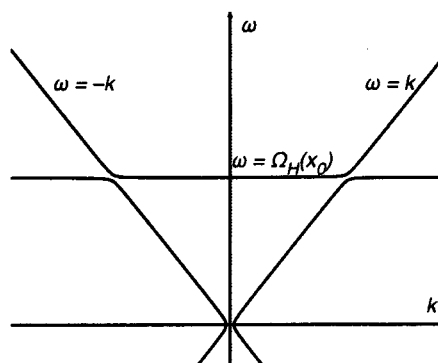


FIGURE 4.6 MODE CONVERSION IN ω - k SPACE FOR FIXED POSITION x_0 . THESE ARE DISPERSION CURVES. NOTE THE AVOIDED CROSSINGS.

In Figure 4.7 we draw the *rays* in phase space. These are representational only to illustrate what the avoided crossing phenomena looks like in the x - k space for fixed ω_0 . Signals propagate *along* the rays (unlike the dispersion surfaces of the previous figure).

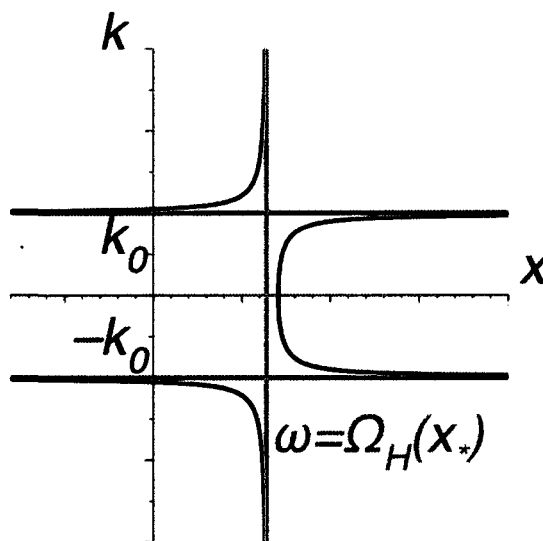


FIGURE 4.7 MODE CONVERSION IN x - k SPACE FOR FIXED FREQUENCY ω_0 . THE BLACK CURVES ARE RAYS.

We now consider how to apply these ideas to the original cold plasma model.

4.4 WKB method on the Cold plasma problem

In this section we will revisit our cold plasma equations by using the WKB method when away from the resonances. Before we focus on the uncoupled modes, we first examine the dispersion curves for a fixed x point for a 50%Deuterium-50% Hydrogen density ratio plasma. Figure 4.8 shows the dispersion curves, now for our full cold-plasma model, in the ion-cyclotron frequency range for the full cold-plasma model with this density ratio. Compare this Figure 4.8 with Figure 4.6, which are the dispersion curves for our 2×2 'toy' model, Equation (4.21).

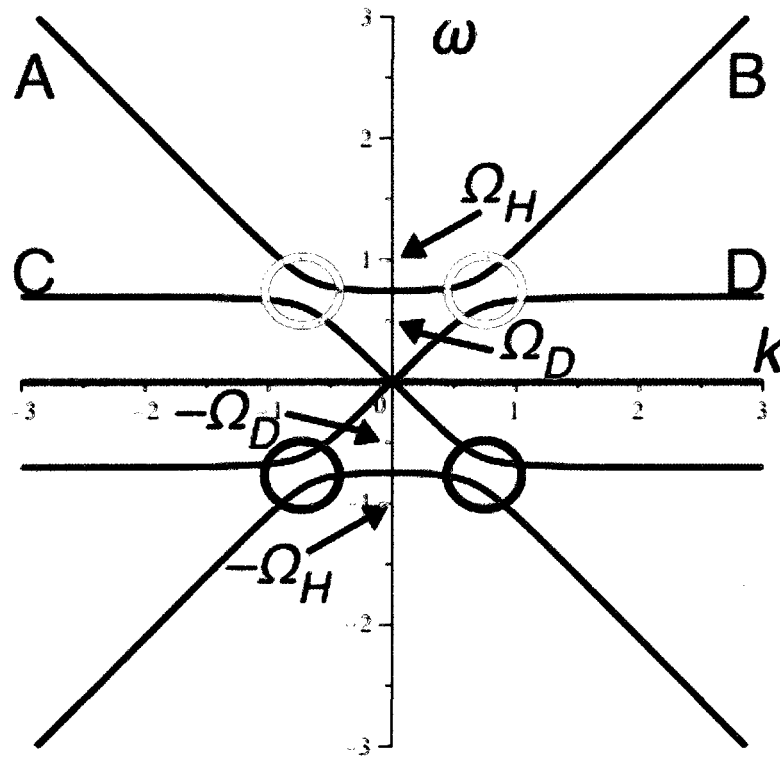


FIGURE 4.8 DISPERSION CURVES FOR 50% DEUTERIUM-50% HYDROGEN WITH ELECTRON IN ω - k SPACE FOR A FIXED POSITION $x_0 > x^*$. THESE ARE DISPERSION CURVES CALCULATED USING THE FULL COLD PLASMA EQUATIONS.

In Figure 4.8 the red circles are the mode conversions of the positive ion-ion hybrid mode and the fast wave mode; the blue circles are the mode conversions of the negative ion-ion hybrid mode coupled with the fast wave mode. Note that we have chosen our time scale to be the cyclotron period for a proton, hence $\Omega_H=1$ and $\Omega_D=1/2$. Because we will choose a wave packet with positive carrier frequency, we will be more interested in the area of the red circle. Far away from the red circle mode conversion region, the waves behave similar to a fast wave mode *or* a pure resonance. The fast waves propagate to both left and right direction with a well-defined group velocity,

$$v_g \equiv -\frac{\partial D / \partial k}{\partial D / \partial \omega} \text{ and phase velocities } v_g \equiv \frac{\omega}{k}.$$

In area *A*, the fast wave mode is far from the crossing and the wave number for the carrier is negative, which gives a negative group velocity and phase velocity. When the group velocity is negative, it means the envelope is moving to the left. In the area *B*, the fast wave mode is far from the resonance and both the carrier frequency and wave number are positive, which gives a positive group velocity. Hence, the envelope propagates to the right. We set our initial wavenumber and carrier in a region like *A* with the wave packet position to the *right* of the resonance in *x*.

The ‘mode’ associated with the ion-hybrid resonance does not propagate in *x* space but does propagate in *k* space as we discussed in section 3.4. There are no constraints on *k* in this mode. The group velocity is zero, the envelope is stationary in *x* space and the phase velocity can be any value. It is

positive at the point D where k is positive and negative in the area C where k is negative.

Next, we will study the polarization of the dispersion curves away from the crossings. At C and D the amplitudes of the polarization components are dominated by the ion motion with almost zero contribution from the electric field. This means the energy of the gyroresonance mode away from the crossing is mainly carried by the particles' motion, not the field. At A and B , but also away from the crossings, the amplitudes of the polarization components are evenly distributed between the electric field and ion motion. However, the energy is mainly contributed by the fields, as we will show by deriving the wave packet energy in detail in Chapter 6. This completes our discussion of the problem far from resonance, where the WKB approximation is valid. We now turn to the local behavior within the resonance region.

Chapter 5

Waves in nonuniform plasma at resonances

We discussed the wave propagation in nonuniform plasma away from the resonances, where the polarization and amplitude of the eikonal ansatz of WKB method are slowly varying. In this chapter, we will concentrate on the wave equations we studied in Chapter 4 at resonances, where the WKB approximation fails.

5.1 Reduction to the 2×2 form

Although WKB breaks down in mode conversion regions, the ray geometry in the conversion regions can still be employed to develop local wave equations governing the two coupled wave modes undergoing the conversion. At the ray tracing level of description, mode conversion appears as a ray splitting event, where one incoming ray turns into two outgoing rays – the transmitted and converted rays. The local wave equation can be solved to find the initial phase and amplitude of these outgoing rays. These WKB connection formulae are summarized by an S -matrix. [18].

In Chapter 4, we discussed the dispersion curves for a fixed position x_* of the cold plasma equations in (ω, k) space. Here I want to change the

perspective by fixing the frequency in the ion cyclotron frequency range, $\omega = \omega_*$ and show the dispersion curves in the phase space (k, x) .

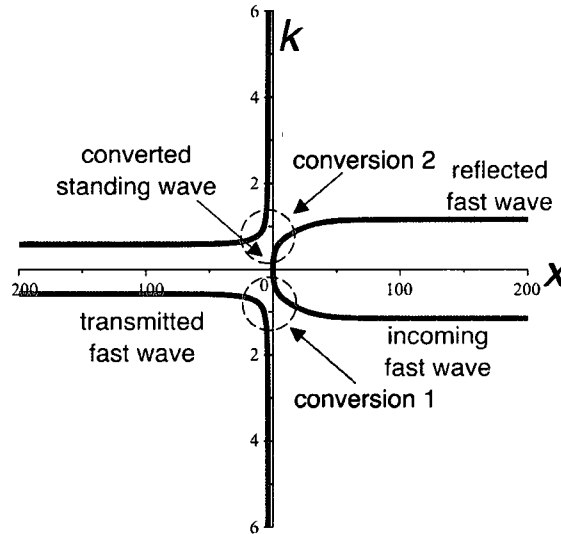


FIGURE 5.1 DISPERSION CURVES FOR THE COLD PLASMA EQUATIONS IN PHASE SPACE FOR A FIXED FREQUENCY ω_* . THESE ARE RAYS, BUT NEAR THE CONVERSIONS WKB BREAKS DOWN.

There are two conversions in Figure 5.1. Let's take a closer look at conversion 1. As mentioned earlier, away from the conversion, the polarizations following the ray change slowly, but they rapidly change near the conversion. We can interpolate to get the polarizations at the conversion point (k_*, x_*) for the two constant *uncoupled* modes $\hat{e}_\alpha(k_*, x_*)$ and $\hat{e}_\lambda(k_*, x_*)$. (We adopt the convention that the *uncoupled* modes are labeled with Greek indices.)

Consider Figure 5.2: There are two rays: ray *a* (in green) and *b* (in purple). Following ray *a*, this transitions smoothly between the incoming ray of uncoupled mode α and the outgoing converted mode λ . Ray *b* behaves similarly. We interpolate between these two pairs of polarizations to the

conversion point (k_*, x_*) and get the two uncoupled constant polarizations

$\hat{e}_\alpha(k_*, x_*)$ and $\hat{e}_\lambda(k_*, x_*)$.

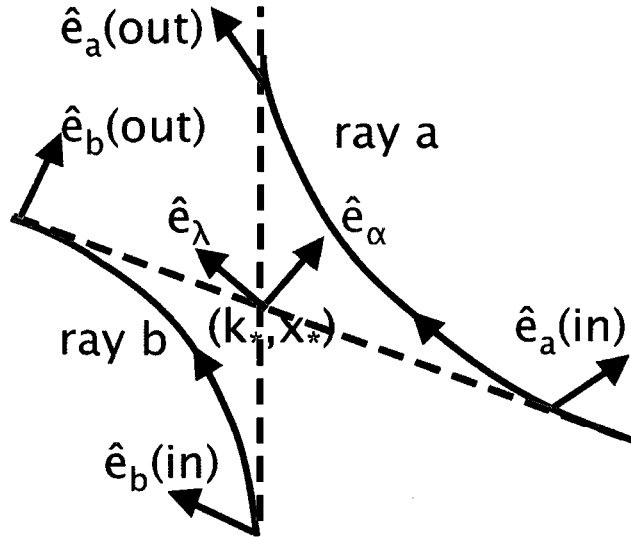


FIGURE 5.2 LOCAL RAY GEOMETRY AND THE POLARIZATION AT EACH POINT ON THE RAYS. $\hat{e}_\alpha(k_*, x_*)$ IS CONSTRUCTED BY LINEARLY TRANSPORTING THE INCOMING AND OUTGOING RED POLARIZATIONS TO THE ORIGIN, THEN AVERAGING $\hat{e}_a(in)$ AND $\hat{e}_b(out)$; $\hat{e}_\lambda(k_*, x_*)$ IS CONSTRUCTED SIMILARLY BY AVERAGING THE BLUE POLARIZATIONS $\hat{e}_a(out)$ AND $\hat{e}_b(in)$.

For each fixed value of frequency $\omega = \omega_*$, the 6×6 cold plasma equations are:

$$\underline{\underline{\hat{D}}}^{6 \times 6}(x, -i\partial_x) \cdot \underline{\underline{\psi}}(x) = 0 \quad (5.1).$$

We now use the uncoupled polarizations for the fixed frequency $\omega = \omega_*$ to introduce a new ansatz appropriate for the neighborhood of the conversion. In that local neighborhood, $\underline{\underline{\psi}}(x)$ is taken to be of the form:

$$\underline{\underline{\psi}}(x) = \psi_\alpha(x) \hat{e}_\alpha(k_*, x_*) + \psi_\lambda(x) \hat{e}_\lambda(k_*, x_*) \quad (5.2).$$

Inserting this new ansatz into the action principle we find:

$$\mathcal{A} \equiv \int dx \underline{\underline{\psi}}^\dagger \cdot \underline{\underline{\hat{D}}} \cdot \underline{\underline{\psi}} = \int dx [\psi_\alpha \hat{e}_\alpha + \psi_\lambda \hat{e}_\lambda]^\dagger \cdot \underline{\underline{\hat{D}}} \cdot [\psi_\alpha \hat{e}_\alpha + \psi_\lambda \hat{e}_\lambda] \quad (5.3).$$

The variation with respect to the uncoupled amplitudes ψ_α and ψ_λ gives the reduced wave equation:

$$\underline{\underline{\hat{D}}}^{2 \times 2}(x, -i\partial_x) \begin{pmatrix} \psi_\alpha(x) \\ \psi_\lambda(x) \end{pmatrix} = 0. \quad (5.4)$$

The 2×2 form of wave operator is

$$\underline{\underline{\hat{D}}}^{2 \times 2}(x, -i\partial_x) = \begin{pmatrix} \hat{D}_{\alpha\alpha}(x, -i\partial_x) & \hat{D}_{\alpha\lambda}(x, -i\partial_x) \\ \hat{D}_{\lambda\alpha}(x, -i\partial_x) & \hat{D}_{\lambda\lambda}(x, -i\partial_x) \end{pmatrix},$$

where the operators $\hat{D}_{mn}(x, -i\partial_x) \equiv \hat{e}_m^\dagger \cdot \underline{\underline{\hat{D}}}^{6 \times 6}(x, -i\partial_x) \cdot \hat{e}_n$, and $m, n = (\alpha, \lambda)$.

The four operators $\hat{D}_{mn}(x, -i\partial_x)$ are linear combinations of the original entries of the 6×6 wave operator $\underline{\underline{\hat{D}}}^{6 \times 6}(x, -i\partial_x)$ because the uncoupled polarizations are constant. And -- just like the 6×6 wave operator for our cold plasma model -- there are terms that mix products of x and $-i\partial_x$ in the 2×2 wave operator. Therefore, we can still avoid invoking the full Weyl symbol calculus and we can easily obtain the symbol of the 2×2 operator by simply replacing $-i\partial_x$ by k :

$$\underline{\underline{D}}^{2 \times 2}(x, k) = \begin{pmatrix} D_{\alpha\alpha}(x, k) & D_{\alpha\lambda}(x, k) \\ D_{\lambda\alpha}(x, k) & D_{\lambda\lambda}(x, k) \end{pmatrix}, \text{ where } D_{mn}(x, k) \equiv \hat{e}_m^\dagger \cdot \underline{\underline{D}}^{6 \times 6}(x, k) \cdot \hat{e}_n, \text{ and}$$

$m, n = (\alpha, \lambda)$. We now Taylor expand the 2×2 symbol of the wave operator [44] around the conversion point (x_*, k_*) . The diagonal terms are zero at the leading order because the polarizations project the 2×2 matrix onto the uncoupled modes. The off-diagonal terms are constant at leading order. The 2×2 form of the wave operator therefore has the following reduced form:

$$\begin{aligned}
\underline{D}^{2 \times 2} &\equiv \left(\begin{array}{cc} (x-x_*) \frac{\partial D_{\alpha\alpha}}{\partial x} \Big|_{x_*,k_*} + (k-k_*) \frac{\partial D_{\alpha\alpha}}{\partial k} \Big|_{x_*,k_*} & \tilde{\eta} \\ \tilde{\eta}^* & (x-x_*) \frac{\partial D_{\lambda\lambda}}{\partial x} \Big|_{x_*,k_*} + (k-k_*) \frac{\partial D_{\lambda\lambda}}{\partial k} \Big|_{x_*,k_*} \end{array} \right) \\
&\equiv \begin{pmatrix} D_\alpha & \tilde{\eta} \\ \tilde{\eta}^* & D_\lambda \end{pmatrix}
\end{aligned} \tag{5.5}$$

where $\tilde{\eta} \equiv \hat{e}_\alpha^\dagger \cdot \underline{D}^{6 \times 6}(x_*, k_*) \cdot \hat{e}_\lambda$.

Referring back to Figure (5.1): If an incoming wave packet is launched in the (red) fast-wave mode, at the lower conversion the transmission coefficient and conversion coefficient are defined as [15]:

$$\tau(\eta) \equiv e^{-\pi|\eta|^2}, \quad \beta(\eta) \equiv \frac{(2\pi\tau)^{1/2}}{\eta\Gamma(-i|\eta|^2)}$$

where the normalized coupling constant is defined $\eta \equiv \frac{\tilde{\eta}}{|\mathcal{B}|^{1/2}}$, with

$\mathcal{B} \equiv \{D_\alpha, D_\lambda\}$ the Poisson bracket of the uncoupled dispersion functions. The bracket is evaluated at the conversion point. In the current case the value of this bracket $\mathcal{B} \equiv \{D_\alpha, D_\lambda\} \propto (c_1 n_D^0 + c_2 n_H^0) \cdot k_* \frac{\partial \Omega_p(x)}{\partial x} \Big|_{x=x_*}$ is proportional to the product of 1] the wavenumber at the conversion point, 2] the gradient of the nonuniform background at the conversion point, and 3] the densities of hydrogen and deuterium; c_1 and c_2 are constants related to the constant uncoupled polarizations.

The wave packet energy splitting at the conversion can be predicted by the transmission and conversion coefficients. The fraction of energy

transmitted is $|\tau|^2$ and the fraction converted is $|\beta|^2$. Energy conservation is guaranteed because by properties of the Γ -function: $|\tau|^2 + |\beta|^2 = 1$ [18].

This is the S matrix prediction for how energy will split when an incoming ray is crossed the conversion region, splits into a converted ray and a transmitted ray. The transmission and conversion coefficients can be used to predict how the energy is transmitted and converted. As we have shown, the whole derivation is for a fixed frequency. We will compare this S matrix prediction for the energy transfers with the full wave calculations for a narrow banded wave packet crossing the conversion region. It is important to note that with a wave packet there is a range of frequencies in a narrow banded wave packet, though the spectrum is dominated by the carrier frequency. Strictly speaking, the frequency dependence of the S -matrix predictions must be taken into consideration. However, the transmission and conversion coefficients are smooth functions of the frequency, hence the results for a narrow-banded wave packet are very close to the single frequency ones. We neglect this subtlety in this thesis, and find we still get good agreement between the ray-based S -matrix predictions and the full-wave simulations.

5.2 Double conversion for the cold plasma models

Figure 5.1 shows that in the resonance-crossing problem, there are two conversions in ray phase space that lie over one another in x -space. We will discuss each of them here in detail. When we launch an initial fast wave packet from the low-field side of the resonance (in Figure (5.1) this

corresponds to the red ray entering from the lower right), it propagates in x -space until it reaches the mode conversion region 1, and the conversion occurs. The wave packet splits into a transmitted fast wave packet and a disturbance in the ion motion that does not propagate in x but propagates in k -space until this converted wave packet arrives at the mode conversion region 2. That is, in x -space the group velocity of the wave packet is zero, but the carrier oscillation evolves. Now the previously converted standing wave packet from conversion 1 is the ‘incoming’ wave packet for conversion 2. The local 2×2 matrix operator for region 2 governs the coupled wave propagation in the second conversion. Part of the energy is now converted to a *reflected* fast wave (the red ray traveling to the upper right in Figure (5.15)) while the rest of the energy is *transmitted* through the second conversion and continues to propagate in k -space. Eventually, the carrier oscillations in the standing wave packet develop very small spatial scales and the wave will dissipate, but this physics is not included in the present model.

Because there are two conversions in this problem, we need to reduce from the 6×6 form of the wave operator to the 2×2 normal form *at each local conversion point*. The cold plasma 6×6 matrix is quadratic in k and therefore, if the conversion point in mode conversion region 1 is $(-k_*, x_*, \omega_*)$, in region 2 the second conversion will be at (k_*, x_*, ω_*) .² In both conversion regions,

² N.B. This is a special property of the one-dimensional problem. In two or three spatial dimensions the ray geometry is much richer and further complications can arise. But, we have found that it is often still possible to

the off-diagonal coupling term is the same. Thus, the transmission and conversion coefficients of these two conversion regions are the same. If we set the incoming wave packet energy to be I , after the conversion region 1 the transmitted fast wave packet energy is $|\tau|^2$ and the converted standing wave packet energy is $|\beta|^2$. When the converted wave packet propagates to arrive later at conversion 2, the reflected wave packet energy has undergone two conversions; hence the reflected wave packet has the energy $|\beta|^2 \cdot |\beta|^2 = |\beta|^4$. After this second conversion, the ‘transmitted’ wave packet will continue propagating in k -space, with the energy $|\beta|^2 \cdot |\tau|^2$. The total energy in all wave packets after the two conversions

is $|\tau|^2 + |\beta|^4 + |\beta|^2 \cdot |\tau|^2 = |\tau|^2 + |\beta|^2 (|\beta|^2 + |\tau|^2) = |\tau|^2 + |\beta|^2 = 1$, which indicates that total energy is conserved after two mode conversion regions.

treat the conversion ray-by-ray and that it is still very useful to think of gyroresonance crossing as a ‘double conversion’.

Chapter 6

Numerical calculations and comparison with theoretical predictions

In the previous chapters, we have derived the 6×6 matrix form of the wave equation for our cold plasma problem, as well as the 2×2 reduction that governs the wave dynamics in the vicinity of the resonance. In this chapter, we will discuss numerical methods to solve these equations, as well as carrying out a direct comparison between the numerical calculations and analytical estimates of the transmission, conversion and reflection coefficients based upon the modular S -matrix approach of Kaufman *et. al.*

6.1 Crank-Nicolson method

The 6×6 matrix equation for cold plasma is a set of partial differential equations. These must be supplemented by appropriate initial conditions, which in the present case we choose to be a magnetosonic wave packet that approaches the resonance from the low-field side (*i.e.* from the right). The numerical solution of PDE's is a very large field of research, which goes well beyond the scope of this thesis. Because the medium is nonuniform in space we cannot use Fourier methods, hence we will use finite difference methods to solve the wave equation.

Recall the cold plasma equation in nonuniform medium is of the form:

$$\underline{\underline{R}}(i\partial_x, x, -i\partial_t) \cdot \underline{V}(x, t) = 0. \text{ The symbol of the operator for our cold}$$

Deuterium-Hydrogen-electron plasma is:

$$\underline{\underline{R}}_{6 \times 6}^{x,y} \equiv \begin{pmatrix} \tilde{D}_{11} & -i\omega \frac{f_1^3 f_3^2}{f_2} n_D^0 e_D & -i\omega \frac{f_1^3 f_3^2}{f_2} n_H^0 e_H & -\frac{1}{2}k^2 & 0 & 0 \\ \frac{f_2}{f_1} \frac{e_D}{m_D} & i(\omega + \Omega_D(x)) & 0 & 0 & 0 & 0 \\ \frac{f_2}{f_1} \frac{e_H}{m_H} & 0 & i(\omega + \Omega_H(x)) & 0 & 0 & 0 \\ -\frac{1}{2}k^2 & 0 & 0 & \tilde{D}_{22} & -i\omega \frac{f_1^3 f_3^2}{f_2} n_D^0 e_D & -i\omega \frac{f_1^3 f_3^2}{f_2} n_H^0 e_H \\ 0 & 0 & 0 & \frac{f_2}{f_1} \frac{e_D}{m_D} & i(\omega - \Omega_D(x)) & 0 \\ 0 & 0 & 0 & \frac{f_2}{f_1} \frac{e_H}{m_H} & 0 & i(\omega - \Omega_H(x)) \end{pmatrix}$$

$$\tilde{D}_{11} \equiv -f_1^2 \omega^2 + \frac{k^2}{2} + f_1^2 f_3^2 \frac{n_e^0 e^2}{m_e} \frac{\omega}{\omega + \Omega_e(x)}$$

$$\tilde{D}_{22} \equiv -f_1^2 \omega^2 + \frac{k^2}{2} + f_1^2 f_3^2 \frac{n_e^0 e^2}{m_e} \frac{\omega}{\omega - \Omega_e(x)}$$

As we discussed in Chapter 3, for nontrivial solutions, the determinant of the matrix has to be zero $\det(\underline{\underline{R}}_{6 \times 6}^{x,y}(k, \omega, x)) = 0$, which gives us the dispersion function of a sixth-order polynomial equation of ω . Figure 6.1 shows the dispersion relation for a fixed spatial position.

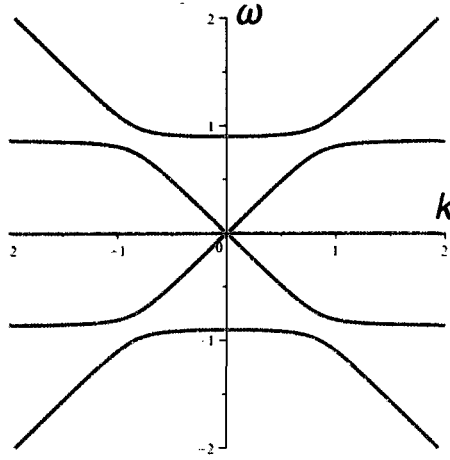


FIGURE 6.1 DISPERSION RELATION OF THE FULL 6×6 COLD PLASMA PROBLEM FOR A FIXED POSITION

The dispersion function (the determinant of the symbol matrix) is a sixth-order polynomial in ω . In the ion-cyclotron range of frequencies we can simplify the dispersion function to a fourth-order polynomial by using the fact that f_i is very small and applying the following approximation for the electron contribution:

$$\tilde{D}_{11} \equiv -f_1^2 \omega^2 + \frac{k^2}{2} + f_1^2 f_3^2 \frac{n_e^0 e^2}{m_e} \frac{\omega}{\omega + \Omega_e(x)} \approx \frac{k^2}{2} + f_1^2 f_3^2 \frac{n_e^0 e^2}{m_e} \frac{\omega}{\Omega_e(x)}$$

$$\tilde{D}_{22} \equiv -f_1^2 \omega^2 + \frac{k^2}{2} + f_1^2 f_3^2 \frac{n_e^0 e^2}{m_e} \frac{\omega}{\omega - \Omega_e(x)} \approx \frac{k^2}{2} - f_1^2 f_3^2 \frac{n_e^0 e^2}{m_e} \frac{\omega}{\Omega_e(x)}$$

The dispersion relations computed under this approximation overlaps the exact result, which means the wave characteristics will not be changed and thus this simplification is valid in this range of frequencies.

We want to study the cold plasma model for an incoming wave packet in the fast wave mode in the space-time domain. We follow its evolution to

study the effect of its crossing the resonance layer at $x = 0$. We performed the Weyl symbol calculation again to obtain the operators in time-space domain. As we explained in Chapter 4, because there is no product term of x and k , we can simply relate: $\frac{\partial}{\partial t} \rightarrow -i\omega$, $\frac{\partial}{\partial x} \rightarrow ik$. The operator in x - t space is therefore:

$$\hat{\underline{R}}_{6 \times 6}^{x,y} \equiv \begin{pmatrix} \hat{D}_{11} & \frac{f_1^3 f_3^2}{f_2} n_D^0 e_D \partial_t & \frac{f_1^3 f_3^2}{f_2} n_H^0 e_H \partial_t & \frac{1}{2} \partial_x^2 & 0 & 0 \\ \frac{f_2 e_D}{f_1 m_D} & -\partial_t + i\Omega_D(x) & 0 & 0 & 0 & 0 \\ \frac{f_2 e_H}{f_1 m_H} & 0 & -\partial_t + i\Omega_H(x) & 0 & 0 & 0 \\ \frac{1}{2} \partial_x^2 & 0 & 0 & \hat{D}_{22} & \frac{f_1^3 f_3^2}{f_2} n_D^0 e_D \partial_t & \frac{f_1^3 f_3^2}{f_2} n_H^0 e_H \partial_t \\ 0 & 0 & 0 & \frac{f_2 e_D}{f_1 m_D} & -\partial_t - i\Omega_D(x) & 0 \\ 0 & 0 & 0 & \frac{f_2 e_H}{f_1 m_H} & 0 & -\partial_t - i\Omega_H(x) \end{pmatrix},$$

$$\hat{D}_{11}(i\partial_x, x, -i\partial_t) \equiv -\frac{\partial_x^2}{2} + i f_1^2 f_3^2 \frac{n_e^0 e^2}{m_e \Omega_e(x)} \partial_t$$

with

$$\hat{D}_{22}(i\partial_x, x, -i\partial_t) \equiv -\frac{\partial_x^2}{2} - i f_1^2 f_3^2 \frac{n_e^0 e^2}{m_e \Omega_e(x)} \partial_t$$

$$\hat{\underline{R}}_{6 \times 6}^{x,y} \cdot \underline{V}_{6 \times 1}^{x,y}(x, t) = 0 \quad \text{and} \quad \underline{V}_{6 \times 1}^{x,y}(x, t) \equiv \begin{pmatrix} E_R(x, t) \\ v_{DR}(x, t) \\ v_{HR}(x, t) \\ E_L(x, t) \\ v_{DL}(x, t) \\ v_{HL}(x, t) \end{pmatrix}.$$

Next, we will use the finite-difference method to numerically solve the PDEs. Because of our simplification, the differential equations all involve first-order derivatives in time. There are also second-order derivatives in space. We can therefore apply the Crank-Nicolson method [45]. This method

has the highly desirable property that the iteration scheme is exactly unitary. This means that the time-step is represented by a unitary matrix operation. This ensures numerical stability for these Schrödinger-type PDEs. Several other numerical methods we used were unstable, sometimes wildly so. Appendix C shows the details about how to express the PDEs in finite difference form.

We can also reduce the 6×6 equation to the 2×2 local form as explained in Chapter 5, then solve the reduced wave equation numerically. We calculate the 2×2 local form numerically to compare with the 6×6 results. We also analytically expand the 2×2 symbol around the local resonance position using methods described in Chapter 5 to obtain the S matrix for each of the two mode conversions in the problem. Thus we get a closed form analytical prediction of the transmission and reflection coefficients to compare with the 6×6 and 2×2 full wave numeric results.

6.2 Initial wave packets

We choose initial conditions consisting of a magnetosonic wave packet that enters the resonance region from the low-field side (*i.e.* it is moving from right to left since we assume the magnetic field strength increases to the left). Firstly, we choose a position $x = x_0$ that is far away from the resonance to the *right* as the center position for the initial wave packet. Secondly, we pick the wave frequency for the initial wave packet that equals the ion-hybrid gyrofrequency at the resonance $\omega_0 = \Omega_{IH}(x = 0)$, and

$x = 0$ is where the resonance takes place. Thirdly, use Maple to calculate when $\det \left[\underline{\underline{R}}_{6 \times 6}^{x,y} (k, \omega = \Omega_{IH}(x = 0), x = x_0) \right] = 0$, which gives the initial value of the wavenumber $k = k_0$. Select the sign of the root to guarantee the wave packet is propagating to the left toward the resonance. Lastly, use the cold plasma equation at the initial wave packet position with the initial wave frequency and wavenumber to determine the initial polarization satisfying:

$$\underline{\underline{R}}_{6 \times 6}^{x,y} (k = k_0, \omega = \omega_0, x = x_0) \cdot \underline{\underline{V}}_{6 \times 1}^{x,y} (k = k_0, \omega = \omega_0, x = x_0) = 0$$

This initial wave packet is now evolved forward in time using the Crank-Nicolson algorithm described in Appendix C. We discuss in a moment how we measure the energy of the incoming wavepacket, as well as the transmitted and reflected packets.

We will also compare the full 6×6 simulation with a numerical solution of the reduced 2×2 wave equation in the vicinity of the resonance. The 2×2 reduced form is obtained from the constant uncoupled polarizations $\hat{e}_\alpha(k_*, \omega_*)$ and $\hat{e}_\lambda(k_*, \omega_*)$ as introduced in Chapter 5. We use the same approach to get the proper wave packet initial conditions which satisfy the local dispersion curves $\det \left[\underline{\underline{D}}_{2 \times 2} (k, \omega = \omega_0, x = x_0) \right] = 0$ and the corresponding polarization that

$$\underline{\underline{D}}_{2 \times 2} (k = k_0, \omega = \omega_0, x = x_0) \cdot \underline{\underline{\psi}}_{2 \times 1} (k = k_0, \omega = \omega_0, x = x_0) = 0.$$

6.3 Numerical results

6.3.1 Wave packet propagation

After the initial wave packet for the 6×6 full wave is determined as above, it propagates in the fast-wave mode until it encounters the mode conversion region. It will excite a disturbance in the resonance layer and the remnant of the fast-wave packet will continue as the transmitted wave. The disturbance in the resonance layer is supported largely by particle motion (the field contribution to the energy is small). The carrier oscillation of this disturbance evolves in k -space while the envelope of the wave packet is stationary in x -space until the resonance condition for the other mode conversion is satisfied. This disturbance then converts partly back into the fast-wave mode. Therefore, after a finite time delay a reflected fast wave packet is emitted. As an example, we show the wave packet propagating before and after mode conversion for a 99% Deuterium and 1% Hydrogen plasma. Figures 6.2-6.4 show what the wave packets look like before and after the resonance crossing.

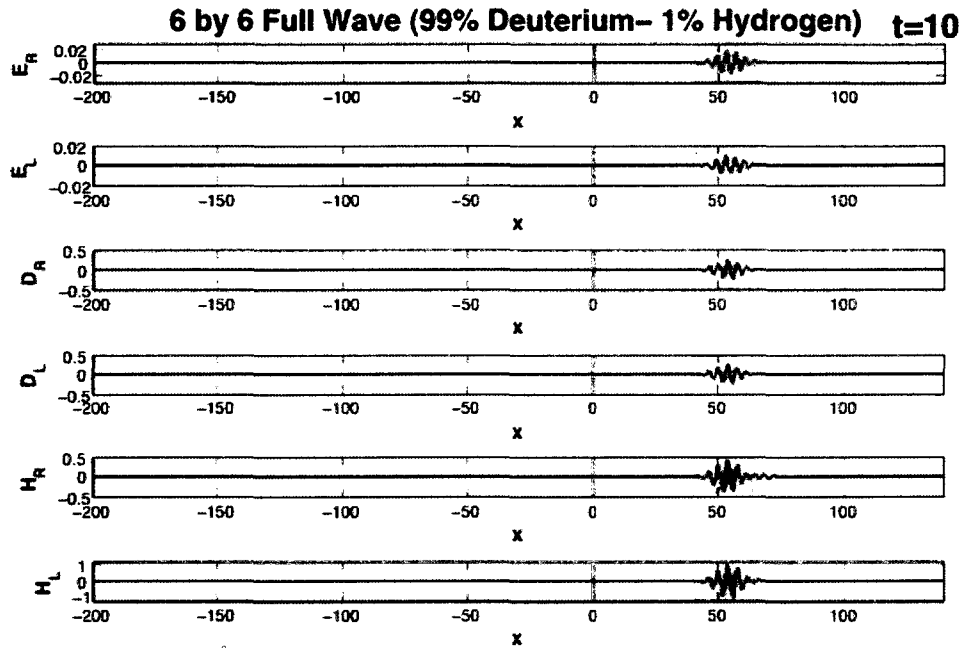


FIGURE 6.2 THE SHADED REGION INDICATES THE INCOMING WAVE PACKET FOR THE FULL 6×6 COLD PLASMA PROBLEM. THE RED LINES ARE THE MODE CONVERSION REGIONS. THE INCOMING WAVE PACKET MOVES TO THE LEFT. THE INCOMING ENERGY IS COMPUTED USING THE SHADED REGION.

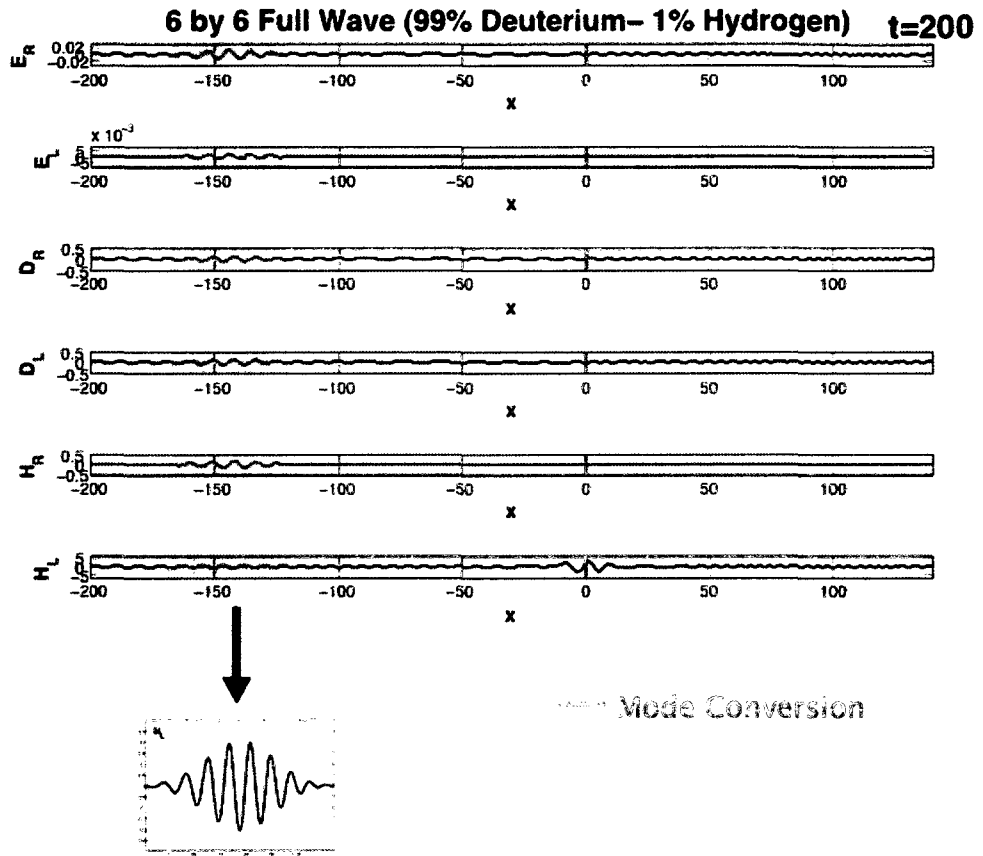


FIGURE 6.3 THE SHADED REGION INDICATES THE TRANSMITTED WAVE PACKET FOR THE FULL 6×6 COLD PLASMA PROBLEM. THE RED LINES ARE THE MODE CONVERSION REGIONS. THE WAVE PACKET MOVES TO THE LEFT. THIS IS THE TRANSMITTED WAVE PACKET AND ITS ENERGY IS COMPUTED USING THE SHADED REGION.

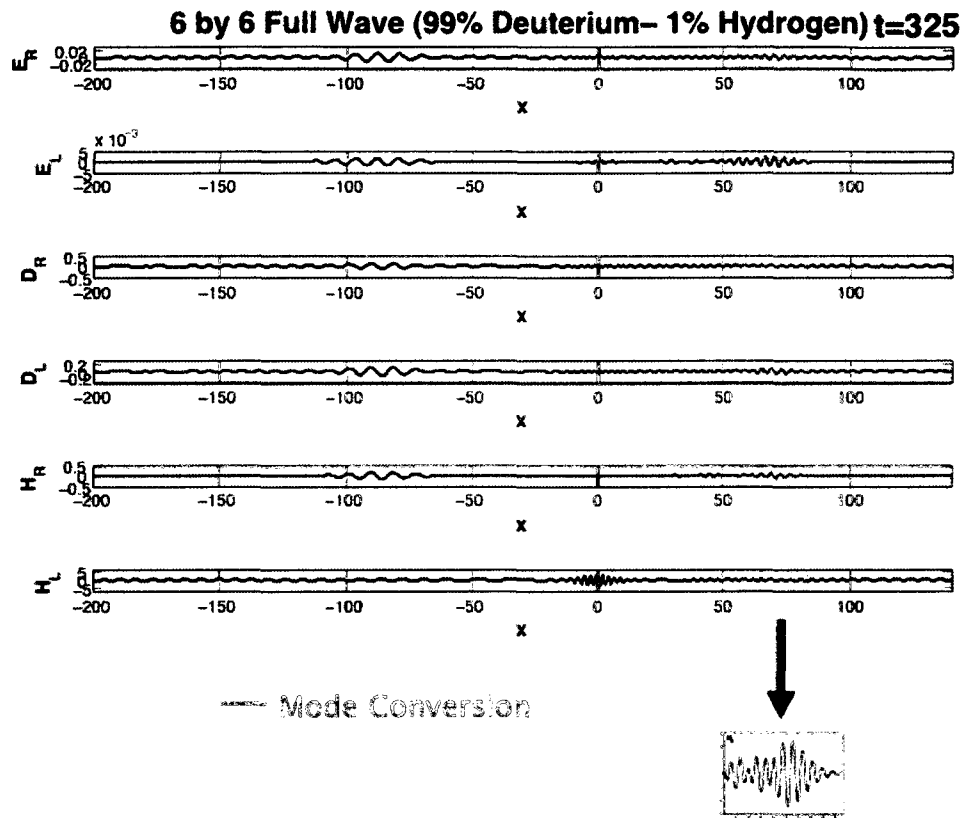


FIGURE 6.4 THE SHADED REGION INDICATES THE REFLECTED WAVE PACKETS FOR THE FULL 6×6 COLD PLASMA PROBLEM. THE RED LINES ARE THE MODE CONVERSION REGIONS. THE REFLECTED WAVE PACKET MOVES TO THE RIGHT. ITS ENERGY IS COMPUTED USING THE SHADED REGION.

Similarly, if we apply Crank-Nicolson to the 2×2 reduction form and use the proper initial conditions introduced in the previous section, we will get the numerical calculation for the 2×2 full wave. For the same 99% Deuterium–1% Hydrogen plasma, Figures 6.5-6.7 show how the wave packets before and after the resonances look like for the 2×2 reduced form. After the initial wave packet is launched, it propagates to the left until it hits the mode conversion region. In the case of the 6×6 full wave, just as the case for the 2×2 full wave,

the incoming wave packets will excite a disturbance in the resonance layer and the remnant of the fast-wave packet will continue as the transmitted wave. In the same way, the carrier oscillation of this disturbance evolves in k -space while the envelope of the wave packet is stationary in x -space until the resonance condition for the other mode conversion is satisfied. And as before, this disturbance then converts partly back into the fast-wave mode. Therefore, it appears that after a finite time delay, a reflected fast wave packet is emitted.

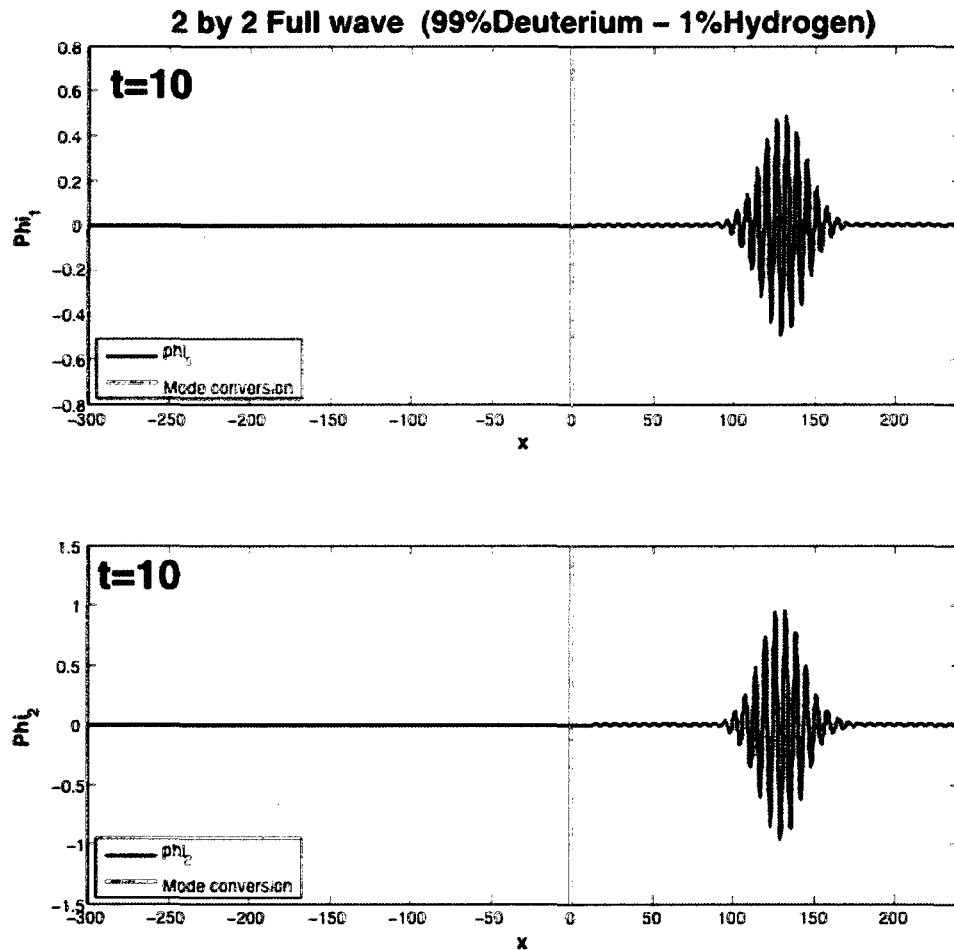


FIGURE 6.5 THE SHADED REGION INDICATES THE INCOMING WAVE PACKET FOR THE 2×2 REDUCED FORM. THE INCOMING ENERGY IS COMPUTED USING THE SHADED REGION.

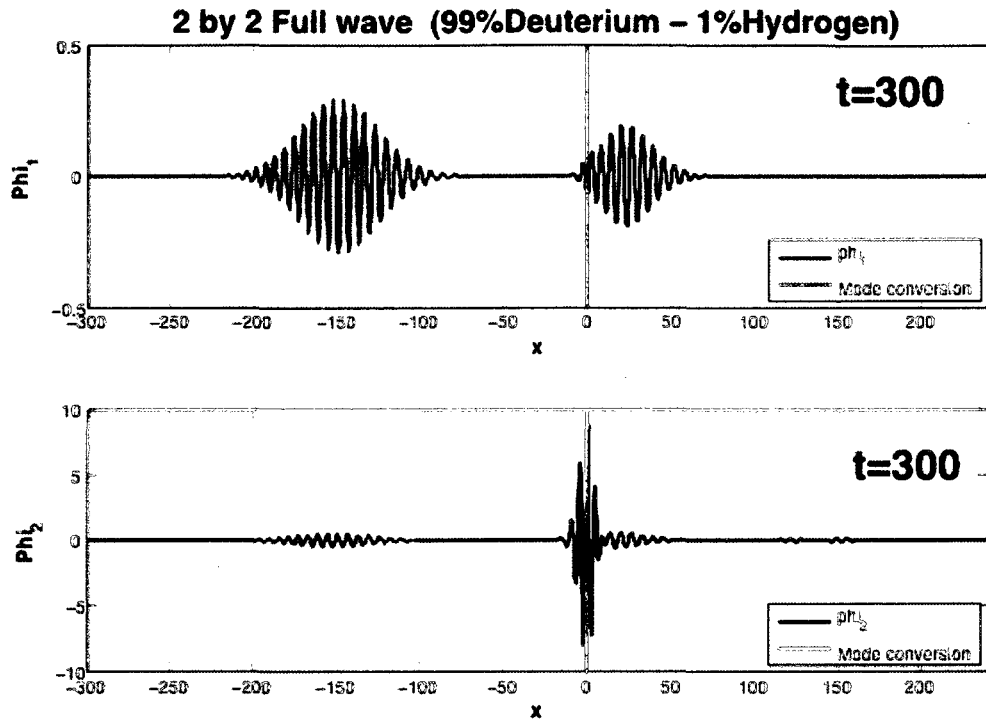


FIGURE 6.6 THE SHADED REGION INDICATES THE TRANSMITTED WAVE PACKET FOR THE 2×2 REDUCTION FORM. NOTE THE DISTURBANCE REMAINING IN THE VICINITY OF THE RESONANCE IN THE LOWER FRAME (WHICH IS LARGELY A COMBINATION OF THE PARTICLE VELOCITIES), AND THE EMERGENCE OF THE REFLECTED WAVE PACKET (WHICH IS LARGELY THE ELECTRIC FIELD).

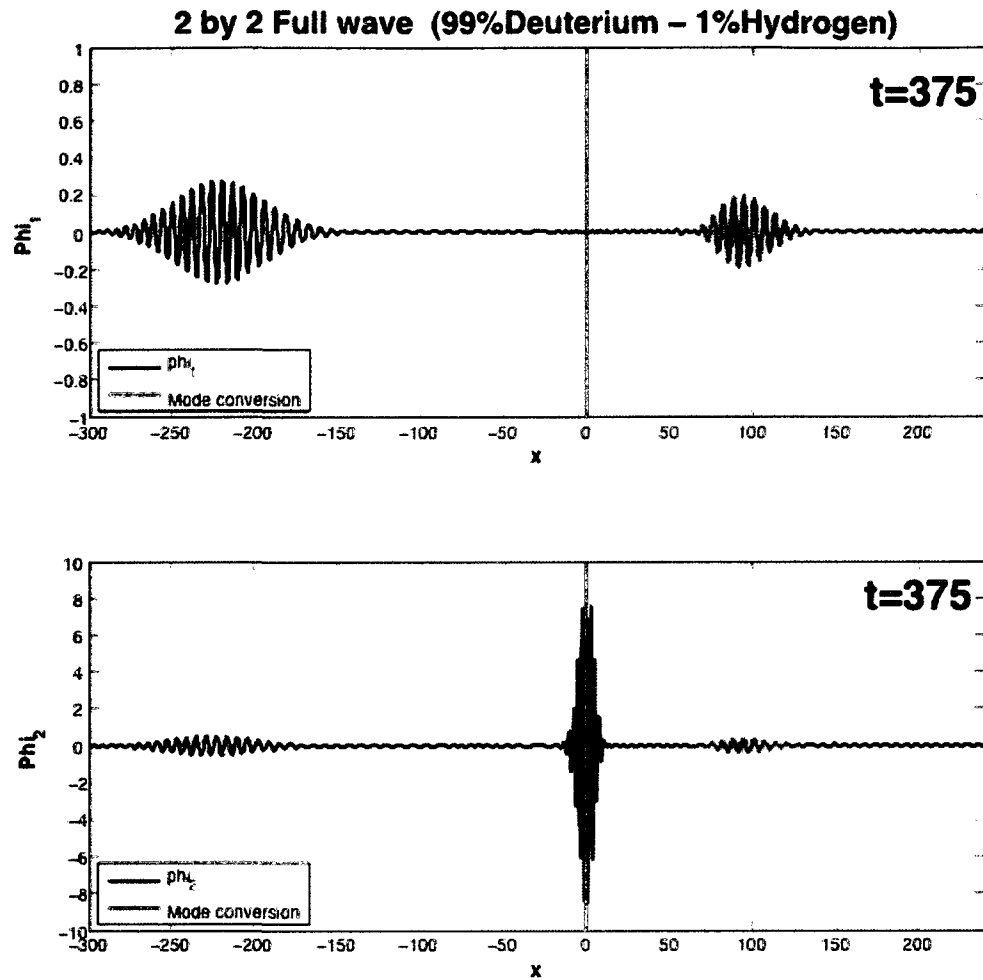


FIGURE 6.7 THE SHADED REGION INDICATES THE REFLECTED WAVE PACKET FOR THE 2×2 REDUCED FORM. THE REFLECTED ENERGY IS COMPUTED USING THE SHADED REGION.

6.3.2 Wave packet energy

Next we will calculate the energy before and after the mode conversions. In Chapter 2.2, we discussed the total energy for the system. We will compare the transmitted energy ratio and reflected energy ratio for the different 6×6 and 2×2 full wave equations and the S matrix prediction. In Figure 6.2, the field energy is:

$$\mathcal{E}_{field} = \int_V \frac{\epsilon_0}{2} \left(|\vec{E}(\vec{x}, t)|^2 + c^2 |\vec{B}(\vec{x}, t)|^2 \right) dV = \epsilon_0 \epsilon_0 E_0^2 \int_V \frac{1}{2} \left(|\vec{E}^*(\vec{x}, t)|^2 + |\vec{B}^*(\vec{x}, t)|^2 \right) dV^*$$

where the ‘*’ quantities are nondimensional and all notations with the subscript 0 represent reference values. For each species s , the kinetic energy is

$$\varepsilon_{s,kinetic} = m_p n_0 V_0^2 x_0 \int_V \frac{1}{2} \left(m_s^* n_s^* |\vec{v}_s^*|^2 \right) dV^* .$$

In the energy calculation, the magnetic field and the electron velocity are unknown variables. We use the Maxwell-Farady equation to get the nondimensionalized \vec{B}^* and by applying the momentum conservation equation, we can represent \vec{v}_e^* by the electric field. In the ion-hybrid region, the electron kinetic energy is very small compared to the ion kinetic energy. Thus we can express the energy in terms of our known parameters

$E_R, E_L, v_{DR}, v_{DL}, v_{HR}, v_{HL}$ which is

$$\varepsilon = \sum_{\substack{\text{envelope} \\ \text{region}}} \underline{V}^\dagger \underline{\mathcal{S}}^{6 \times 6} \underline{V}, \quad \underline{V} = \begin{pmatrix} E_R(x,t) \\ E_L(x,t) \\ v_{DR}(x,t) \\ v_{DL}(x,t) \\ v_{HR}(x,t) \\ v_{HL}(x,t) \end{pmatrix}$$

$$\underline{\mathcal{S}}^{6 \times 6} \equiv \begin{pmatrix} \frac{1}{2} + \frac{1}{2f_1^2} & -\frac{1}{2f_1^2} & & & & \\ -\frac{1}{2f_1^2} & \frac{1}{2} + \frac{1}{2f_1^2} & & & & \\ & & \frac{n_D^* m_D^*}{2} & & & \\ & & & \frac{n_D^* m_D^*}{2} & & \\ & & & & \frac{n_H^* m_H^*}{2} & \\ & & & & & \frac{n_H^* m_H^*}{2} \end{pmatrix}$$

Unlike the total energy that is integrated over the whole space, the wave packet energy is only integrated over the width of the wave envelope (the shaded regions in the previous figures). Since our numerical algorithm uses finite-differences, the integral becomes a summation. We summed up the corresponding shaded areas for the incoming, transmitted and reflected waves to get the corresponding energies. We define the amplitude of the transmission coefficient as the ratio of the transmitted energy to the incoming energy and the amplitude of the reflection coefficient as the ratio of reflected energy to the incoming energy.

In the 2x2 numerical calculation, because we use the constant uncoupled polarization to represent the vector

$$V = \begin{pmatrix} E_R(x,t) \\ E_L(x,t) \\ v_{DR}(x,t) \\ v_{DL}(x,t) \\ v_{HR}(x,t) \\ v_{HL}(x,t) \end{pmatrix} = \psi_1(x)\hat{e}_\alpha + \psi_2(x)\hat{e}_\lambda, \text{ the energy can be expressed from the}$$

2x2 numerical calculation.

We performed this calculation for the various number density fractions of Deuterium and Hydrogen (50% D-50% H, 80% D-20% H, 95% D-5% H, 97% D-3% H, 99% D-1% H, 99.5% D-0.5% H, 99.8% D-0.2% H). And these results are plotted in two figures to illustrate what the amplitude of transmission (Figure 6.8) and reflection coefficients (Figure 6.9) obtained from our three methods for different proportions of ion densities.

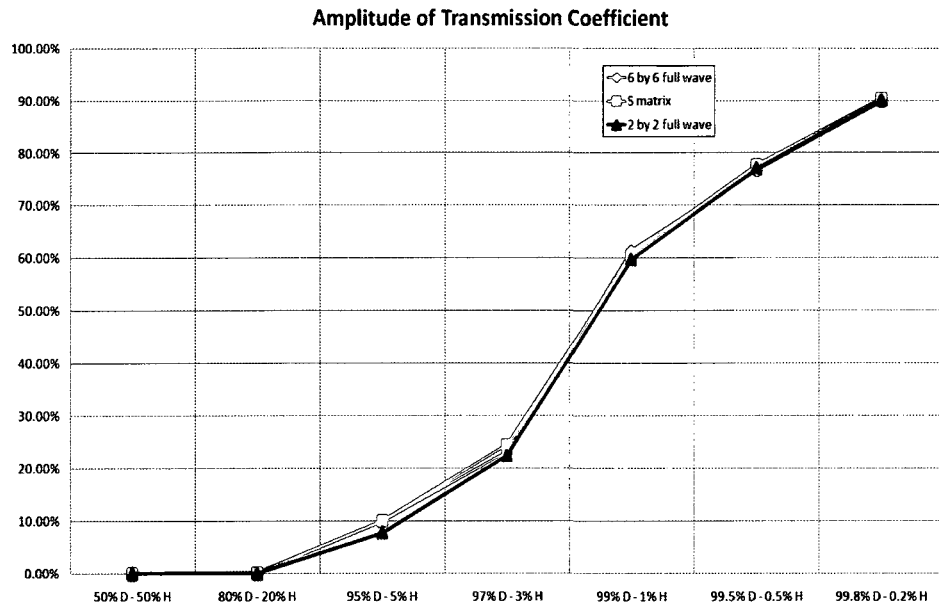


FIGURE 6.8 THE TRANSMISSION COEFFICIENT FROM THE 'FULL-WAVE' 6×6, 'REDUCED' 2×2 FULL WAVE AND 'RAY-BASED' S MATRIX PREDICTIONS FOR DIFFERENT ION DENSITIES.

Figure 6.8 shows that as the deuterium density increases and hydrogen density decreases correspondingly, the amplitude of transmission coefficient increases too, which means more energy transmits through the ion-hybrid gyroresonance layer.

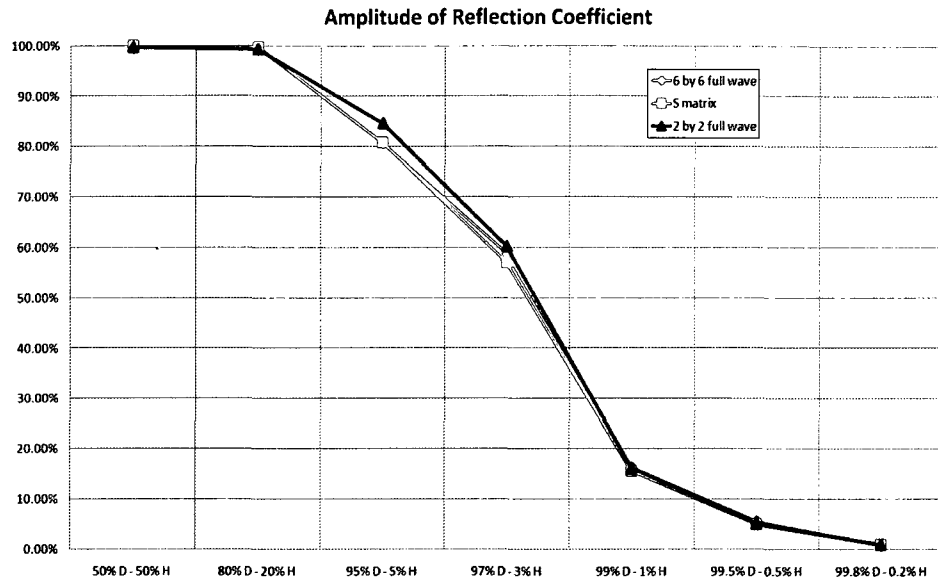


FIGURE 6.9 THE REFLECTION COEFFICIENT FROM THE 'FULL-WAVE' 6×6, 'REDUCED' 2×2 FULL WAVE AND 'RAY-BASED' S MATRIX PREDICTIONS FOR DIFFERENT ION DENSITIES.

Figure 6.8 shows that as the deuterium density increases and hydrogen decreases accordingly, the amplitude of reflection coefficient decreases, which means less energy converts back to the fast wave mode.

For each density, we find the 6×6 and 2×2 full wave results and the S matrix prediction match each other well, which shows that the ray tracing method of prediction is valid. The errors between the full-wave and ray-based S matrix prediction comes from several causes: 1] We used the finite-difference numerical calculations. 2] The polarizations used for the Galerkin projection we chose to reduce the 6×6 to the 2×2 form at the conversion point are obtained by linear interpolation. The resulting local wave operator is linearized, so higher order corrections are neglected. Physically, the Galerkin projection is accurate in the mode conversion region and it is less accurate

farther away from the conversion. 3] As discussed in Chapter 5, the S -matrix prediction is for a fixed frequency. However, our numerical calculation is for a (narrow-banded) wave packet which has a spread of frequencies.

Despite all the estimates we have made and the numerical errors we brought in, these results match very well with each other, which gives us confidence that ray-based methods give good results over the whole range of density ratios.

Chapter 7

Summary and conclusion

In this thesis I have provided the first direct comparison between full-wave and ray-based calculations of the important phenomenon of resonance crossing in nonuniform plasma.

In Chapter 2, we introduced our cold plasma model consisting of two ion species, deuterium and hydrogen, and electrons. We model the plasma as comprised of ideal charge-carrying fluids satisfying mass and momentum conservation equations. After sketching the derivation of this set of nonlinear partial differential equations, we linearized and then nondimensionalized them. We also discussed how to compute the total energy of the system. These cold plasma model equations are the focus of this dissertation, and the energy is the quantity we used for comparison to test the validity of our ray-based method.

We first studied this plasma in a uniform magnetic field in Chapter 3. Because of the uniformity, we could Fourier transform the partial differential equations and find the dispersion relations. The traditional approach eliminates all the variables in favor of the electric field. This obscures the physics when a magnetosonic wave packet and an ion-hybrid wave are resonant. When this resonance occurs, energy and action are exchanged between the two modes. This is the ‘mode conversion’ phenomenon. The

approach of Ye and Kaufman, which retains the ion velocities as dynamical variables in addition to the electric field, shows that the mode conversion is essentially a pair of avoided crossings. The ray-based approach, the real power of which only becomes apparent in nonuniform plasma, is based upon this fundamental insight.

In Chapter 4 we then extended our study from a uniform background to allow for nonuniformity in space, but the background is still assumed to be stationary in time. The avoided crossing now is local in x . Because of the nonuniformity, we cannot Fourier transform in space as we did in Chapter 3 but we can use WKB (ray tracing) methods away from the conversion region. The models we are studying have a nice property: there are no terms in the wave operator that involve products of x and $-i\partial_x$. Therefore we can avoid the full complication of the Weyl Symbol calculation to get the dispersion relations and can freely substitute k for $-i\partial_x$ to find the symbol of our dispersion matrix, Equation (4.10), which is dependent on x , k , and ω . Taking the determinant of the dispersion matrix gives the dispersion function. The zeros of the dispersion function give the dispersion surfaces, Figure (4.8). The dispersion function plays the role of Hamiltonian for the rays, Equation (4.20). These ray equations are valid away from the mode conversion region. We provided a very short summary of WKB methods for a general vector wave equation. As an illustration we also applied these methods to a simplified wave equation governing the interaction of the fast wave and

gyroresonance. We then went back to our cold plasma model and applied these WKB concepts away from the conversion.

In Chapter 5, we focused on the conversion region. We defined the notion of ‘uncoupled modes’, and used them to reduce our 6×6 matrix wave operator to a 2×2 reduced form *via* Galerkin projection. We then expand the symbol of this 2×2 wave operator around the two conversion points to get the S matrix at each of the two conversions, where we could get the transmission and conversion coefficients. Also, we investigated the double conversion and found that – as predicted by the Ye and Kaufman approach -- after launching an incoming wave in the fast wave mode, reflected waves appeared after a finite time delay in the $x-t$ domain.

In Chapter 6, we introduced the numerical calculations for our models. We applied the Crank-Nicolson method to our 6×6 full-wave equations and the 2×2 reduced model. The great advantage of the Crank-Nicolson method is that it gives unitary evolution (under discrete-time iteration), hence stability is assured. Other numerical methods we had examined for this calculation were not stable. We also compared transmission and conversion coefficients with the ray-based S -matrix predictions for a wide range of hydrogen/deuterium density ratios. Combining these predictions together in the appropriate way gives a ray-based prediction for the overall transmission and reflection coefficients from the ion-hybrid resonance. These three predictions matched very well, see Fig. 6.8 and 6.9, which verified both the 2×2 reduction and the related ray-based S -matrix method, which is based upon a local approximation

to the 2×2 reduced wave equation. This is an important result that supports the use of ray methods. One advantage of ray-based methods is that they only involve ordinary differential equations, which are much easier and faster to solve than partial differential equations.

We should comment on aspects of real plasma experiments that were left out of our study. Inclusion of these effects would provide fruitful extensions of the work presented in this thesis, but would have significantly complicated the analysis. We note that other full-wave simulations, even the most powerful computer codes currently available, also leave out many of these effects. This shows how much work there remains to be done. We used a linearized ideal fluid model assuming a quiescent and simple background magnetic field geometry, hence we did not include nonlinear effects, nontrivial magnetic field geometries characteristic of real fusion experiments, turbulent fluctuations in the background, viscous effects, or finite pressure. Because we used a fluid model, we did not include wave-particle resonance effects, or particle collisions, hence the eventual mechanism by which wave energy is finally thermalized by the ions is left out of our model. We assumed a globally-fixed density ratio of ion species. We included only three species (electrons, hydrogen and deuterium) and assumed full ionization, while a real experiment would have far more charged particle species due to impurities from the wall, and neutrals in the cooler plasma near the edge. Furthermore, we used very simple boundary conditions. The boundary of a real physical plasma is anything but simple. The coupling to the antenna was not treated

either, while real antenna physics is complex and hard to model because of near-field effects and the back-reaction of the plasma on the antenna.

In conclusion, this dissertation compared the full-wave calculation with the ray-based prediction for a one-dimensional cold plasma model including mode conversion and we successfully tested the validity of ray-based methods for this model. As a potential topic for future research, this work should be extended to multi-dimensional plasma problems including mode conversion. There now exist full-wave simulation tools that include mode conversion in realistic plasma models [46, 47,48]. The ray-based RAYCON algorithm [19] has also been developed which can be applied to the same models. But, they have yet to undergo careful benchmark comparison with one another, and neither have been validated against experimental results as of yet. Much remains to be done.

Appendix A

The momentum conversion equation gives a relationship between the particle disturbances and the electric field. When the unperturbed magnetic field is constant in time and homogenous in space, as we assume in Chapter 3, we linearize and Fourier transform the equations. Expressing the results in x, y, z components gives:

$$\begin{aligned}
 -i\omega \tilde{v}_{sx}^1(\vec{k}, \omega) &= \frac{1}{f_1} \frac{e_s}{m_s} \tilde{E}_x^1(\vec{k}, \omega) + \frac{e_s B^0}{m_s} \tilde{v}_{sy}^1(\vec{k}, \omega) \\
 -i\omega \tilde{v}_{sy}^1(\vec{k}, \omega) &= \frac{1}{f_1} \frac{e_s}{m_s} \tilde{E}_y^1(\vec{k}, \omega) - \frac{e_s B^0}{m_s} \tilde{v}_{sx}^1(\vec{k}, \omega) \\
 -i\omega \tilde{v}_{sz}^1(\vec{k}, \omega) &= \frac{1}{f_1} \frac{e_s}{m_s} \tilde{E}_z^1(\vec{k}, \omega)
 \end{aligned} \tag{A.1}$$

Define $\Omega_s \equiv \frac{e_s}{m_s} B^0$

Rearrange equation (A.1)

$$\begin{pmatrix} -i\omega & -\Omega_s & 0 \\ \Omega_s & -i\omega & 0 \\ 0 & 0 & -i\omega \end{pmatrix} \begin{pmatrix} \tilde{v}_{sx}^1 \\ \tilde{v}_{sy}^1 \\ \tilde{v}_{sz}^1 \end{pmatrix} = \frac{1}{f_1} \frac{e_s}{m_s} \begin{pmatrix} \tilde{E}_x^1 \\ \tilde{E}_y^1 \\ \tilde{E}_z^1 \end{pmatrix} \tag{A.2}$$

The matrix is not diagonal, but it is i multiplying a Hermitian matrix, so it has pure imaginary eigenvalues and can be diagonalized using the eigenvectors.

Here are the details:

Define a 3 by 3 transformation matrix $Q = \begin{pmatrix} \frac{\sqrt{2}}{2} & \frac{\sqrt{2}}{2} & 0 \\ \frac{\sqrt{2}}{2}i & -\frac{\sqrt{2}}{2}i & 0 \\ 0 & 0 & 1 \end{pmatrix}$ and its

$$\text{Hermitian adjoint } Q^\dagger = \begin{pmatrix} \frac{\sqrt{2}}{2} & -\frac{\sqrt{2}}{2}i & 0 \\ \frac{\sqrt{2}}{2} & \frac{\sqrt{2}}{2}i & 0 \\ 0 & 0 & 1 \end{pmatrix}, \quad QQ^\dagger = I.$$

Use Q and Q^\dagger to perform a similarity transformation on the matrix of equation (A.2).

$$\text{And } Q^\dagger \begin{pmatrix} -i\omega & -\Omega_s & 0 \\ \Omega_s & -i\omega & 0 \\ 0 & 0 & -i\omega \end{pmatrix} Q = \begin{pmatrix} -i\omega - i\Omega_s & & \\ & -i\omega + i\Omega_s & \\ & & -i\omega \end{pmatrix}$$

Define

$$Q^\dagger \begin{pmatrix} \tilde{v}_{sx}^1 \\ \tilde{v}_{sy}^1 \\ \tilde{v}_{sz}^1 \end{pmatrix} \equiv \begin{pmatrix} \tilde{v}_{sR}^1 \\ \tilde{v}_{sL}^1 \\ \tilde{v}_{sz}^1 \end{pmatrix} = \begin{pmatrix} \frac{\sqrt{2}}{2}(\tilde{v}_{sx}^1 - i\tilde{v}_{sy}^1) \\ \frac{\sqrt{2}}{2}(\tilde{v}_{sx}^1 + i\tilde{v}_{sy}^1) \\ \tilde{v}_{sz}^1 \end{pmatrix}, \quad Q^\dagger \begin{pmatrix} \tilde{E}_x^1 \\ \tilde{E}_y^1 \\ \tilde{E}_z^1 \end{pmatrix} \equiv \begin{pmatrix} \tilde{E}_R^1 \\ \tilde{E}_L^1 \\ \tilde{E}_z^1 \end{pmatrix} = \begin{pmatrix} \frac{\sqrt{2}}{2}(\tilde{E}_x^1 - i\tilde{E}_y^1) \\ \frac{\sqrt{2}}{2}(\tilde{E}_x^1 + i\tilde{E}_y^1) \\ \tilde{E}_z^1 \end{pmatrix}$$

So we get a diagonalized matrix by changing the basis from the x - y to the R - L basis.

$$\begin{pmatrix} -i\omega - i\Omega_s & & \\ & -i\omega + i\Omega_s & \\ & & -i\omega \end{pmatrix} \begin{pmatrix} \tilde{v}_{sR}^1 \\ \tilde{v}_{sL}^1 \\ \tilde{v}_{sz}^1 \end{pmatrix} = \frac{1}{f_1} \frac{e_s}{m_s} \begin{pmatrix} \tilde{E}_R^1 \\ \tilde{E}_L^1 \\ \tilde{E}_z^1 \end{pmatrix}. \quad (\text{A.3})$$

The Fourier transforms of Ampere's law and Faraday's equation are:

$$i\vec{k} \times \vec{\tilde{B}}^1(\vec{k}, \omega) = f_1^2 f_3^2 \sum_s n_s^0 e_s \vec{\tilde{v}}_s^1(\vec{k}, \omega) + f_1(-i\omega) \vec{\tilde{E}}^1(\vec{k}, \omega) \quad (\text{A.4})$$

$$i\vec{k} \times \vec{\tilde{E}}^1(\vec{k}, \omega) = i\omega f_1 \vec{\tilde{B}}^1(\vec{k}, \omega) \quad (\text{A.5})$$

From equations (A.4) and (A.5), we can eliminate $\vec{\tilde{B}}^1$ by multiplying both sides of equation (A.5) from the left by \vec{k} using the cross product and substituting $\vec{k} \times \vec{\tilde{B}}^1$ term by equation (A.4) yielding:

$$\begin{aligned} f_1^2 \omega^2 \vec{\tilde{E}}^1(\vec{k}, \omega) + \vec{k} \times \vec{k} \times \vec{\tilde{E}}^1(\vec{k}, \omega) &= -i\omega f_1^3 f_3^2 \sum_s n_s^0 e_s \vec{\tilde{v}}_s^1(\vec{k}, \omega) \\ &= -i\omega f_1^3 f_3^2 \left[n_D^0 e_D \vec{\tilde{v}}_D^1(\vec{k}, \omega) + n_H^0 e_H \vec{\tilde{v}}_H^1(\vec{k}, \omega) + n_e^0 e_e \vec{\tilde{v}}_e^1(\vec{k}, \omega) \right] \end{aligned} \quad (\text{A.6})$$

Multiply Q^\dagger from the left in equation (A.6)

$$\begin{aligned} f_1^2 \omega^2 Q^\dagger \vec{\tilde{E}}^1 + Q^\dagger \vec{k} \times \vec{k} \times \vec{\tilde{E}}^1 + i\omega f_1^3 f_3^2 n_D^0 e_D Q^\dagger \vec{\tilde{v}}_D^1 \\ + i\omega f_1^3 f_3^2 n_H^0 e_H Q^\dagger \vec{\tilde{v}}_H^1 = -i\omega f_1^3 f_3^2 n_e^0 e_e Q^\dagger \vec{\tilde{v}}_e^1 \end{aligned} \quad (\text{A.7})$$

And

$$\vec{k} \times \vec{k} \times \vec{\tilde{E}}^1 = \vec{k}(\vec{k} \cdot \vec{\tilde{E}}^1) - \vec{k}^2 \vec{\tilde{E}}^1 = \begin{pmatrix} k_x k_y \tilde{E}_y^1 + k_x k_z \tilde{E}_z^1 - k_y^2 \tilde{E}_x^1 - k_z^2 \tilde{E}_x^1 \\ k_x k_y \tilde{E}_x^1 + k_y k_z \tilde{E}_z^1 - k_x^2 \tilde{E}_y^1 - k_z^2 \tilde{E}_y^1 \\ k_x k_z \tilde{E}_x^1 + k_y k_z \tilde{E}_y^1 - k_x^2 \tilde{E}_z^1 - k_y^2 \tilde{E}_z^1 \end{pmatrix}$$

$$\begin{aligned}
Q^\dagger \bar{k} \times \bar{k} \times \tilde{E}^1 &= \begin{pmatrix} \frac{\sqrt{2}}{2} & -\frac{\sqrt{2}}{2}i & 0 \\ \frac{\sqrt{2}}{2} & \frac{\sqrt{2}}{2}i & 0 \\ 0 & 0 & 1 \end{pmatrix} \begin{pmatrix} k_x k_y \tilde{E}_y^1 + k_x k_z \tilde{E}_z^1 - k_y^2 \tilde{E}_x^1 - k_z^2 \tilde{E}_x^1 \\ k_x k_y \tilde{E}_x^1 + k_y k_z \tilde{E}_z^1 - k_x^2 \tilde{E}_y^1 - k_z^2 \tilde{E}_y^1 \\ k_x k_z \tilde{E}_x^1 + k_y k_z \tilde{E}_y^1 - k_x^2 \tilde{E}_z^1 - k_y^2 \tilde{E}_z^1 \end{pmatrix} \\
&= \frac{\sqrt{2}}{2} \begin{pmatrix} k_x k_y (\tilde{E}_y^1 - i\tilde{E}_x^1) + k_x k_z \tilde{E}_z^1 - ik_y k_z \tilde{E}_z^1 + ik_x^2 \tilde{E}_y^1 - k_y^2 \tilde{E}_x^1 - k_z^2 (\tilde{E}_x^1 - i\tilde{E}_y^1) \\ k_x k_y (\tilde{E}_y^1 + i\tilde{E}_x^1) + k_x k_z \tilde{E}_z^1 + ik_y k_z \tilde{E}_z^1 - ik_x^2 \tilde{E}_y^1 - k_y^2 \tilde{E}_x^1 - k_z^2 (\tilde{E}_x^1 + i\tilde{E}_y^1) \\ \sqrt{2} (k_x k_z \tilde{E}_x^1 + k_y k_z \tilde{E}_y^1 - k_x^2 \tilde{E}_z^1 - k_y^2 \tilde{E}_z^1) \end{pmatrix}
\end{aligned}$$

Because we defined $\begin{pmatrix} \tilde{E}_R^1 \\ \tilde{E}_L^1 \\ \tilde{E}_z^1 \end{pmatrix} = \begin{pmatrix} \frac{\sqrt{2}}{2} (\tilde{E}_x^1 - i\tilde{E}_y^1) \\ \frac{\sqrt{2}}{2} (\tilde{E}_x^1 + i\tilde{E}_y^1) \\ \tilde{E}_z^1 \end{pmatrix}$ and we have

$$\begin{pmatrix} \tilde{E}_x^1 \\ \tilde{E}_y^1 \\ \tilde{E}_z^1 \end{pmatrix} = \begin{pmatrix} \frac{\sqrt{2}}{2} (\tilde{E}_R^1 + \tilde{E}_L^1) \\ \frac{\sqrt{2}}{2} i (\tilde{E}_R^1 - \tilde{E}_L^1) \\ \tilde{E}_z^1 \end{pmatrix}, \text{ after substituting } E_x, E_y \text{ with } E_R \text{ and } E_L, \text{ we get:}$$

$$\begin{aligned}
Q^\dagger \bar{k} \times \bar{k} \times \tilde{E}^1 &= \begin{pmatrix} -ik_x k_y \tilde{E}_L^1 + \frac{\sqrt{2}}{2} k_x k_y \tilde{E}_z^1 - \frac{\sqrt{2}}{2} ik_x k_y \tilde{E}_z^1 - \frac{1}{2} k_y^2 (\tilde{E}_R^1 - \tilde{E}_L^1) - \frac{1}{2} k_y^2 (\tilde{E}_R^1 + \tilde{E}_L^1) - k_y^2 \tilde{E}_R^1 \\ ik_x k_y \tilde{E}_R^1 + \frac{\sqrt{2}}{2} k_x k_y \tilde{E}_z^1 + \frac{\sqrt{2}}{2} ik_x k_y \tilde{E}_z^1 + \frac{1}{2} k_y^2 (\tilde{E}_R^1 - \tilde{E}_L^1) - \frac{1}{2} k_y^2 (\tilde{E}_R^1 + \tilde{E}_L^1) - k_y^2 \tilde{E}_L^1 \\ \frac{\sqrt{2}}{2} k_x k_y (\tilde{E}_R^1 + \tilde{E}_L^1) \frac{\partial^2}{\partial x \partial z} + \frac{\sqrt{2}}{2} ik_x k_y (\tilde{E}_R^1 - \tilde{E}_L^1) \frac{\partial^2}{\partial y \partial z} - (k_x^2 + k_y^2) \tilde{E}_z^1 \end{pmatrix}
\end{aligned}$$

(A.8)

Substituting equation (A.8) into equation (A.7), we get

$$\begin{aligned}
& - \left(\begin{aligned}
& -ik_x k_y \tilde{E}_L^1 + \frac{\sqrt{2}}{2} k_x k_y \tilde{E}_z^1 - \frac{\sqrt{2}}{2} ik_x k_y \tilde{E}_z^1 - \frac{1}{2} k_y^2 (\tilde{E}_R^1 - \tilde{E}_L^1) - \frac{1}{2} k_y^2 (\tilde{E}_R^1 + \tilde{E}_L^1) - k_y^2 \tilde{E}_R^1 \\
& ik_x k_y \tilde{E}_R^1 + \frac{\sqrt{2}}{2} k_x k_y \tilde{E}_z^1 + \frac{\sqrt{2}}{2} ik_x k_y \tilde{E}_z^1 + \frac{1}{2} k_y^2 (\tilde{E}_R^1 - \tilde{E}_L^1) - \frac{1}{2} k_y^2 (\tilde{E}_R^1 + \tilde{E}_L^1) - k_y^2 \tilde{E}_L^1 \\
& \frac{\sqrt{2}}{2} k_x k_y (\tilde{E}_R^1 + \tilde{E}_L^1) \frac{\partial^2}{\partial x \partial z} + \frac{\sqrt{2}}{2} ik_x k_y (\tilde{E}_R^1 - \tilde{E}_L^1) \frac{\partial^2}{\partial y \partial z} - (k_x^2 + k_y^2) \tilde{E}_z^1
\end{aligned} \right) \\
& + f_1^2 \omega^2 \begin{pmatrix} \tilde{E}_R^1 \\ \tilde{E}_L^1 \\ \tilde{E}_z^1 \end{pmatrix} + i\omega f_1^3 f_3^2 n_D^0 e_D Q^\dagger \tilde{v}_D^1 + i\omega f_1^3 f_3^2 n_H^0 e_H Q^\dagger \tilde{v}_H^1 = -i\omega f_1^3 f_3^2 n_e^0 e_e Q^\dagger \tilde{v}_e^1
\end{aligned} \tag{A.9}$$

As stated before, we want to express all the variables in terms of the electric field and ion velocities, so we have to invert the equation (A.3) to express the *electron* velocity in terms of the electric field. The frequency range of interest is far below the electron gyrofrequency, so there are no singular denominator to worry about:

$$\begin{pmatrix} \tilde{v}_{eR}^1 \\ \tilde{v}_{eL}^1 \\ \tilde{v}_{ez}^1 \end{pmatrix} = \frac{1}{f_1} \frac{e_e}{m_e} \begin{pmatrix} \frac{i}{\omega + \Omega_e} & & \\ & \frac{i}{\omega - \Omega_e} & \\ & & \frac{i}{\omega} \end{pmatrix} \begin{pmatrix} \tilde{E}_R^1 \\ \tilde{E}_L^1 \\ \tilde{E}_z^1 \end{pmatrix} \tag{A.10}$$

$$\begin{aligned}
& \left(\begin{array}{c} -ik_x k_y \tilde{E}_L^1 + \frac{\sqrt{2}}{2} k_x k_y \tilde{E}_z^1 - \frac{\sqrt{2}}{2} ik_x k_y \tilde{E}_z^1 - \frac{1}{2} k_y^2 (\tilde{E}_R^1 - \tilde{E}_L^1) - \frac{1}{2} k_y^2 (\tilde{E}_R^1 + \tilde{E}_L^1) - k_y^2 \tilde{E}_R^1 \\ ik_x k_y \tilde{E}_R^1 + \frac{\sqrt{2}}{2} k_x k_y \tilde{E}_z^1 + \frac{\sqrt{2}}{2} ik_x k_y \tilde{E}_z^1 + \frac{1}{2} k_y^2 (\tilde{E}_R^1 - \tilde{E}_L^1) - \frac{1}{2} k_y^2 (\tilde{E}_R^1 + \tilde{E}_L^1) - k_y^2 \tilde{E}_L^1 \\ \frac{\sqrt{2}}{2} k_x k_y (\tilde{E}_R^1 + \tilde{E}_L^1) \frac{\partial^2}{\partial x \partial z} + \frac{\sqrt{2}}{2} ik_x k_y (\tilde{E}_R^1 - \tilde{E}_L^1) \frac{\partial^2}{\partial y \partial z} - (k_x^2 + k_y^2) \tilde{E}_z^1 \end{array} \right) \\
& - f_1^2 \omega^2 \begin{pmatrix} \tilde{E}_R^1 \\ \tilde{E}_L^1 \\ \tilde{E}_z^1 \end{pmatrix} - i\omega f_1^3 f_3^2 n_D^0 e_D Q^\dagger \tilde{v}_D^1 - i\omega f_1^3 f_3^2 n_H^0 e_H Q^\dagger \tilde{v}_H^1 \\
& = -f_1^2 f_3^2 n_e^0 \frac{e_e^2}{m_e} \begin{pmatrix} \frac{\omega}{\omega + \Omega_e} & & \\ & \frac{\omega}{\omega - \Omega_e} & \\ & & 1 \end{pmatrix} \begin{pmatrix} \tilde{E}_R^1 \\ \tilde{E}_L^1 \\ \tilde{E}_z^1 \end{pmatrix}
\end{aligned} \tag{A.11}$$

We can write equation (A.11) in a neat matrix form:

$$\underline{\underline{\tilde{D}}}_M \begin{pmatrix} \tilde{E}_R^1 \\ \tilde{E}_L^1 \\ \tilde{E}_z^1 \end{pmatrix} = i\omega f_1^3 f_3^2 n_D^0 e_D \begin{pmatrix} \tilde{v}_{DR}^1 \\ \tilde{v}_{DL}^1 \\ \tilde{v}_{Dz}^1 \end{pmatrix} + i\omega f_1^3 f_3^2 n_H^0 e_H \begin{pmatrix} \tilde{v}_{HR}^1 \\ \tilde{v}_{HL}^1 \\ \tilde{v}_{Hz}^1 \end{pmatrix} \tag{A.12}$$

Where the operator $\underline{\underline{\tilde{D}}}_M$ is defined as

$$\underline{\underline{\tilde{D}}}_M \equiv \begin{pmatrix} \tilde{D}_{11} & -\frac{1}{2} k_x^2 + \frac{1}{2} k_y^2 + ik_x k_y & \frac{\sqrt{2}}{2} (-k_x k_z + ik_y k_z) \\ -\frac{1}{2} k_x^2 + \frac{1}{2} k_y^2 - ik_x k_y & \tilde{D}_{22} & \frac{\sqrt{2}}{2} (-k_x k_z + ik_y k_z) \\ -\frac{\sqrt{2}}{2} (k_x k_z + ik_y k_z) & \frac{\sqrt{2}}{2} (-k_x k_z + ik_y k_z) & \tilde{D}_{33} \end{pmatrix} \tag{A.13}$$

$$\begin{aligned}\tilde{D}_{11} &\equiv -f_1^2 \omega^2 + \frac{(k_x^2 + k_y^2)}{2} + k_z^2 + f_1^2 f_3^2 \frac{n_e^0 e^2}{m_e} \frac{\omega}{\omega + \Omega_e} \\ \tilde{D}_{22} &\equiv -f_1^2 \omega^2 + \frac{(k_x^2 + k_y^2)}{2} + k_z^2 + f_1^2 f_3^2 \frac{n_e^0 e^2}{m_e} \frac{\omega}{\omega - \Omega_e} \\ \tilde{D}_{33} &\equiv -f_1^2 \omega^2 + k_x^2 + k_y^2 + f_1^2 f_3^2 \frac{n_e^0 e^2}{m_e}\end{aligned}$$

Recall that the deuterium and hydrogen ion velocities are subject to the linearized Lorentz force:

$$\begin{aligned}\begin{pmatrix} -i\omega - i\Omega_D & & \\ & -i\omega + i\Omega_D & \\ & & -i\omega \end{pmatrix} \begin{pmatrix} \tilde{v}_{DR}^1 \\ \tilde{v}_{DL}^1 \\ \tilde{v}_{Dz}^1 \end{pmatrix} &= \frac{1}{f_1} \frac{e_D}{m_D} \begin{pmatrix} \tilde{E}_R^1 \\ \tilde{E}_L^1 \\ \tilde{E}_z^1 \end{pmatrix} \\ \begin{pmatrix} -i\omega - i\Omega_H & & \\ & -i\omega + i\Omega_H & \\ & & -i\omega \end{pmatrix} \begin{pmatrix} \tilde{v}_{HR}^1 \\ \tilde{v}_{HL}^1 \\ \tilde{v}_{Hz}^1 \end{pmatrix} &= \frac{1}{f_1} \frac{e_H}{m_H} \begin{pmatrix} \tilde{E}_R^1 \\ \tilde{E}_L^1 \\ \tilde{E}_z^1 \end{pmatrix}\end{aligned}\tag{A.14}$$

If we combine the two sets of matrix (A.13) and (A.14), we will get a 9×9 matrix:

$$\begin{pmatrix}
\tilde{D}_{11} & -i\omega f_1^1 f_1^2 n_p^0 e_p & -i\omega f_1^1 f_1^2 n_H^0 e_H & -\frac{1}{2}k_x^2 + \frac{1}{2}k_y^2 + ik_x k_y & 0 & 0 & \frac{\sqrt{2}}{2}(-k_x k_z + ik_y k_z) & 0 & 0 \\
\frac{1}{f_1} \frac{e_p}{m_p} & i(\omega + \Omega_p) & 0 & 0 & 0 & 0 & 0 & 0 & 0 \\
\frac{1}{f_1} \frac{e_H}{m_H} & 0 & i(\omega + \Omega_H) & 0 & 0 & 0 & 0 & 0 & 0 \\
-\frac{1}{2}k_x^2 + \frac{1}{2}k_y^2 - ik_x k_y & 0 & 0 & \tilde{D}_{22} & -i\omega f_1^1 f_1^2 n_p^0 e_p & -i\omega f_1^1 f_1^2 n_H^0 e_H & \frac{\sqrt{2}}{2}(-k_x k_z - ik_y k_z) & 0 & 0 \\
0 & 0 & 0 & \frac{1}{f_1} \frac{e_p}{m_p} & i(\omega - \Omega_p) & 0 & 0 & 0 & 0 \\
0 & 0 & 0 & \frac{1}{f_1} \frac{e_H}{m_H} & 0 & i(\omega - \Omega_H) & 0 & 0 & 0 \\
\frac{\sqrt{2}}{2}(-k_x k_z - ik_y k_z) & 0 & 0 & \frac{\sqrt{2}}{2}(-k_x k_z + ik_y k_z) & 0 & 0 & D_{33} & -i\omega f_1^1 f_1^2 n_p^0 e_p & -i\omega f_1^1 f_1^2 n_H^0 e_H \\
0 & 0 & 0 & 0 & 0 & 0 & \frac{1}{f_1} \frac{e_p}{m_p} & i\omega & 0 \\
0 & 0 & 0 & 0 & 0 & 0 & \frac{1}{f_1} \frac{e_H}{m_H} & 0 & i\omega
\end{pmatrix}
\begin{pmatrix}
\tilde{E}_x \\
\tilde{v}_{2p} \\
\tilde{v}_{2H} \\
\tilde{E}_y \\
\tilde{v}_{1p} \\
\tilde{E}_z \\
\tilde{v}_{1H}
\end{pmatrix} = 0$$

This is the result we needed for the discussion of the Kaufman-Ye method in

Chapter 3

APPENDIX B

In Appendix A, we dealt with uniform plasma. Here we extend our analysis to nonuniform plasma. The momentum conservation equation provides a relationship between the particle disturbances and the electric and magnetic fields. When the undisturbed magnetic field is constant in time and slowly varying in space, linearize the equations and Fourier transform in time. In x, y, z components the result is:

$$\begin{aligned}
 -i\omega \tilde{v}_{sx}^1(\vec{x}, \omega) &= \frac{1}{f_1} \frac{e_s}{m_s} \tilde{E}_x^1(\vec{x}, \omega) + \frac{e_s B^0(x)}{m_s} \tilde{v}_{sy}^1(\vec{x}, \omega) \\
 -i\omega \tilde{v}_{sy}^1(\vec{x}, \omega) &= \frac{1}{f_1} \frac{e_s}{m_s} \tilde{E}_y^1(\vec{x}, \omega) - \frac{e_s B^0(x)}{m_s} \tilde{v}_{sx}^1(\vec{x}, \omega) \\
 -i\omega \tilde{v}_{sz}^1(\vec{x}, \omega) &= \frac{1}{f_1} \frac{e_s}{m_s} \tilde{E}_z^1(\vec{x}, \omega)
 \end{aligned} \tag{B.1}$$

The gyrofrequency for each plasma species is defined as usual

$$\Omega_s(x) \equiv f_2 \frac{e_s}{m_s} B^0(x), \text{ but it is now spatially dependent.}$$

Rearranging equation (B.1) we have:

$$\begin{pmatrix} -i\omega & -\Omega_s(x) & 0 \\ \Omega_s(x) & -i\omega & 0 \\ 0 & 0 & -i\omega \end{pmatrix} \begin{pmatrix} \tilde{v}_{sx}^1 \\ \tilde{v}_{sy}^1 \\ \tilde{v}_{sz}^1 \end{pmatrix} = \frac{1}{f_1} \frac{e_s}{m_s} \begin{pmatrix} \tilde{E}_x^1 \\ \tilde{E}_y^1 \\ \tilde{E}_z^1 \end{pmatrix}. \tag{B.2}$$

As in Appendix A, this matrix can be diagonalized.

The linearized Fourier transformation of Ampere's law and Faraday's law are:

$$\nabla \times \tilde{\vec{B}}^1(\vec{x}, \omega) = \frac{f_1^2 f_3^2}{f_2} \sum_s n_s^0 e_s \tilde{\vec{v}}_s^1(\vec{x}, \omega) + f_1 (-i\omega) \tilde{\vec{E}}^1(\vec{x}, \omega) \tag{B.3}$$

$$\nabla \times \tilde{\tilde{E}}^1(\vec{x}, \omega) = i\omega f_1 \tilde{\tilde{B}}^1(\vec{x}, \omega) \quad (\text{B.4})$$

From equations (B.3) and (B.4), we can eliminate \tilde{B}^1 by taking the curl of both sides of Equation (B.5) and using Equation (B.3), yielding:

$$\begin{aligned} f_1^2 \omega^2 \tilde{\tilde{E}}^1(\vec{x}, \omega) + \nabla \times \nabla \times \tilde{\tilde{E}}^1(\vec{x}, \omega) &= -i\omega f_1^3 f_3^2 \sum_s n_s^0 e_s \tilde{\tilde{v}}_s^1(\vec{x}, \omega) \\ &= -i\omega f_1^3 f_3^2 \left[n_D^0 e_D \tilde{\tilde{v}}_D^1(\vec{x}, \omega) + n_H^0 e_H \tilde{\tilde{v}}_H^1(\vec{x}, \omega) + n_e^0 e_e \tilde{\tilde{v}}_e^1(\vec{x}, \omega) \right] \end{aligned} \quad (\text{B.5})$$

Multiply Q^\dagger on the right of equation (B.5)

$$\begin{aligned} f_1^2 \omega^2 Q^\dagger \tilde{\tilde{E}}^1 + Q^\dagger \nabla \times \nabla \times \tilde{\tilde{E}}^1 + i\omega f_1^3 f_3^2 n_D^0 e_D Q^\dagger \tilde{\tilde{v}}_D^1 \\ + i\omega f_1^3 f_3^2 n_H^0 e_H Q^\dagger \tilde{\tilde{v}}_H^1 = -i\omega f_1^3 f_3^2 n_e^0 e_e Q^\dagger \tilde{\tilde{v}}_e^1 \end{aligned} \quad (\text{B.6})$$

And

$$\nabla \times \nabla \times \tilde{\tilde{E}}^1 = \nabla(\nabla \cdot \tilde{\tilde{E}}^1) - \nabla^2 \tilde{\tilde{E}}^1 = \begin{pmatrix} \frac{\partial^2 \tilde{E}_y^1}{\partial x \partial y} + \frac{\partial^2 \tilde{E}_z^1}{\partial x \partial z} - \frac{\partial^2 \tilde{E}_x^1}{\partial y^2} - \frac{\partial^2 \tilde{E}_x^1}{\partial z^2} \\ \frac{\partial^2 \tilde{E}_x^1}{\partial x \partial y} + \frac{\partial^2 \tilde{E}_z^1}{\partial y \partial z} - \frac{\partial^2 \tilde{E}_y^1}{\partial x^2} - \frac{\partial^2 \tilde{E}_y^1}{\partial z^2} \\ \frac{\partial^2 \tilde{E}_x^1}{\partial x \partial z} + \frac{\partial^2 \tilde{E}_y^1}{\partial y \partial z} - \frac{\partial^2 \tilde{E}_z^1}{\partial x^2} - \frac{\partial^2 \tilde{E}_z^1}{\partial y^2} \end{pmatrix}$$

$$\begin{aligned}
Q^\dagger \nabla \times \nabla \times \tilde{\mathbf{E}}^1 &= \begin{pmatrix} \frac{\sqrt{2}}{2} & -\frac{\sqrt{2}}{2}i & 0 \\ \frac{\sqrt{2}}{2} & \frac{\sqrt{2}}{2}i & 0 \\ 0 & 0 & 1 \end{pmatrix} \begin{pmatrix} \frac{\partial^2 \tilde{E}_y^1}{\partial x \partial y} + \frac{\partial^2 \tilde{E}_z^1}{\partial x \partial z} - \frac{\partial^2 \tilde{E}_x^1}{\partial y^2} - \frac{\partial^2 \tilde{E}_x^1}{\partial z^2} \\ \frac{\partial^2 \tilde{E}_x^1}{\partial x \partial y} + \frac{\partial^2 \tilde{E}_z^1}{\partial y \partial z} - \frac{\partial^2 \tilde{E}_y^1}{\partial x^2} - \frac{\partial^2 \tilde{E}_y^1}{\partial z^2} \\ \frac{\partial^2 \tilde{E}_x^1}{\partial x \partial z} + \frac{\partial^2 \tilde{E}_y^1}{\partial y \partial z} - \frac{\partial^2 \tilde{E}_z^1}{\partial x^2} - \frac{\partial^2 \tilde{E}_z^1}{\partial y^2} \end{pmatrix} \\
&= \frac{\sqrt{2}}{2} \begin{pmatrix} \frac{\partial^2 (\tilde{E}_y^1 - i\tilde{E}_x^1)}{\partial x \partial y} + \frac{\partial^2 \tilde{E}_z^1}{\partial x \partial z} - i \frac{\partial^2 \tilde{E}_z^1}{\partial y \partial z} + i \frac{\partial^2 \tilde{E}_y^1}{\partial x^2} - \frac{\partial^2 \tilde{E}_x^1}{\partial y^2} - \frac{\partial^2 (\tilde{E}_x^1 - i\tilde{E}_y^1)}{\partial z^2} \\ \frac{\partial^2 (\tilde{E}_y^1 + i\tilde{E}_x^1)}{\partial x \partial y} + \frac{\partial^2 \tilde{E}_z^1}{\partial x \partial z} + i \frac{\partial^2 \tilde{E}_z^1}{\partial y \partial z} - i \frac{\partial^2 \tilde{E}_y^1}{\partial x^2} - \frac{\partial^2 \tilde{E}_x^1}{\partial y^2} - \frac{\partial^2 (\tilde{E}_x^1 + i\tilde{E}_y^1)}{\partial z^2} \\ \sqrt{2} \left(\frac{\partial^2 \tilde{E}_x^1}{\partial x \partial z} + \frac{\partial^2 \tilde{E}_y^1}{\partial y \partial z} - \frac{\partial^2 \tilde{E}_z^1}{\partial x^2} - \frac{\partial^2 \tilde{E}_z^1}{\partial y^2} \right) \end{pmatrix}
\end{aligned}$$

Because we defined $\begin{pmatrix} \tilde{E}_R^1 \\ \tilde{E}_L^1 \\ \tilde{E}_z^1 \end{pmatrix} = \begin{pmatrix} \frac{\sqrt{2}}{2} (\tilde{E}_x^1 - i\tilde{E}_y^1) \\ \frac{\sqrt{2}}{2} (\tilde{E}_x^1 + i\tilde{E}_y^1) \\ \tilde{E}_z^1 \end{pmatrix}$ and we have

$$\begin{pmatrix} \tilde{E}_x^1 \\ \tilde{E}_y^1 \\ \tilde{E}_z^1 \end{pmatrix} = \begin{pmatrix} \frac{\sqrt{2}}{2} (\tilde{E}_R^1 + \tilde{E}_L^1) \\ \frac{\sqrt{2}}{2} i (\tilde{E}_R^1 - \tilde{E}_L^1) \\ \tilde{E}_z^1 \end{pmatrix}$$

After substituting E_x, E_y with E_R and E_L , we get:

$$Q^\dagger \nabla \times \nabla \times \tilde{\mathbf{E}}^1 = \begin{pmatrix} -i \frac{\partial^2 \tilde{E}_L^1}{\partial x \partial y} + \frac{\sqrt{2}}{2} \frac{\partial^2 \tilde{E}_z^1}{\partial x \partial z} - \frac{\sqrt{2}}{2} i \frac{\partial^2 \tilde{E}_z^1}{\partial y \partial z} - \frac{1}{2} \frac{\partial^2 (\tilde{E}_R^1 - \tilde{E}_L^1)}{\partial x^2} - \frac{1}{2} \frac{\partial^2 (\tilde{E}_R^1 + \tilde{E}_L^1)}{\partial y^2} - \frac{\partial^2 \tilde{E}_R^1}{\partial z^2} \\ i \frac{\partial^2 \tilde{E}_R^1}{\partial x \partial y} + \frac{\sqrt{2}}{2} \frac{\partial^2 \tilde{E}_z^1}{\partial x \partial z} + \frac{\sqrt{2}}{2} i \frac{\partial^2 \tilde{E}_z^1}{\partial y \partial z} + \frac{1}{2} \frac{\partial^2 (\tilde{E}_R^1 - \tilde{E}_L^1)}{\partial x^2} - \frac{1}{2} \frac{\partial^2 (\tilde{E}_R^1 + \tilde{E}_L^1)}{\partial y^2} - \frac{\partial^2 \tilde{E}_L^1}{\partial z^2} \\ \frac{\sqrt{2}}{2} \frac{\partial^2 (\tilde{E}_R^1 + \tilde{E}_L^1)}{\partial x \partial z} + \frac{\sqrt{2}}{2} i \frac{\partial^2 (\tilde{E}_R^1 - \tilde{E}_L^1)}{\partial y \partial z} - \left(\frac{\partial^2 \tilde{E}_z^1}{\partial x^2} + \frac{\partial^2 \tilde{E}_z^1}{\partial y^2} \right) \end{pmatrix}$$

(B.7)

Substituting equation (B.7) into equation (B.6), we get

$$\begin{aligned}
& - \left(-i \frac{\partial^2 \tilde{E}_L^1}{\partial x \partial y} + \frac{\sqrt{2}}{2} \frac{\partial^2 \tilde{E}_z^1}{\partial x \partial z} - \frac{\sqrt{2}}{2} i \frac{\partial^2 \tilde{E}_z^1}{\partial y \partial z} - \frac{1}{2} \frac{\partial^2 (\tilde{E}_R^1 - \tilde{E}_L^1)}{\partial x^2} - \frac{1}{2} \frac{\partial^2 (\tilde{E}_R^1 + \tilde{E}_L^1)}{\partial y^2} - \frac{\partial^2 \tilde{E}_R^1}{\partial z^2} \right. \\
& \left. + i \frac{\partial^2 \tilde{E}_R^1}{\partial x \partial y} + \frac{\sqrt{2}}{2} \frac{\partial^2 \tilde{E}_z^1}{\partial x \partial z} + \frac{\sqrt{2}}{2} i \frac{\partial^2 \tilde{E}_z^1}{\partial y \partial z} + \frac{1}{2} \frac{\partial^2 (\tilde{E}_R^1 - \tilde{E}_L^1)}{\partial x^2} - \frac{1}{2} \frac{\partial^2 (\tilde{E}_R^1 + \tilde{E}_L^1)}{\partial y^2} - \frac{\partial^2 \tilde{E}_L^1}{\partial z^2} \right. \\
& \left. + \frac{\sqrt{2}}{2} \frac{\partial^2 (\tilde{E}_R^1 + \tilde{E}_L^1)}{\partial x \partial z} + \frac{\sqrt{2}}{2} i \frac{\partial^2 (\tilde{E}_R^1 - \tilde{E}_L^1)}{\partial y \partial z} - \left(\frac{\partial^2 \tilde{E}_z^1}{\partial x^2} + \frac{\partial^2 \tilde{E}_z^1}{\partial y^2} \right) \right) \\
& + f_1^2 \omega^2 \begin{pmatrix} \tilde{E}_R^1 \\ \tilde{E}_L^1 \\ \tilde{E}_z^1 \end{pmatrix} + i \omega f_1^3 f_3^2 n_D^0 e_D Q^\dagger \tilde{v}_D^1 + i \omega f_1^3 f_3^2 n_H^0 e_H Q^\dagger \tilde{v}_H^1 = -i \omega f_1^3 f_3^2 n_e^0 e_e Q^\dagger \tilde{v}_e^1
\end{aligned}
\tag{B.8}$$

As stated before, we want to express all the variables in terms of the electric field and ion velocities, so we to express the electron velocity in terms of the electric field.

$$\begin{pmatrix} \tilde{v}_{eR}^1 \\ \tilde{v}_{eL}^1 \\ \tilde{v}_{ez}^1 \end{pmatrix} = \frac{1}{f_1} \frac{e_e}{m_e} \begin{pmatrix} \frac{i}{\omega + \Omega_e(x)} & & \\ & \frac{i}{\omega - \Omega_e(x)} & \\ & & \frac{i}{\omega} \end{pmatrix} \begin{pmatrix} \tilde{E}_R^1 \\ \tilde{E}_L^1 \\ \tilde{E}_z^1 \end{pmatrix}$$

(B.9)

$$\begin{aligned}
& \left(\begin{array}{c} -i \frac{\partial^2 \tilde{E}_L^1}{\partial x \partial y} + \frac{\sqrt{2}}{2} \frac{\partial^2 \tilde{E}_z^1}{\partial x \partial z} - \frac{\sqrt{2}}{2} i \frac{\partial^2 \tilde{E}_z^1}{\partial y \partial z} - \frac{1}{2} \frac{\partial^2 (\tilde{E}_R^1 - \tilde{E}_L^1)}{\partial x^2} - \frac{1}{2} \frac{\partial^2 (\tilde{E}_R^1 + \tilde{E}_L^1)}{\partial y^2} - \frac{\partial^2 \tilde{E}_R^1}{\partial z^2} \\ i \frac{\partial^2 \tilde{E}_R^1}{\partial x \partial y} + \frac{\sqrt{2}}{2} \frac{\partial^2 \tilde{E}_z^1}{\partial x \partial z} + \frac{\sqrt{2}}{2} i \frac{\partial^2 \tilde{E}_z^1}{\partial y \partial z} + \frac{1}{2} \frac{\partial^2 (\tilde{E}_R^1 - \tilde{E}_L^1)}{\partial x^2} - \frac{1}{2} \frac{\partial^2 (\tilde{E}_R^1 + \tilde{E}_L^1)}{\partial y^2} - \frac{\partial^2 \tilde{E}_L^1}{\partial z^2} \\ \frac{\sqrt{2}}{2} \frac{\partial^2 (\tilde{E}_R^1 + \tilde{E}_L^1)}{\partial x \partial z} + \frac{\sqrt{2}}{2} i \frac{\partial^2 (\tilde{E}_R^1 - \tilde{E}_L^1)}{\partial y \partial z} - \left(\frac{\partial^2 \tilde{E}_z^1}{\partial x^2} + \frac{\partial^2 \tilde{E}_z^1}{\partial y^2} \right) \end{array} \right) \\
& - f_1^2 \omega^2 \begin{pmatrix} \tilde{E}_R^1 \\ \tilde{E}_L^1 \\ \tilde{E}_Z^1 \end{pmatrix} - i \omega f_1^3 f_3^2 n_D^0 e_D Q^\dagger \tilde{v}_D^1 - i \omega f_1^3 f_3^2 n_H^0 e_H Q^\dagger \tilde{v}_H^1 \\
& = -f_1^2 f_3^2 n_e^0 \frac{e_e^2}{m_e} \begin{pmatrix} \frac{\omega}{\omega + \Omega_e(x)} & & \\ & \frac{\omega}{\omega - \Omega_e(x)} & \\ & & 1 \end{pmatrix} \begin{pmatrix} \tilde{E}_R^1 \\ \tilde{E}_L^1 \\ \tilde{E}_Z^1 \end{pmatrix}
\end{aligned}$$

(B.10)

Write equation (B.10) in a matrix operator form:

$$\underline{\underline{\tilde{D}}}_M \begin{pmatrix} \tilde{E}_R^1 \\ \tilde{E}_L^1 \\ \tilde{E}_Z^1 \end{pmatrix} = i \omega f_1^3 f_3^2 n_D^0 e_D \begin{pmatrix} \tilde{v}_{DR}^1 \\ \tilde{v}_{DL}^1 \\ \tilde{v}_{Dz}^1 \end{pmatrix} + i \omega f_1^3 f_3^2 n_H^0 e_H \begin{pmatrix} \tilde{v}_{HR}^1 \\ \tilde{v}_{HL}^1 \\ \tilde{v}_{Hz}^1 \end{pmatrix} \quad (\text{B.11})$$

Where operator $\underline{\underline{\tilde{D}}}_M$ is defined as

$$\underline{\underline{\tilde{D}}}_M \equiv \begin{pmatrix} \hat{D}_{11} & \frac{1}{2} \partial_x^2 - \frac{1}{2} \partial_y^2 - i \partial x \partial y & \frac{\sqrt{2}}{2} (\partial x \partial z - i \partial y \partial z) \\ \frac{1}{2} \partial_x^2 - \frac{1}{2} \partial_y^2 + i \partial x \partial y & \hat{D}_{22} & \frac{\sqrt{2}}{2} (\partial x \partial z + i \partial y \partial z) \\ \frac{\sqrt{2}}{2} (\partial x \partial z + i \partial y \partial z) & \frac{\sqrt{2}}{2} (\partial x \partial z - i \partial y \partial z) & \hat{D}_{33} \end{pmatrix} \quad (\text{B.12})$$

$$\begin{aligned}\hat{D}_{11} &\equiv -f_1^2 \omega^2 - \frac{(\partial_x^2 + \partial_y^2)}{2} + k_z^2 + f_1^2 f_3^2 \frac{n_e^0 e^2}{m_e} \frac{\omega}{\omega + \Omega_e} \\ \hat{D}_{22} &\equiv -f_1^2 \omega^2 - \frac{(\partial_x^2 + \partial_y^2)}{2} + k_z^2 + f_1^2 f_3^2 \frac{n_e^0 e^2}{m_e} \frac{\omega}{\omega - \Omega_e} \\ \hat{D}_{33} &\equiv -f_1^2 \omega^2 - \partial_x^2 - \partial_y^2 + f_1^2 f_3^2 \frac{n_e^0 e^2}{m_e}\end{aligned}$$

Recall that the deuterium and hydrogen ions motions are given by the linearized Lorentz force law:

$$\begin{aligned}\begin{pmatrix} -i\omega - i\Omega_D(x) & & \\ & -i\omega + i\Omega_D(x) & \\ & & -i\omega \end{pmatrix} \begin{pmatrix} \tilde{v}_{DR}^1 \\ \tilde{v}_{DL}^1 \\ \tilde{v}_{Dz}^1 \end{pmatrix} &= \frac{1}{f_1} \frac{e_D}{m_D} \begin{pmatrix} \tilde{E}_R^1 \\ \tilde{E}_L^1 \\ \tilde{E}_z^1 \end{pmatrix} \\ \begin{pmatrix} -i\omega - i\Omega_H(x) & & \\ & -i\omega + i\Omega_H(x) & \\ & & -i\omega \end{pmatrix} \begin{pmatrix} \tilde{v}_{HR}^1 \\ \tilde{v}_{HL}^1 \\ \tilde{v}_{Hz}^1 \end{pmatrix} &= \frac{1}{f_1} \frac{e_H}{m_H} \begin{pmatrix} \tilde{E}_R^1 \\ \tilde{E}_L^1 \\ \tilde{E}_z^1 \end{pmatrix}\end{aligned}\tag{B.13}$$

If we combine the two sets of matrix (B.12) and (B.13), we will get – finally –
- the 9 by 9 matrix operator for the non-uniform Deuterium-Hydrogen-
Electron plasma we quoted in Chapter 4:

$$\begin{pmatrix}
\tilde{D}_n & -i\omega f_1 f_1^2 n_0^2 \epsilon_0 & -i\omega f_1 f_1^2 n_0^2 \epsilon_n & \frac{1}{2} \partial_t^2 - \frac{1}{2} \partial_t^2 - i\partial_t \partial_z & 0 & 0 & \frac{\sqrt{2}}{2} (i\partial_z - i\partial_t \partial_z) & 0 & 0 \\
\frac{1}{f_1 m_0} \epsilon_0 & f(\omega + \Omega_n(x)) & 0 & 0 & 0 & 0 & 0 & 0 & 0 \\
\frac{1}{f_1 m_n} \epsilon_n & 0 & f(\omega + \Omega_n(x)) & 0 & 0 & 0 & 0 & 0 & 0 \\
\frac{1}{2} \partial_t^2 - \frac{1}{2} \partial_t^2 + i\partial_t \partial_z & 0 & 0 & \tilde{D}_n & -i\omega f_1 f_1^2 n_0^2 \epsilon_0 & -i\omega f_1 f_1^2 n_0^2 \epsilon_n & \frac{\sqrt{2}}{2} (i\partial_z + i\partial_t \partial_z) & 0 & 0 \\
0 & 0 & 0 & \frac{1}{f_1 m_0} \epsilon_0 & f(\omega - \Omega_n(x)) & 0 & 0 & 0 & 0 \\
0 & 0 & 0 & \frac{1}{f_1 m_n} \epsilon_n & 0 & f(\omega - \Omega_n(x)) & 0 & 0 & 0 \\
\frac{\sqrt{2}}{2} (i\partial_z + i\partial_t \partial_z) & 0 & 0 & \frac{\sqrt{2}}{2} (i\partial_z - i\partial_t \partial_z) & 0 & 0 & \tilde{D}_n & -i\omega f_1 f_1^2 n_0^2 \epsilon_0 & -i\omega f_1 f_1^2 n_0^2 \epsilon_n \\
0 & 0 & 0 & 0 & 0 & 0 & \frac{1}{f_1 m_0} \epsilon_0 & i\omega & 0 \\
0 & 0 & 0 & 0 & 0 & 0 & \frac{1}{f_1 m_n} \epsilon_n & 0 & i\omega
\end{pmatrix}
\begin{pmatrix}
\tilde{E}_n^+ \\
\tilde{E}_{nm}^+ \\
\tilde{E}_{nm}^- \\
\tilde{E}_n^- \\
\tilde{E}_z^+ \\
\tilde{E}_z^- \\
\tilde{E}_n^+ \\
\tilde{E}_n^-
\end{pmatrix}
= 0$$

Appendix C

The Crank-Nicolson method is an implicit finite differencing method that gives unconditionally stable numerical results for certain types of partial differential equations. We represent a function $\phi(x,t)$ by its values at the discrete set of points in space and discrete time by choosing equally spaced points along both time and space axes.

$$\begin{aligned}x_j &= x_0 + j\Delta x, \quad j = 0, 1, \dots, x_j \\t_n &= t_0 + n\Delta t, \quad n = 0, 1, \dots, t_N\end{aligned}$$

Let ϕ_j^n denote $\phi(x_j, t_n)$. We used the zero boundary condition for simplicity, which is $\phi(1, t_n) = 0, \phi(x_j, t_n) = 0$. This will cause artificial reflections, but we make the computational box large enough so the conversion process we are interested in can complete itself before the wave packets reflected at the box boundaries reenter the conversion region.

There are several ways to represent the time derivative term. The obvious one is $\frac{\partial \phi}{\partial t} \Big|_{j,n} \simeq \frac{\phi_j^{n+1} - \phi_j^n}{\Delta t}$. This is called forward Euler differencing and is first-order accurate in Δt . By giving the value at timestep n , we can obtain the value at $n+1$. For the second order spatial derivative, we will use Crank-Nicolson differencing:

$$\frac{\partial^2 \phi}{\partial x^2} \Big|_{j,n} \simeq \frac{(\phi_{j+1}^{n+1} - 2\phi_j^{n+1} + \phi_{j-1}^{n+1}) + (\phi_{j+1}^n - 2\phi_j^n + \phi_{j-1}^n)}{2(\Delta x)^2}$$

which is the two-step time average of implicit and explicit centered spatial differencing schemes.

Replace the differential equations $\hat{\underline{R}} \cdot \underline{V}(x, t) = 0$ with the Crank-

Nicolson differencing where

$$\hat{\underline{R}} \equiv \begin{pmatrix} \hat{D}_{11} & \frac{f_1^3 f_3^2}{f_2} n_D^0 e_D \partial_t & \frac{f_1^3 f_3^2}{f_2} n_H^0 e_H \partial_t & \frac{1}{2} \partial_x^2 & 0 & 0 \\ \frac{f_2 e_D}{f_1 m_D} & -\partial_t + i\Omega_D(x) & 0 & 0 & 0 & 0 \\ \frac{f_2 e_H}{f_1 m_H} & 0 & -\partial_t + i\Omega_H(x) & 0 & 0 & 0 \\ \frac{1}{2} \partial_x^2 & 0 & 0 & \hat{D}_{22} & \frac{f_1^3 f_3^2}{f_2} n_D^0 e_D \partial_t & \frac{f_1^3 f_3^2}{f_2} n_H^0 e_H \partial_t \\ 0 & 0 & 0 & \frac{f_2 e_D}{f_1 m_D} & -\partial_t - i\Omega_D(x) & 0 \\ 0 & 0 & 0 & \frac{f_2 e_H}{f_1 m_H} & 0 & -\partial_t - i\Omega_H(x) \end{pmatrix}$$

$$\hat{D}_{11}(i\partial_x, x, -i\partial_t) \equiv -\frac{\partial_x^2}{2} + i f_1^2 f_3^2 \frac{n_e^0 e_e^2}{m_e \Omega_e(x)} \partial_t$$

$$\hat{D}_{22}(i\partial_x, x, -i\partial_t) \equiv -\frac{\partial_x^2}{2} - i f_1^2 f_3^2 \frac{n_e^0 e_e^2}{m_e \Omega_e(x)} \partial_t$$

$$\underline{V}(x, t) \equiv \begin{pmatrix} E_R(x, t) \\ v_{DR}(x, t) \\ v_{HR}(x, t) \\ E_L(x, t) \\ v_{DL}(x, t) \\ v_{HL}(x, t) \end{pmatrix}.$$

and $\underline{\underline{A}}_1, \underline{\underline{A}}_2, \underline{\underline{A}}_3, \underline{\underline{B}}_1, \underline{\underline{B}}_2, \underline{\underline{B}}_3$ are all 6×6 matrices. Recall we used the zero boundaries here.

After inverting the matrix $\underline{\underline{A}}$, we will get an explicit result:

$$\begin{pmatrix} \underline{V}_1 \\ \underline{V}_2 \\ \vdots \\ \underline{V}_{x_j} \end{pmatrix}^{n+1} = \underline{\underline{A}}^{-1} \underline{\underline{B}} \cdot \begin{pmatrix} \underline{V}_1 \\ \underline{V}_2 \\ \vdots \\ \underline{V}_{x_j} \end{pmatrix}^n. \text{ With given initial conditions, this iteration scheme}$$

generates the vector values for later times. The Crank-Nicolson finite difference method guarantees this is a unitary iteration scheme [45]. In our problem, we have numerically verified the matrix $\underline{\underline{A}}^{-1} \underline{\underline{B}}$ has eigenvalues that are pure phases, which proves that this method is unitary.

Bibliography

- [1] A. N. Kaufman, A. J. Brizard, and E. R. Tracy, in RADIO FREQUENCY POWER IN PLASMAS: 16th Topical Conference on Radio Frequency Power in Plasmas (2005), vol. 787 of AIP Conference Proceedings, pp. 146–149.
- [2] Yu. Krasniak and E. R. Tracy, “Emission from mode conversion regions”, in Radio Frequency Power in Plasmas, 13th Topical Conference (AIP Conference Proceedings, No. 485, 1999).
- [3] A. N. Kaufman, J. J. Morehead, A. J. Brizard and E. R. Tracy, “Modular approach for conversion to the ion-hybrid wave and α -gyroresonance,” in Radio Frequency Power in Plasmas, 12th Topical Conference, AIP Conference Proceedings 403 (1997) 359.
- [4] T. K. Mau and J. deGrassie, eds., RF Power in Plasmas, AIP Conference Proceedings (American Institute of Physics, Melville, NY, 2001) Vol. 595.
- [5] L. Friedland, G. Goldner, and A.N. Kaufman, “Four-dimensional eikonal theory of linear mode conversion” Phys. Rev. Lett. 58, 1392 (1987).
- [6] A. N. Kaufman and L. Friedland, “Phase space solution of the linear mode-conversion problem,” Phys. Lett. A 123, 387 (1987).
- [7] H. Ye and A. N. Kaufman, “Wave propagation in k-space and the linear ion-cyclotron echo,” Physical Review Letters 60 (1988) 1642.
- [8] H. Ye and A. N. Kaufman, “Analytic solution for second-harmonic gyroresonant absorption and mode conversion ,” Physical Review Letters 61 (1988) 2762.

-
- [9] H. Ye and A. N. Kaufman, "Self-consistent theory for ion gyroresonance," *Physics of Fluids*, 4B (1992), 1735-53.
- [10] A. N. Kaufman, "Phase-space action principles, linear mode conversion, and the generalized Fourier transformation", in *Nonlinear and chaotic phenomena in plasmas, fluids and solids*, W. Rozmus and J. A. Tuszynski, eds. (World Scientific, New Jersey, 1991).
- [11] R. G. Littlejohn, *Physics Reports* 138, 193 (1986).
- [12] W. G. Flynn and R. G. Littlejohn, *Annals of Physics* 234, 334 (1994).
- [13] A. N. Kaufman, E. R. Tracy, J. J. Morehead, and A. J. Brizard, *Physics Letters A* 252, 43 (1999).
- [14] R. G. Littlejohn and W. G. Flynn, "Chaos: An Interdisciplinary" *Journal of Nonlinear Science* 2, 149 (1992).
- [15] E. R. Tracy and A. N. Kaufman, *Phys. Rev. E* 48, 2196 (1993).
- [16] A. N. Kaufman, E. R. Tracy, and A. J. Brizard, *Physics of Plasmas* 12, 022101 (2005).
- [17] E. R. Tracy, A. N. Kaufman, and A. Jaun, *Physics of Plasmas* 14, 082102 (2007)
- [18] E. R. Tracy, A. N. Kaufman, and A. J. Brizard, *Physics of Plasmas* 10, 2147 (2003).
- [19] A. Jaun, E. R. Tracy and A. N. Kaufman, *Plasma Physics and Controlled Fusion* 49 (2007) 43.

-
- [20] Yi-Ming Liang, James J. Morehead, Daniel R. Cook, Tor Fla and Allan N. Kaufman, "Multiple mode conversion: an analytical and numerical comparison," *Physics Letters* 193A (1994) 1.
- [21] A.J. Brizard, J.J. Morehead, A.N. Kaufman, and E.R. Tracy, "Double-crossing mode conversion in nonuniform medium", *Physics of Plasmas* (1998) 5, 45-59.
- [22] P.S. Cally, J. Andries, "Resonance absorption as mode conversion/transmission." (In preparation for submission to *Solar Physics*)
- [23] J. D. Jackson, *Classical Electrodynamics* (Wiley, New York, 3rd ed., 1998).
- [24] D. R. Nicholson, *Introduction to Plasma Theory* (Wiley, New York, 1992).
- [25] D. R. Cook, A. N. Kaufman, E. R. Tracy and T. Fla, "Collective wave spin-off and the gyroballistic continuum in gyronresonant absorption," *Physics Letters* 175A (1993) 326.
- [26] D. R. Cook, A. N. Kaufman, A. J. Brizard, H. Ye and E. R. Tracy, "Two-dimensional reflection of magnetosonic radiation by gyroballistic waves: an analytical theory," *Physics Letters* 178A (1993) 413.
- [27] Alfvén, H. (1942), "Existence of electromagnetic-hydrodynamic waves", *Nature* **150** (3805): 405–406.
- [28] T. H. Stix, *Waves in Plasmas* (AIP, New York 1992).
- [29] Sakurai, J. J. (1967). *Advanced Quantum Mechanics*. Addison Wesley
- [30] A. N. Kaufman, A. J. Brizard and E. R. Tracy, "Triplicate Budden

resonance in the presence of sheared flow,” AIP Conference Proceedings 787 (2005) 146.

[31] A. N. Kaufman, E. R. Tracy and A. J. Brizard, “Helical rays in two-dimensional resonant wave conversion,” *Physics of Plasmas* 12 (2005) 22101-1-10.

[32] D. A. Gurnett and A. Bhattacharjee, *Introduction to Plasma Physics* (Cambridge, United Kingdom, 2005)

[33] C. Zener, *Proceedings of the Royal Society of London. Series A, Containing Papers of a Mathematical and Physical Character* (1905-1934) 137, 696 (1932).

[34] R. G. Littlejohn, “Landau-Zener transitions in two dimensions”, in *Path Integrals from meV to MeV*, Proceedings of the 4th International Conference, Tutzing, Bavaria, May 18-21 (1992), edited by Hermann Grabert, et al. (World Scientific, Singapore, 1993).

[35] Y. Colin de Verdière, “The level crossing problem in semi-classical analysis I: the symmetric case”, *Annales de l’Institut Fourier*, Special Issue: Proceedings of Frédéric Pham’s Congress, 53 (2003) 1023-1054.

[36] Y. Colin de Verdière, “The level crossing problem in semi-classical analysis I: the symmetric case”, *Annales de l’Institut Fourier*, Special Issue: In Honor of Louis Boutet de Monvel, 54 (2004) 1423-1441.

[37] A. S. Richardson, “Group theoretical foundations of path integrals with application in mode conversion,” (PhD. dissertation, William and Mary, 2007).

-
- [38] G. B. Whitham, *Linear and nonlinear waves*, Pure and applied mathematics (Wiley, New York, 1974).
- [39] Goldstein H. *Classical Mechanics* (2nd ed.). (Wesley, MA, 2nd ed. 1980).
- [40] J. B. Delos, “Catastrophes and stable caustics in bound-states of Hamiltonian-Systems” *Journal of Chemical Physics* 86, 1 (1987).
- [41] R. G. Littlejohn and J. M. Robbins, “New way to compute Maslov indices”, *Phys. Rev. A* 36, 2953 (1987).
- [42] A. N. Kaufman, H. Ye, and Y. Hui, “Variational formulation of covariant eikonal theory for vector waves,” *Phys. Lett. A*, 120, 327, 1987.
- [43] R. G. Littlejohn and W. G. Flynn, “Geometric phases in the asymptotic theory of coupled wave equations” *Phys. Rev. A*. 44, 5239–5256 (1991).
- [44] E. R. Tracy, A.J. Brizard, “Allan Kaufman’s contributions to plasma wave theory”, *Journal of Physics: Conference Series* **169** (2009) 012008.
- [45] W. H. Press, S.A. Teukolsky, W.T. Vettereling, B.P. Flannery, *Numerical recipes in C* (Cambridge, UK, 2002).
- [46] E. F. Jaeger, L. A. Berry, J. R. Myra, D. B. Batchelor, E. D’Azevedo, P. T. Bonoli, C. K. Phillips, D. N. Smithe, D. A. D’Ippolito, M. D. Carter, R. J. Dumont, J. C. Wright, and R. W. Harvey *Phys. Rev. Lett.* **90**, 195001 (2003).
- [47] E. Nelson-Melby, M. Porkolab, P. T. Bonoli, Y. Lin, A. Mazurenko, and S. J. Wukitch, *Phys. Rev. Lett.* **90**, 155004 (2003).
- [48] C. C. Petty, R. I. Pinsky, M. J. Mayberry, M. Porkolab, F. W. Baity, P. T. Bonoli, S. C. Chiu, J. C. M. de Haas, R. H. Goulding, D. J. Hoffman, T. C. Luce, and R. Prater *Phys. Rev. Lett.* **69**, 289 (1992).

VITA

Yanli Xiao

Yanli Xiao was born on October 15, 1982, in Shanghai, China. She was educated in Shanghai through high school and in 2004 she entered Fudan University in Shanghai to study physics. She graduated with honors in June 2004, and in Fall 2004 she entered the physics graduate program at the College of William and Mary in Williamsburg, Virginia. In December 2005, she received a Master of Science degree from William and Mary and joined Professor Tracy's research group, studying plasma dynamics theory. She successfully defended her PhD dissertation in May 13, 2010.